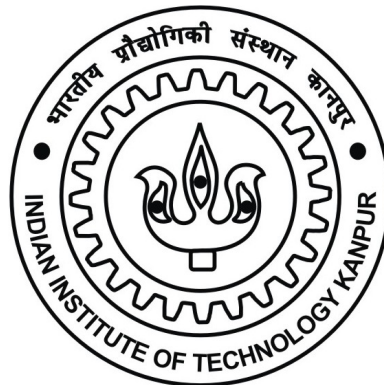# DEVELOPMENT OF CUTTING TOOL CONDITION MONITORING SYSTEM FOR TURNING OPERATION

By

H.CHELLADURAI

DEPARTMENT OF MECHANICAL ENGINEERING

INDIAN INSTITUTE OF TECHNOLOGY KANPUR

July, 2008

DEVELOPMENT OF CUTTING TOOL CONDITION MONITORING SYSTEM FOR TURNING OPERATION
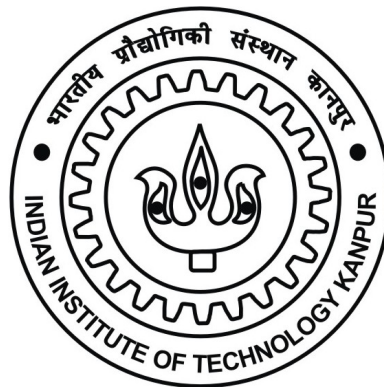
A Thesis Submitted

in Partial Fulfillment of the Requirements

for the Degree of

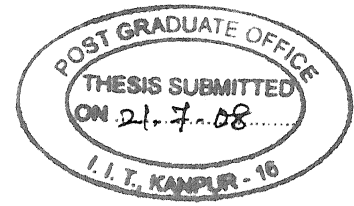**Doctor of Philosophy**

By

H.CHELLADURAI

to the

DEPARTMENT OF MECHANICAL ENGINEERING

INDIAN INSTITUTE OF TECHNOLOGY KANPUR

July, 2008

CERTIFICATE

It is certified that the work contained in the thesis entitled *"Development Of Cutting Tool Condition Monitoring System For Turning Operation"* by *H.Chelladurai* has been carried out under our supervision and that this work has not been submitted elsewhere for a degree.

Dr.V.K.Jain

Professor

Department of Mechanical Engineering

Indian Institute of Technology Kanpur

Kanpur-208 016

India

July 2008

Dr.N.S.Vyas

Professor

Department of Mechanical Engineering

Indian Institute of Technology Kanpur

Kanpur-208 016

India

Synopsis

Name of Student : H.Chelladurai   Roll Number : Y210563

Degree for Which Submitted : Ph.D.   Department : Mechanical Engineering

Thesis Title: **Development Of Cutting Tool Condition Monitoring System For Turning Operation**

Thesis Supervisor(s) :Prof. N.S.Vyas and Prof. V.K. Jain

Month and Year of Submission : July, 2008

Cutting tool wear monitoring in machining operations has been an active area of research for nearly last two decades. Cutting tool wear plays an important role in deciding economic strategies, product quality, tooling cost, tool-changing cost, rejection of products and productivity. Metal cutting processes are in general non-linear and stochastic in nature. It is therefore difficult to represent them as a mathematical model and they usually require simplifying assumptions. As a result, such models are not capable of representing real metal cutting process. For an automated industry, all the machining input parameters (cutting speed, feed rate, depth of cut) are controllable except cutting tool condition. Major problem in the machining process is cutting tool wear prediction. In this research work an attempt has been made to develop neural network models using sensors' signals to predict the health of a cutting tool. Properties of signals from the sensors depend on many factors such as machining conditions (cutting conditions), workpiece material, and cutting tool geometry. Apart from the complexity of the process, signals from the sensors are disturbed for many reasons: outbreak at cutting edges, chatter (i.e. self-exited vibrations), sensor non-linearity, noise of digitizers, crosstalk effects between sensor's channels, etc.

An intensive investigation has been carried out in the area of Tool Condition

Monitoring (TCM) system, covering various metal cutting processes such as turning, milling, drilling, grinding, etc. However, none of these systems have been accepted universally by shop-floor engineers. There is still a need for a reliable, universal TCM system, which is suitable for industrial applications. A good cutting tool condition monitoring system should be characterized by fast detection of impact or collision, (i.e. unwanted movement between tool and workpiece, or tool and any component of the machine tool), tool chipping (cutting edge breakage), and gradual tool wear caused by abrasion due to friction between flank face of cutting tool and workpiece. A human operator can detect condition of a cutting tool by sensing noise (or sound) generated during machining, observation of chip color (visual), presence of smoke (smell), surface roughness of workpiece and so on.

Cutting tool wear sensing techniques are broadly classified into two categories: direct and indirect. Direct methods are those that utilize effect caused directly by tool wear, and measured by using optical microscope, radioactive, or camera vision. However, direct methods of measuring tool wear have not been easily adaptable for shop floor applications. They are not suitable for on-line condition monitoring. However, they can be easily applied to off-line measurements which require more time. Indirect tool sensing techniques generally employ one or more of the responses of a machining process like temperature, cutting force, vibration, surface finish, acoustic emission, motor current and so on. These indirect methods can be implemented for an unmanned automated industry; however they have a lower sensitivity compared to direct methods. Availability of computational power and reliability of electronics have lately helped in the development of a reliable tool condition monitoring system using indirect methods. A major problem in TCM system is selection of a proper sensor and its location. Sensors have to be placed as close as possible to the target location (close to the tool tip). Hardware components of a cutting tool wear monitoring

system have been developed to a reasonable satisfaction but software components need to be improved significantly. In view of this, a multi-sensor approach has been proposed to monitor the condition of a cutting tool.

Accurate and repeatable physical simulations of a flank wear as well as chipped off cutting edge of a tool is a difficult task. Hence, in this work an attempt has been made to create artificial flank wear and chipped off cutting edge using Electrical Discharge Machining (EDM) process in a controlled manner. Use of such tool results in very close to real life flank wear and chipping failure experienced by a tool during machining process. Artificially created flank wear and chipped off cutting edge are more uniform and well defined while in real life they are not so uniform, and non-uniformity always persists. This difference would definitely lead to the deviation between the results obtained by these two classes of tools (tool worn out during normal cutting and worn out tool created by EDM). Using this (artificial worn out) cutting tool, experiments are carried out on a CNC GILDMEISTER CTX 400 Serie 2 turning centre for various machining conditions using EN-8 steel as workpiece.

In order to study the dynamic behaviour of cutting tool, Finite Element Analysis (FEA) has been carried out by using ANSYS. In this analysis, a solid model of a cutting tool has been developed. The natural fundamental frequencies and modes of vibration have been analysed by using free vibration concepts (modal analysis).

Experiments are conducted on EN-8 steel using DNMG 150608 insert with Seco tool holder PDJNR 2020 K15 without cutting fluid. The tool is instrumented with strain gauges (TML-120Ω) and two accelerometers (NP-3331-ONO-SOKKI). The strain gauge signals are taken to a PXI system and accelerometer signals are taken to an ONOSOKKI FFT analyzer. The PXI system is equipped with a

Wheatstone bridge configuration and an amplifier. By using design of experiments (DOE) theory, the analysis of variance (ANOVA) has been carried out for different machining input parameters and each parameter has been tested with the level of significance at 99% confidence limit. Empirical models have been developed with respect to machining parameters and the predicted results have been compared with the experimental results. From the experimental results, it is observed that the magnitude of strain and amplitude of vibration increase with depth of cut and feed rate, and decrease with cutting speed. The amplitude of vibration (acceleration, g) and amplitude of strain are substantially more for a chipped off tool compared to a flank worn-out tool.

One of the aims of this research work is to enhance the feature extraction procedure from the signals of the sensors (accelerometers and strain gauges). Time domain and Power spectral analysis are carried out and an Artificial Neural Networks (ANN) back propagation algorithm is used to classify and estimate the wear parameters. A real condition monitoring system is expected to replace the knowledge and experience of a skilled machine operator. This can be achieved through proper learning and training of ANN. Neural networks based condition monitoring systems employ feed forward multi layer perceptrons (MLP). The behaviour of neural networks architecture depends upon various parameters like input patterns to networks, target vectors, number of layers, number of neurons, activation function, training function, number of epochs and so on. Back-propagation training algorithms were tried. Training and validation results from various architectures are presented and a comparison is made. An attempt has also been made to develop an ANN algorithm that can identify whether a tool has flank wear or a chipping failure. Cutting tool vibration and strain signals are found to carry useful information for predicting flank wear as well as chipping failure. For this purpose, four statistical moments are extracted from time domain data and then used in ANN analysis as the input data.

Similarly frequency domain analysis has been carried out and extracted features are fed in to ANN as input data for training. After training, the best architecture of ANN has been chosen by trial and error analysis and then the same architecture of ANN has been tested with new experimental data. It is observed that the response (output) of ANN is good enough to classify both, the flank wear and chipping failure at different levels. On the basis of the condition of the cutting tool this neural network model may be further employed to develop an adaptive feed back system to control the machining process.

This research work focuses on the development of instrumentation system to monitor the condition of cutting tool in on-line, development of the method to artificially create flank wear and chipped off cutting edge, and to identify the state of a cutting tool on-line. This thesis comprises following eight chapters.

- Chapter 1 discusses introduction of condition monitoring systems and its applications in the area of cutting tool condition monitoring system.

- Chapter 2 deals with literature survey. In this chapter various indirect TCM systems have been discussed. Based on the literature survey, the present thesis is placed in an appropriate context and objectives of the work have been identified. It is decided to develop a sensor based tool condition monitoring system to identify the cutting tool condition.

- Chapter 3 deals with various flanks wear levels and their maximum limitation; selection of tool material with respect to workpiece has also been discussed. Based on the understanding of flank wear and chipping mechanism, a systematic procedure has been formulated to create an artificial flank wear (including nose wear) and chipping failure by EDM process.

- Chapter 4 details about the experimental design, selection of machine tool and selection of machining parameters according to the design of

experiments criterion. It also includes sensors and instrumentation systems, data acquisition and retrieval systems namely FFT analyzer and NI-SCXI strain gauge module.

- Chapter 5 discusses the empirical models development and analysis using ANOVA. These models are validated with the experimental results. In this chapter flank wear as well as chipping failure analysis are compared and it is observed that cutting tool with chipping failure vibrates more when compare with flank wear tool.

- Chapter 6 discusses the development of ANN models. Three ANN models have been developed to predict the flank wear and chipping failure for various machining conditions. These models are validated with experimental results.

- Chapter 7 discusses conclusions, major results and contributions of this work. It also suggests a few areas of future study.

This system can be useful to on-line predict the condition of a cutting tool which would help in improving the quality of the products. The experimental, empirical and ANN results are promising to implement TCM system in an industry.

Acknowledgment

I am deeply indebted to my supervisors Prof N.S.Vyas and Prof.V.K.Jain who constantly provided me the excellent guidance, invaluable suggestions and encouragement during the entire course of my study. They always guided me on the right path when ever I had a trouble time. It was a great pleasure for me to work with them as a lot of care and personal touch was always available . It would not have been possible for me to complete the thesis work without their continuous encouragement and guidance during the entire period of thesis work.

I am grateful to Prof.J.Ramkumar and Dr.V.Raghuram for their constructive criticism and suggestion, which helped in improving quality of the work. I also thank all other faculty members and the staff of Department of Mechanical Engineering for their timely help.

I express my gratitude to Mr.T.V.K. Gupta, Research Engineer, 4i-Lab providing me the freedom and utilisation of 4i- Lab facilities during my thesis period. I express my hearty gratitude to Dr.G.Saravanakumar (Asst. Professor, IITG), for extending his helping hands whenever it was needed the most.

I wish to acknowledge my lab mates Mr.Ankur kumar, Mr.Prashanth Dalawai, Mr.Mohan Kumar, Mr.Ravi Kumar, Mr.A.K.Sahani, Mr.N.R.K.Reddy, Mr.R.K.Singh, Dr.Sunil jha, Mr.M. Ravisankar, Mr.Manas Das, Dr.B.V.Dharmendar, Mr.Asish Nayak, Mr.Anupam Agrawal, Mr.Nitin galphat, Mr.Manoj Nayani, Mr.R.K.Porwal, Major.Jasdeep singh, Mr.Pradeep sarkar, Mr.Rohit and Sanjay shukla, Ms.Noopur shukla, Ms.Ruchira for their cooperation, help and maintaining a good working atmosphere.

I sincerely thank Mr.J.P. Verma, Mr.R.C. Agnihotri, Mr.Mohamed Mohsin and Mr.Manoj kumar Rawat for proper maintenance and when required, speedy repair of the lab equipments and providing technical help while conducting experiments.

Contents

List of Figures

List of Tables

Chapter 1

Introduction

1.1 Condition monitoring

Condition monitoring and diagnostics of machines is a subject of increased importance in the course of progressive automation. It is essential in order to ensure operation within design consideration and anticipate problems in time, so as to prevent catastrophic failures. It is concerned with extracting information from cutting tools and machine tools to indicate their conditions, and to enable them to be operated smoothly throughout their serviceable life. Manufacturing industries mainly pertaining to computer integrated manufacturing system, robot controlled machining system, have undergone tremendous changes in the past three decades. Today customer demands high quality products for lowest possible price. In order to meet such demands and to face global competition, modern industries are aiming towards achieving high dimensional accuracy. Manufacturers are focusing on the technical aspects of , how to achieve uninterrupted automated machining for longer duration with least human supervision. Cutting tool wear condition monitoring is one such important aspect that needs to be looked into in automated cutting processes and unmanned factories. In a metal cutting operation, a major hurdle in realizing total automation is cutting tool state prediction and consequently maintenance.

Cutting tool condition monitoring can help in on-line realization of the tool wear, tool breakage, and workpiece surface roughness [1].   Worldwide investment in metal cutting industries remains steady or continues to increase year by year, and it decides economic condition or wealth of the country [2]. Researchers and engineers have been trying to evolve a cutting tool condition monitoring system with high reliability [3].   There is a need for reliable, universal cutting tool condition monitoring (TCM) system, which is suitable for industrial applications.   Various sensing techniques [4] have been reported which deal with detecting edge chipping, fracture, tool wear and surface finish. Various sensors were adopted in the area of metal cutting tool condition monitoring system namely, touch sensors, power sensors, acoustic emission sensors [5, 6], vibration sensors, torque sensors, force sensors, vision sensors and so on . In any automated process, sensors and their signal interpretation play an important role. The processing and analysis of signals is important because it improves production capacity, reliability, reduced downtime and improved machining quality [7, 8, 9]. Sensors and their utilization were implemented in many areas like machine tool manufacture, automotive industry, tool manufacturing and so on.   Byrne et al [10] reported that 46% of the sensors monitoring systems were fully functional, 16% had limited functionality, 25% of the systems were non functional due to technical limitations and 13% were replaced by or switchover to alternate systems.

In sensors based system, the accurate prediction of cutting tool condition using signal responses is an important aspect. In many cases wrong interpretation of the sensor signals by an operator leads to the wrong decision to switch off the machine tool which affects the quality of the product as well as production rate. The training of the personnel also plays a vital role in successful implementation of tool condition monitoring systems.   Now-a-days, modern machines and

machine tools are complex systems. It is difficult to monitor each element or each system without the addition of numerous sensors. If number of sensors are more, the difficulty further compounds to handle a large number of data, their interpretation and analysis.

Generally, machining processes are non-linear and stochastic in nature, and it is hard to build a mathematical model. Such mathematical models are based on suitable assumptions and they may not be matching with real world metal cutting process. An intensive research has been carried out related to TCM systems, covering various metal cutting processes such as turning , milling , drilling and grinding, over the past two decades or so [11]. A good cutting tool condition monitoring system [23] should be characterized by fast detection of (a) impact or collisions, (i.e. unwanted movement between tool and workpiece, or tool and any other component of the machine tool), (b) tool chipping (cutting edge breakage), and (c) gradual tool wear (crater and flank) caused by abrasion between cutting tool and workpiece (flank wear) and cutting tool and chip (crater wear), respectively.

Tool wear sensing techniques are broadly classified into two categories: direct and indirect as shown in Table 1.1. The direct tool wear monitoring methods can be applied when cutting tools are not in contact with the work piece [7, 12] like radioactive, microscope, camera vision and so on. However, direct methods of measuring tool wear have not been easily adaptable for shop floor application. They are not suitable for on-line condition monitoring system however they can be easily applied to off-line measurements and it consumes more time. Indirect tool sensing methods use relationship between cutting conditions and response of machining process which is a measurable quantity through sensor signals output (such as force, acoustic emission, vibration, or current) and may be used to predict the condition of the cutting tool. These indirect methods are used

Table 1.1: Tool wear sensing methods.

Direct Methods	Indirect Methods
Electrical Resistance	Torque and power
Optical Measurements	Temperature
Radio active	Vibration and Acoustic Emission
Contact sensing	Cutting forces and Strain measurements

extensively by various researchers and the detailed analyses have been carried out in the past two decades. These indirect methods can be implemented on to an industrial problem, but they have a lower sensitivity compared to direct methods. Nowadays, availability of computational power and reliability of electronics help in the development of a reliable condition monitoring system by using indirect methods. However, a problem in TCM is selection of proper sensor and its location. The sensors have to be placed as close as possible to the target location (close to the tool tip) being monitored.

It is interesting to note that an indirect TCM system [7] consists of four steps: (i) collection of data in terms of signals from sensors [30] for assessing cutting force, vibration, temperature, acoustic emission and/or motor current, (ii) extraction of features from the signals, (iii) classification or estimation of tool wear using [84] pattern recognition, fuzzy logic, neural networks, or regression analysis, and (iv) development of an adaptive system [87, 98, 96] to control the machining process based on information from the sensors.

There have been many investigations on tool wear based on periodic measurements of wear levels using optical microscope. In the present study, an artificial wear has been created (externally) using Electric Discharge Machining

(EDM) process in a controlled manner. This is similar to a real wear (Flank and Chipping failure) experienced by the tool during machining process. Artificially created wear is neat and clean (Figure3.6) while on-line actual wear is irregular. Because of irregular shape of wear it is difficult to judge or measure level of severity of wear. In artificially created wear, the bulk temperature during EDM is very small compared to on-line tool wear during cutting. It may lead to very fine micro-cracks while on-line tool wear, during metal cutting, the tool is subjected to reasonably high temperature and quenching it coolant is used resulting in micro-cracks. In Artificially created wear, the final conditions of the tool exist in the beginning itself while in on-line tool wear it has to be simulated or guessed which will be an involve approximation. Using this (artificially worn) cutting tool, cutting experiments are performed and signals are captured.

1.2   Objectives of the Thesis

In actual metal cutting experiments, the tool wear geometry generated is not uniform hence its dimensions have to be averaged out. Artificially created worn out tool may also have thermal defects like micro-cracks and thermal residual stresses [13]. The concept of artificially creating flank wear on the tool can be applied for non-uniform shape and size provided they are mathematically representable. However, while interpreting the captured signals, this difference should be kept in mind. Therefore, for purpose of algorithm development and calibration it was decided to artificially create the uniform flank wear of the desired averaged dimension on the tool using EDM machine.

This created wear is well defined shape and easy to measure (using USB port microscope). In this thesis two sets of sensors (strain gauge and accelerometers) were used to monitor the cutting tool condition. These were placed very close to cutting tool tip. The aim of the thesis is to develop a systematic feature

extraction procedure from the output responses (accelerometers and strain gauges) of a machining process. Artificial Neural Network (ANN) schemes are developed for classification or estimation of tool wear. The output from the sensors, after necessary processing is fed as input to the networks. Back propagation and probabilistic neural networks have been designed. Their efficiency has been investigated for various internal architectures, activation functions and learning algorithms. Major contributions of this work are briefly mentioned as follows:

- Development of systematic procedure to create an artificial tool wear (externally) by using EDM process.

- Development of experimental design and instrumentation systems to predict the flank wear and chipping failure level for different machining conditions which is very helpful to predict the condition of a cutting tool.

- FEM analysis and solid models are developed using ANSYS to study the dynamic characteristics of the cutting tool, and workpiece, and validated with the experimental results.

- Using the concept of DOE, the empirical models had been developed to predict the flank wear and chipping failure levels, and validated the same with experimental results.

- ANN models have been developed and these models were trained and validated with experimental data to predict the flank wear level and chipping failure.

1.3   Constraints and limitations

The present study has focused on a specific application and its limitations are listed below

- The study is limited to DNMG inserts cutting tool for turning operation.

- The feature of the selected tool DNMG inserts is that it ensures that crater wear does not take place because of chip breaker mechanism in the tool system.

- This DNMG inserts experiences only flank wear and chipping failure.

- The study of interaction between flank wear and chipping failure in the tool was not in the scope of the simulated Artificial Neural Network (ANN) experiments.

- As flank wear and chipping failure are considered simultaneously for the first time, FEM analysis and ANN applications to DNMG tool failures give new directions and confidence for future studies.

- The results of this study with DNMG inserts fitted with cutting tool can not be extended for monitoring non grooved inserts or solid cutting tool where crater wear is significant. Theses two studies have to be carried out totally independent because of different designs of the tool.

- To find out any possible interaction between flank wear and chipping failure, it is necessary to apply fracture mechanism because of creation of notch irregularities and resulting stress raisers and stress concentrations by real life flank wear. The geometry of these notches and stress raisers will have to be simulated and considered.

- Initiation of surface crack or crack at the sub-surface and crack growth in the cutting tool in the presence of fatigue loading and dynamic stresses need to be considered in the study.

Chapter 2

Literature survey

2.1 Literature survey

The vast amount of literature in this field suggests that a variety of process parameters in the metal cutting environment can be tapped and used to predict the cutting tool-state. In this chapter, following typical methods are discussed along with their correlation to tool wear during experimentation.

- Acoustic emission (AE),

- Cutting forces (static and dynamic),

- Vibration signature (accelerometer signals),

- Cutting tool temperature, and

- Miscellaneous method such as ultrasonic, optical measurements, workpiece surface finish measurements, workpiece dimensions, stress/strain analysis, spindle motor current and so on.

2.1.1   Acoustic emission

In metal cutting operations,workpiece undergoes plastic deformation when the cutting tool penetrates in it. Due to deformation (dislocation movements),

localised strain energy is released spontaneously in the form of acoustic emission. In addition to metal cutting, acoustic emission are also released in many other practical situations such as phase transformations, friction mechanisms (tool-workpiece contact), crack formation or fracture or fracture extension and so on. In the literature [14, 9, 15, 16, 17], various researchers have employed different methodologies and sensors for capturing signals and their interpretation. Out of many methods, some important methods are discussed below.

Choi *et al*. [16] developed a real-time TCMS for turning operations using AE and cutting force signals. Two sets of experiments were conducted using tungsten carbide insert tips with one set slotted by wire EDM to accelerate fracture while the second was brazed to the workpiece to induce tool breakage. The recorded data was analysed through a fast block-averaging algorithm for features and patterns indicative of tool fracture, and it showed the occurrence of a large burst of AE at tool breakage. Similar work conducted by Jemielniak and Otman [17] used a statistical signal processing algorithm to identify the root mean square (RMS), skew and kurtosis of the AE signal in the detection of catastrophic tool failure. Cutting force measurements recorded simultaneously were used as reference signals to indicate when the failure actually occurred. Inspection of the test results indicated the skew and kurtosis to be better indicators of catastrophic tool failure than the RMS values.

Kakade *et al*. [18] used AE analysis to predict tool wear as well as chip condition by selecting AE parameters (ring-down count, rise time, event duration, frequency and event rate) recorded simultaneously with the corresponding flank wear land length measured at the selected intervals. Analysis of the results concluded that AE signals could distinguish clearly the cutting actions of a sharp and a worn out or a broken tool.

Zheng *et al*. [19] presented an intrinsic method for AE sensing based on an optic fiber sensor. The sensor consisted of two distinct parts: the sensing element and an interferometer. The sensing element principally was used to produce a shift of phase in the light transmitted through the optical fiber allowing the interferometer to detect and measure the photo elastic modulations in the light intensity. Preliminary drilling and milling operation tests were conducted and the AE signal measured using an optic fiber sensor and a commercially available PZT AE sensor. The obtained results were compared and these showed a reasonable degree of agreement.

Knig *et al*. [20] performed test cuts to detect fracture and/or monitor the condition of small drills using AE features. They circumvented the time consuming and cost-intensive signal processing usually accompanying AE applications by employing simple process-adapted band pass filters, a rectifier and a low pass filter to convert the normally high frequency AE signals to low frequency signals. Drilling operations were performed and a ceramic knock detector sensor designed for industrial application was used to measure AE signals. The recorded AE-RMS was plotted for the number of holes that each drill performed before it failed. Inspection of their plots showed that at the closing phase of tool life (i.e. tertiary phase of tool wear), the RMS value increased dramatically. The rise, one could argue, was a direct response to the fractured tool. Hence Knig *et al*. [20] used this as a prescribed threshold which the RMS for normal operating drills should not exceed. This method however was found to be sensitive to tool chipping.

Blum and Inasaki [5] performed experimental tests to determine amongst other things, the influence of flank wear on the generation of AE signals. They were particularly interested in the use of the AE mode, a parameter describing the

characteristic of the cutting process as the DC component of the measured signal. Experiments were conducted from which AE and the cutting forces were recorded simultaneously for pre-ground and sharp tool inserts. The ensuing analysis involved studying the effects of the cutting conditions on the chosen AE features and tool flank wear. With knowledge of the former, it was possible for its influence in flank wear interpretation not to be misconstrued. Inspection of the obtained graphs for AE-mode/cutting forces and flank wear for various cutting speeds showed an indispensable correlation of AE-mode to flank wear. A not-so-good correlation was realised with the cutting forces, as their slopes were significantly smaller compared to the AE-mode ones that were almost linear. This was interpreted as the flank wear length being extremely sensitive to AE-mode. They, however, concluded that extraction of such information from the AE signal was difficult.

Moriwaki and Tobito [21] proposed a method based on AE measurement and analysis for coated tool life estimation. The underlying principle behind their devised method for coated tool life estimation was that, during progressive tool wear, the tool material changes from one substrate layer to another and emits AE signals that could be monitored to determine tool life. An experimental test rig was set up and tests were conducted on it. The AE and tool wear (flank and crater) were measured together with the surface roughness. Typically, AE RMS values for the recorded AE signal and the wear values (initial, middle and tertiary stages of tool wear) were graphed on the same scale for comparison. Inspection of the presented plots indicated a strong correlation of AE RMS amplitude to tool wear, increasing with wear progression. Further analysis to extract statistical features (mean, variance and the coefficient of RMS) were performed and plots made for the complete cutting cycle. The variance was the most sensitive to tool wear, as it had the largest amplitude in the final phase of tool life. The recorded data was applied to a pattern recognition system and it

performed reasonably well. Thus, by measuring the AE emitted from specially treated coatings on a cutting tool, it was possible to identify and predict the ensuing tool life. The only drawback to the application of this method, it could be argued, was its exclusive use of coated tool inserts.

Roget et al. [22] carried out machining tests from which the captured AE signals were used to predict the state of the cutting tool. They concluded that such task could only be successfully accomplished under specific and limited conditions. Using custom-made AE sensors, turning and milling tests were carried out with normal grade and alloyed steels as workpiece . The parameters of AE signals were recorded (RMS, mean and peak values). Further, statistical features such as variance, kurtosis and skew were extracted from the recorded parameters. A comparison of the recorded AE signals and measured flank wear curves were carried out, and showed a remarkable similarity with the characteristic three distinct phases depicted on both the wear-time and AE-time plots. There was a corresponding initial rise in both curves due to the tool being engaged in cutting. A slowing down of the wear rate reciprocated on the AE signal curve by a much gentle slope followed this. As soon as the flank wear began to increase to catastrophic levels, the AE signal reflected the increase and its undulations became more erratic. They extended their method to identifying tool breakage as well but using a milling operation instead of the test bed. Their final conclusion was that AE provided sufficient warning of the ensuing changes in both cutting conditions, tool breakage and tool wear.

During metal cutting , a little AE is thought to be generated compared to a larger AE accompanying tool breakage and fracture [9, 15]. AE, it could be argued, is dependent on the structure of the cutting material than on the cutting tool, with its signal reflecting the behaviour of the response from the machine tool set-up rather than the cutting tool. As the emphasis on any TCMS would generally be

on tool wear rather than tool fracture, AE is not a suitable tool wear indicator in monitoring applications, but could be used to detect tool tip breakage in machining centers. On another note, Lister and Dimla [23] were of the opinion that the most profound limiting factor in the application of AE to a TCMS does not lie on the sensing technology, but on the ensuing analysis. This void is due primarily to a lack of a suitable database on AE, implying that the user has to experiment and establish the necessary trigger responses to a variety of machining conditions thereby placing a considerable burden upon him/her. When compared to instances where for example, the concept of lowering and increasing the force limits might be understood, spectral analysis is not so easily comprehended. Hence instead of the system being an aid to the operator, it rather presents a real-time quandary. Furthermore, because AE might be sufficiently available on the entire machining area, choosing a suitable area to place the AE sensor to trap sufficient AE signals is debatable, as an understanding of the AE path has to be established. A drawback to the application of AE as an indicator of tool wear is the fact that its signals are more sensitive to variations in the cutting conditions and noise than of the tool condition itself. Using AE on its own to monitor the state of a cutting tool is a difficult task [24]. AE in the view of the present author is deemed only suitable as an additional sensing method for increased reliability for TCM. Dornfeld [25] presented compelling reviews on the application of AE sensing techniques in manufacturing processes particularly applied in tool wear detection in machining.

2.1.2 Cutting force

It has been widely established that variation in cutting force can be correlated to tool wear. In practice, application and interpretation of cutting force parameter has been diverse with more effort concentrated on studying the dynamic

characteristic of the cutting force signal and interpreting its relation to tool wear levels. This can largely be attributed to the fact that force becomes important in worn tool conditions as a result of the variations produced due to friction between cutting tool flank and the workpiece [26, 27].

Existing force based tool condition monitoring systems (TCMSs) typically operate independently of absolute force levels, measuring the relative change of force that occurs as a new tool wears or when it fractures [28, 16]. Experiments have shown that the three components of the cutting force respond differently to the various wear forms occurring on the tool. For example, the feed force may be insensitive to crater wear where as the feed and radial forces may be influenced more by tool wear than the main cutting force.

Dimla [30] undertook an extensive and elaborate experimental investigation into the development of an on-line tool wear monitoring system for metal turning operation using cutting force measurements fused with vibration signatures. An experimental test-bed consisting of a center lathe with a tool post dynamo meter was used to generate cutting force data. Interrupted test cuts were conducted using double coated carbide grade tool inserts (with chip-breaker geometry) of the P15 type and P25 were used to machine EN-24 alloy steel. Measurements of flank, nose and notch wear lengths were made immediately proceeding recording the on-line data.

Purushothaman and Srinivasa [31], Yao and Fang [32] have used the cutting force signal as input to an ANN, but implemented TCM via different neural network architectures. Using force ratios (F_x/F_y) as an input to neural network (MLP) and the output from this network depicting the severity of tool wear. Having established and understood the effects the parameters had on the force ratios, they proceeded to conduct tests using worn out tools in order to examine

how the force ratios could be used to monitor tool. Results showed that two of the force ratios were particularly sensitive to the accrued flank wear, thus demonstrating potential applicability in TCM operations.

Ravindra *e*t al. [33]developed a mathematical model for tool wear estimation that involved carrying out turning experiments from which the wear progression was studied and the cutting forces were modelled by a multiple regression analysis method. The experiments indicated that the wear propagated faster with an increase in cutting speed, and the occurrence of inflections on the wear display curves indicated a predominant thermally controlled mechanism. An increase in the magnitude of the components of the triaxial cutting force was evident as the wear on the used inserts increased. The wear-time and wear-force plots seemed to support their propositions, from which they concluded that the experiments had provided vital evidence of a good correlation between flank wear and radial forces.

Lee *e*t al [34]in their quest for an on-line TCMS developed a personal computer based fast Fourier transform software to track the dynamic cutting force signal. Intermittent test cuts were performed on a Colchester mascot lathe at 100 mm intervals using two workpieces and single tool insert type (P30). The cutting forces and wear levels were measured and recorded. Subsequent analysis of the obtained data showed that the feed and tangential dynamic force components had a good relationship to flank wear trend.

Marques and Mesquita [35] investigated the relationship between wear of sintered high-speed steel cutting tools and the associated cutting forces. A wear-force model equation was established and the same was experimentally verified. The models considered the independent influence of the flank and crater wear. Experimental tests were conducted from which the forces were

measured. The experiments were conducted for a short duration to establish force-wear relationship, and longer duration cuts to observe the progressive influence of wear on the forces. They reported a good correlation between experimental and theoretical results.

Kim and Lee [36]developed a model of dynamic cutting forces and compared its results with experimental data. A good agreement between theoretical limits of stability and experimental data was reported. However, in low cutting speed range, deterioration between the model results and the experimental results was observed , a fact, which they attributed to the effect of built-up edge. Grabec [1988] and Khraisheh *e*t al [1988] have developed similar model of the dynamic cutting force for chatter prediction.

Oraby and Hayhurst [86] developed a model for tool wear analysis in a turning operation by force characteristics within the different phases of tool wear. Quantification of the developed model was performed by measurement of the vibration of radial/vertical force component ratios, accomplished through force/wear inter-relationship formulated on simple 2-D plots. The experimental data for these models were obtained from machining test cuts of an alloy steel using a Colchester mascot lathe and triple-coated carbide tool inserts. These test were carried out following a central composite design strategy comprising of 24 tests at variable cutting speeds, feed rate and depth of cut.for each test, the wear values (nose,flank and notch) were measured and recorded.To establish a universal rather than a case-based example of individual characteristics, they proposed a mathematical method to quantitatively formulate the wear-cutting force relation to the cutting speed(V), feed-rate(f) and depth of cut(d)to achieve repeatability and reliability for practical applications. The equation below was used and a statistical method adopted in order to obtain the constants $a_0, \alpha, \beta, \gamma$.

$$T = a_0 V^\alpha f^\beta d^\gamma \qquad (2.1)$$

From the statistical analysis, they concluded that there existed a strong correlation between force variation and wear progression. However their model was only applicable when the tool insert was in the primary or secondary phase of wear.

Yao *et al* [38] and, Yao and Fang [39] investigated what they described as a comprehensive TCMS which included the measurement of major and minor flank, crater, and nose wear based on the analysis of dynamic cutting forces. Tool wear experiments were carried out on a Colchester lathe at varying cutting conditions using only one tool insert and workpiece type and the three orthogonal pre-processed force components recorded. Two distinct frequency bands were obtained in all three axes associated with a wear rate mechanism of some sort: a low frequency band 0.5 - 1 Hz and a higher band 2.6 - 3.5 kHz. These trends were in agreement with the recorded wear values, thus, indispensable as a wear monitoring system.

Ghasempoor *et al* [40] concluded machining tests to investigate the feasibility of using different force components for on-line TCM. Through their investigation, they were able to correlate the feed and cutting force components to flank wear length though it also become evident that these parameters were sensitive to changes in the cutting conditions. Experimental observation of the effect of feed force to cutting force ratio showed sensitivity to flank wear but was insensitive to process changes (cutting speed and depth of cut).By combining a prior fast tool fracture detection scheme with their developed flank wear sensing method, it was possible to develop a new TCM strategy.

Lee *et al* [15] pointed out that significant variation existed in the findings of

various researchers who attempted to correlate static cutting forces to tool wear. Some limitations of the static force approach such as disturbances caused by variation in workpiece material, depth of cut, and tool edge geometry were put forward as evidence that approaches based upon static forces had not made any significant gains. They proceeded to examine the nature and principal source of the dynamic force frequency and its correlation to flank wear. Experiments were carried out from which both the static and dynamic forces, and flank wear length were measured.

An inter-relationship between the tangential and normal components of the dynamic cutting forces have been established in Dan and Mathew [41]. In their review, the dynamic forces are reported to fluctuate with excursions to zero and then to higher magnitudes during cutting. A consequence of these excursions has been onset of tool holder vibration whereby chattering at high magnitudes often results. The measurement of the static cutting forces or the fluctuation of its components would provide valuable information on the static behaviour of the cutting process. The nature of the cutting process is such that it can not be regarded as 'without deflections and instability'. The joints and couplings of the machine tool and minute changes in the cutting conditions lead to fluctuations in the static force components. The cyclic variations of the static forces if not limited leads to dimensional inaccuracy of the cutting operation as chatter results. It is difficult to predict the conditions under which it occurs or select cutting conditions necessary to correct this phenomenon. Therefore, to get an indication of the system fluctuations, the dynamic forces were more useful.

2.1.3   Vibration signatures (Accelerometer signals)

Vibrations are produced by cyclic variations in the dynamic components of the cutting force. Usually, these vibrational motions start as small chatter

responsible for the serrations on the finished surface and chip thickness irregularities. Mechanical vibrations generally result from periodic wave motions. The nature of the vibration signal arising from the metal cutting process is such that it incorporates facets of free, forced, periodic and random types of vibration. Direct measurement of vibration is difficult to achieve because its determining characteristic feature, the vibration mode is frequency dependent. Hence, related parameters such as the rate at which dynamic forces change per unit time (acceleration) are measured and characteristics of the vibration derived from patterns obtained.

Dimla and Lister [42] presents a detailed investigation of progressive tool wear results obtained during turning operation. Dry cutting was conducted using P15 and P25 tool inserts from which the three principal components of vibration signal were obtained. A tool life picture was constructed in both time and frequency domains for each vibration component using three tool wear form measurements (flank, nose and notch). The accumulative sum total power of the spectra signal was used to interpret the time domain characteristics while spectra and contour plots described the frequency characteristics. The accumulative power features were ineffective in gradual tool wear monitoring but reasonable at chipping/fracture detection. Spectra plots for tool characteristics at first contact (i.e. when tool was new and therefore sharp) to those describing the severely worn tool characteristics (or the occasional chipping/failure modes) were produced. observation of the waterfall spectral plots showed the cutting direction (z-axis) components of the vibration signals to be most sensitive and the x-axis generally the least sensitive wear accrued. Contour plots clarified observations from the spectra plots i.e. pinpointed the exact principal frequency peaks. The two types of tool inserts used showed slight difference in their active tool lives as a result of the hot hardness effect of the coatings, but the investigations indicated that the amount of wear and its

form was reliant more on the prevailing cutting conditions.

Yan *et al* [24] investigated the use of vibration signature characteristics in on-line drill wear monitoring and breakage. Vibration signature features sensitive to tool wear were identified in time (ratio of absolute mean value to kurtosis) and frequency (power spectra and cepstra ratio) domains. Experimental results showed that the kurtosis values increased drastically with drill breakage while frequency analysis revealed sharp peaks indicating drill breakage. By combining both the techniques, it was possible to devise an effective drill monitoring system.

Yao *et al* [43] investigated detection and estimation of groove wear at the minor cutting edge of the tool by monitoring vibration signatures. A high precision lathe on to which was attached a miniature 3-D accelerometer, a single tool geometry and material combination with five cutting conditions were utilised. Each cut was interrupted to take measurements of the wear mark values. A multivariate time series analysis was carried out on the recorded vibration signals using a combination of autoregressive moving averages and some explicit functions to be obtain a dispersion of the signals auto-covariance, decomposed into the various Eigen values and normalised to within a range of -1 and 1. The dispersion analysis showed that the thrust cutting force and vibration were sensitive to the length of groove wear with two peaks one at a very low frequency ≤ 200 Hz and the other at a high frequency ≥ 10 kHz.

Dan and Mathew [41] employed discrete modelling method called data dependent system to correlate vibration signals to cutting tool wear. The implementation of this method involved the isolation of vibration signal deemed to be most sensitive to tool wear. Obtained results showed some variation in the amount of vibration energy within a specific frequency band

that was consistently observed regardless of cutting parameter. The application of spectral analysis to the acceleration signals revealed a linear relationship between the cutting speed and tool wear showing that vibration signals were sensitive to tool wear.

Rotberg *et al*[88] were investigated in mechanical signature analysis (vibration) for tool state prediction during interrupted cutting. They emphasis on the milling tool entry and exit conditions. Face milling experiments were conducted and the ensuing flank and crater wear measured. Detailed signal processing of the recorded signals was carried out. Wear curves, average envelop at three points of tool life (sharp, part worn, worn) and spectral descriptions of the three wear phases were established. Inspection of the plots indicated that the vibration signal was a suitable indicator of tool wear as it demonstrated considerable change during tool life.

Jiang *et al* [45] using purposely-built test-rig was able to investigate the effects of vibration in the cutting and feed directions on the cutting tool. Using fixed cutting conditions, tests were conducted utilising plane-faced P10 tool inserts with each cut lasting 10 minutes in a single pass. During the time of active tool engagement, the wear on the tool gradually increased until it catastrophically failed. The recorded signals were post-processed and power spectra density (PSD) of the vibration signals was produced. Three distinctive regions identified on the PSD could be divided into the frequency ranges: up to 100 Hz, 117-510 Hz and 510-1000 Hz, from which they performed an in-process method of tool wear monitoring based on frequency band energy analysis. They concluded that their experimental investigations provided sufficient evidence that vibration signals were sensitive to tool wear states.

The inter-relationship between vibration signals and the cutting forces

determines the dynamic nature of the cutting process, making the utilisation of these process parameters attractive in the development of TCMSs [30]. The static behaviour is governed by the cutting forces and and momentum (or torsion of the tool holder). The dynamic behaviour on the other hand embodies vibration and certain aspects of the dynamic cutting force. The combination of elements of the cutting force and the vibration signals fused in developing a multiple sensor-based TCMS would prove indispensable in the shop floor.

2.1.4   The tool tip/ cutting edges temperature

Metal cutting generates a significant amount of heat.   The resultant high temperatures around the cutting tool edges has a direct controlling influence on the rate and mode of cutting tool wear, the friction between chip and cutting tool, and also that between the cutting tool and the newly formed surface. Frictional behaviour on the tool faces is thought to affect the geometry of the cutting process by some mechanism not completely understood. Two metallic surfaces in sliding contact would normally experience dry friction commonly referred to as Coulomb friction. In metal cutting, the coefficient of friction is independent of sliding speed and area of contact. Force is therefore required for the continual shearing of the tips of the asperities or hills. This required force (or load) is proportional to the frictional force in dry sliding. The coefficient of friction between tool and chip varies considerably due to changes in cutting speed and rake angle resulting in high pressures. In the meantime, the real area of contact would approach unity thereby giving rise to high frictional forces that eventually lead to high temperatures and render sliding at the interfaces almost impossible.   Removal of the generated heat is through the chip, workpiece and/or tool. As the temperature distribution is not uniform, knowing the exact amount of heat transferred via the tool is not straightforward. It is however thought that the amount of heat removed or conducted via the chip is as high as

90% of the overall heat generated, implying that less than 10% of the heat is either absorbed or dispersed through the tool and workpiece material.

Lin [46] in his attempt to measure the cutting tool temperature on-line during a milling process devised an inverse approach for real-time tool/workpiece interface temperature. Infrared pyrometry was employed to measure the actual temperature on the machined surface and a least square inverse method applied through an ellipsoidal mapping model of the heat conduction equation. Using a 1-D co-ordinate transformation of a moving heat source system, the measured temperature and heat dissipation to the workpiece was calculated inversely by finite element analysis (FEA) to predict the tool-workpiece interface temperature considered as the heat source. The designed model was tested through application of a known heat flux input and the inverse output verified. Plots of the actual temperature of heat source and that estimated by the proposed method showed minute deviations. He proceeded to test the model further using flame heating to primarily verify the uncertainties in temperature measurement of a moving heat body.

Raman *et al* [47] proposed and developed a mathematical model for cutting tool temperature measurement based on the remote thermocouple sensing (RTS) principle. Differential quadrature modelling of the forward thermal behaviour of the insulated cutting tool was pursued. The credibility of the method lied in the fact that the tool/chip interface temperature distribution had a unique characteristic relationship between the tool-chip temperature and the remote thermocouple temperature. Cutting process temperature change was then determined by observing the behaviour of the rest of the tool temperature (sink response) to variations in the source of temperature (tool tip).

Stephenson and Ali [48] performed studies on tool temperature effects on

interrupted metal cutting and reported theoretical and experimental results. The experimental analysis involved using both infrared and tool-chip contact thermocouple temperature measurements. The measured temperatures for a series of machining conditions were found to be dependent upon two main factors:

- length of cutting cycles, and

- length of cooling interval between cycles.

They pointed out that it was difficult to instrument a thermocouple for tool-chip or tool-workpiece interface temperature sensing when the workpiece was not hollow. The best option was the use of a non-contact measurement technique such as infrared thermal imaging where taking measurements required a detailed understanding of black body radiation. This technique was only capable of temperature measurements that might be considered at best averages rather than the true temperatures, and therefore tended to be dominated by chip images.

Chow and Wright [49] devised an on-line method for tool-chip interface temperature measurement in a turning process using a standard thermocouple inserted at the bottom of the tool insert. Experiments were conducted from which practical cutting data were collected for comparison with predicted interface temperatures from a theoretical model. The test cuts involved dry machining performed on plain steel tube (AISI 1020) with coated and un-coated controlled contact tool inserts. Analysis of the experimental results obtained and verified by the theoretical model showed that an increase in the tool wear resulted in an increase in the cutting temperature. They concluded that the temperature increases were primarily due to tool wear, which could be used to effect TCM during metal cutting.

Usui *et al* [50] presented what could be regarded as the most interesting experimental approach of cutting tool edge temperature measurement. A special purpose thermocouple was constructed from first principles using two carbide tip parts and a quartz glass for insulation. By changing the exit position of the circuitry wire involved, they claim that it was possible to measure the interface temperature anywhere on the flank face of the tool (i.e. the cutting edges). To validate this design, a series of test cuts were conducted using nominally sharp and artificially worn tool inserts. From the ensuing analyses and discussions, the dependency of temperature change rates on flank wear length for both interrupted and continuous cuttings were established. From the viewpoint of tool life estimation, observation of wear characteristics were in agreement with the wear rate equation 2.2:

$$\frac{dW}{\sigma_t dL} C^{\frac{\lambda}{\theta_t}} \tag{2.2}$$

where, C and λ are tooling and workpiece material constants; W and L are wear volume per unit length of the tool insert face and wear distance, respectively; θ_t and σ_t are the absolute temperature and normal stress distribution respectively. However, beyond designing the thermocouple, their aim was not to perform TCM but to establish the mechanisms principally responsible for flank wear rate.

Shaw [51] cited the complexity involved in any attempt to predict the mean tool face temperature as it defies exact solutions. He proposed and evaluated an approximate solution based on the principle of moving heat source.

2.1.5 Sensors and measurements

Generally speaking, other varieties of sensors have been employed in various attempts at tool wear prediction, monitoring or process parameter measurements in a metal cutting process. These methods fall principally into the

following categories:

- optical methods,

- stress/strain measurement,

- methods based on measuring the workpiece dimension,

- spindle motor current/torque/power,

- surface finish quality measurement, and

- ultrasonic methods

Stress/strain measurements

Noori-Khajavi and Komanduri [52] used amongst other sensors, strain sensors in their study of the correlation of process parameters to drill wear. The recorded signals were analysed in both time and frequency domains but meaningful correlation of the drill wear could only be achieved in the frequency domain. The area under the x-axis PSD for the strain sensor was found to correlate well to drill wear and they proceeded to base their study on this assumption.

Zhou *et al.* [53] proposed to monitor the stresses acting in a cutting edge during a machining process in order to predict tool spontaneous failure. However, because of the impracticalities of in-process measurement of the cutting tool stress, an on-line stress estimation based on in-process cutting forces, load functions and the cutting conditions were used instead. They designed and implemented a real-time TCMS based on VME computer system and real time kernel. This incorporated a fast data acquisition unit that analysed the stresses from force measurements. By monitoring the risk factor defined as a ratio of the instantaneous stresses, they reported that it was possible to predict spontaneous failures.

Lee *et al* [15] proposed another method based on stress analysis of three-dimensional loading. They combined FEA and detailed stress analysis of the cutting edges and tips of sharp and worn tools from which they concluded that it was possible to predict the mode and location of tool failure.

Out of all these methods, most of the researchers used conventional cutting tool dynamometer with any one the other sensors to apply sensor fusion methods to develop ANN models. In general. dynamometers can measure the static and dynamic forces accurately and they can be used as a part of cutting tool condition monitoring systems. But, their frequency range is usually limited by the natural frequency f_0 of piezoelectric components of about 3 kHz. In order to avoid amplitude distortion, the usable frequency of a piezoelectric transducer is restricted to about 0.6 times of f_0 . In view of this, an attempt has been made to measure both static and dynamic components of cutting force using resistance type strain gauges (TML-120Ω -3 mm gauge length). Such gauges can follow the static and dynamic response of a system up to 350 kHz. These strain gauges are economical and get easily pasted on the surface of the tool. Also, they do not affect the stiffness of the tool holder. In this thesis, sensor fusion and above mentioned sensors (Strain gauge and accelerometers)were used to capture the signals. Using these signals, ANN models and empirical models (using ANOVA)have been developed. Some of the researchers were developed TCM systems using sensor-less approach such as motor current monitoring systems and so on. But most of the researchers developed sensor based TCM systems to increase the reliability and consistency of the system. As mentioned above, accelerometers ans strain gauge sensors were used to develop TCM systems.

2.2   Artificial Neural Network

Artificial Neural Networks technology is of a relatively old origin and enormous studies are available which relate to vibrations and dynamics of machinery. Most of the work has been carried out in the last few decades. Mayes [61] applied ANN for on-line vibration monitoring of large turbo-generators. The investigations focused on data processing and the use of the neural networks were discussed. Elkordy et al. [62] investigated the applicability of ANN for vibration signature analysis of a five-store steel structure. The primary investigations showed that ANNs have considerable potential to assess structural damage.

Kram et al. [63] applied the neural net software for the validation and recovery of the distorted vibration of electro machine systems. Vibration signals, which represent the lateral displacement of a shaft, were obtained from proximity probes and the Discrete Fourier coefficients were calculated. These were used as inputs to the network to classify fault and no-fault signal. Fuzzy-input neural net adaptive expert systems were presented for rotor diagnosis and prognosis. A traditional binary classification system was adopted to diagnose the fault in rotating machinery. The two possible states, fault and non-fault were described by 1 or 0. Available knowledge for failure diagnosis in turbo machinery was utilised to initially teach the system. Ahn and Cho [64] proposed a new vibration control scheme using the ANN along with electromagnetic and pneumatic principles as a hybrid type active vibration isolation system. The characteristics were investigated via computer simulation as well as experimentation. The proposed control scheme could suppress the transmissibility of the vibration isolation system to below 0.63 over the entire frequency range, including the resonance frequency, without complex calculation or prior manipulation.

Haung and Lian [65] proposed a different hybrid scheme with a combination of fuzzy logic and neural network algorithms for active vibration control. A fuzzy logic controller was designed for controlling the main influence part of the MIMO (multi-input/multi-output) system.

Recently, Han et al. [69] presented the adaptation of neural network for fast-valve controlling of a power generation plant. The back propagation neural network was used to train the feed-forward neural network controller.The computer simulated back propagation network results were compared with the conventional fast valving methods applied to the same system. The investigations proved that the ANN controller, has satisfactory generalization capability, reliability and accuracy for the critical control operation.

McCormick and Nandi [67] contemplated the application of ANN for real-time classification of rotating shaft conditions. The vibration signals were collected from the machinery in time-domain. Simple signal processing techniques were applied to prepare the training vector set. The use of the ANN was described to classify the load and no-load of the rotating machinery. The network results were compared with the frequency domain analysis.

2.2.1 Applications of ANN

The ANN can be applied in various fields of engineering. In problems like pattern classification, associative memories, optimization, vector quantization, filtering, and control system applications and its principles are directly applied. Many real world problems are formulated as one of these problems, identifying the relation between the parameters from the physical data with the input output data and other parameters describing a neural network. Pattern

classification problems have been successfully solved by the researchers in [104] and [105] using neural networks. The various researchers [106, 107] have used the neural networks for the identification of nonlinear control system dynamics. There are several situations in control applications where the neural networks can be applied. The applications include process control, robotics, industrial manufacturing, aerospace and others [95]. The neural networks have been extensively used in speech recognition, speech synthesis and speaker identification [108, 109]. The main problem in these speech applications is the processing of the speech signal similar to the human auditory processing mechanism, so that the features relevant to a particular task can be extracted. Neural networks have been successfully applied to texture classification and segmentation [110, 111]. In the sigma-pi-sigma neural networks have been used to determine the satellite orbital parameters and other engineering applications. The most important issue for solving practical problems using neural networks is still in coming up with a suitable architecture to solve a problem. We propose neuron models for solving the real-time applications on condition monitoring of cutting tools for turning operation using ANN principles.

2.3 Gaps in the literature

Though a lot of work has been done in TCM, still there is a need is being felt for a reliable and universal monitoring system. Such a system would involve two inherent components: hardware and software. Presently, the hardware component is more developed and many sensors and transducers have been applied in industrial conditions. However, the software component requires improvement, as there are more difficult and complex tasks yet to be solved. Generally, one would like to have a recipe describing how to design a tool wear monitoring system using neural networks.

In the past two decades, various researchers have attempted to analyze the cutting tool failure (flank wear, nose wear and crater wear) by using Artificial Neural Networks (ANN) and mainly focused on either flank wear prediction or crater wear prediction or both. In the literature, a few neural network models are available in the area of cutting tool condition monitoring (TCM) system , which are able to predict all types of tool failure.

From the literature review the following areas are identified as which need further research work to be carried out.

- The methodology to create cutting tool wear of the desired dimensions and shape.

- Most of the TCM systems have applied supervised learning process to identify the condition of cutting tool. One of the main problems in ANN is design of network architecture. In the literature [7], optimum ANN structure (number of neurons, number of layers) is obtained by using 'trial and error' method. Future research should be engaged in optimisation of ANN structure to minimise the computation time.

- Most of the researchers have developed ANN models to predict the condition of the cutting tool having either flank wear, crater wear or nose wear. Hardly any ANN models is available which can take into account all of them at one time and predict the actual condition of the cutting tool.

- Many researchers have used the sensor fused (sensors' output are mixed) system with an additional sensor to increase the confidence limit of machining process. These data are used to develop ANN models to monitor the condition of cutting tool.

In this direction, an attempt has been made in this research work to create artificial wear (well defined shape and size) using EDM process. A systematic

procedure and instrumentation system has been developed to predict the condition of cutting tool. In this thesis an attempt made to create neural network model in such a way that it should predict both flank wear and chipping failure using back propagation algorithms.

2.4 Scope and objectives of the present work

The motivation behind the development of cutting tool condition monitoring system is to develop an on-line condition monitoring system to predict the condition or health of the cutting tool. It requires an instrumentation system comprising of sensors, condition monitoring units (charge amplifiers, filters) and analysis and predictive algorithms. Main aim of this work is to develop instrumentation system which shows the condition of the cutting tool in on-line. To achieve this objective the following methodology have been adopted. The methodology involves acquisition of experimental data, data processing, feature extraction, development of analysis and predictive algorithms. Strain gauge and accelerometers sensors were fitted on the cutting tool and signals were acquired by respective strain gauge module (LabVIEW) and an FFT analyzer. Signals have been processed and information extracted to develop ANN and statistical models. These models have been validated with experimental results. To generate experimental results, the flank wear and chipped off cutting edge have been produced using EDM process. The empirical models have been developed and the ANOVA has been carried out to understand the developed system in depth.

Chapter 3

Cutting tool wear and creation of artificial tool wear

3.1 Tool failure

In general the cutting tool failure may be classified in the following three categories [54]:

- **Fracture failure** - This mode of failure occurs when the cutting force becomes excessive, causing the cutting tool to fail by brittle fracture

- **Temperature failure** - This failure occurs when the cutting temperature is too high for the tool material, causing the material at the tool point to soften, which leads to plastic deformation and loss of the sharp edge.

- **Gradual wear** - Gradual wear of the cutting edge causes loss of tool shape, reduction in cutting efficiency, an accelerated wear as the tool has worn out heavily, and finally tool failure takes place in a manner similar to the temperature failure.

Fracture and temperature failures result in premature loss of the cutting tool. These two modes of failure are undesirable and depend upon machining

conditions namely cutting speed, feed rate and depth of cut. Out of the three possible modes of failure, gradual wear leads to the longest possible use of the tool, with the associated economic advantage of the longer use.

Gradual wear occurs at two locations on a cutting tool: the top rake face (Crater wear) and flank face (Flank wear) as shown in Figure 3.1. Crater wear consists of a concave section (Figure 3.1) on the rake face of the tool, formed by the action of the chip sliding over the surface. High stresses and temperatures characterize the tool-chip contact interface, contributing to the wearing action. Flank wear (Figure 3.1) occurs on the flank, or relief face, of the tool. It results from rubbing between newly generated work surface and the flank face adjacent to the cutting edge. As cutting proceeds, various mechanisms result in increasing levels of wear on a cutting tools. The general relationship of tool wear versus cutting time is shown in Figure 3.2. The first is the **break-in period**, in which the sharp cutting edge (or new tool) wears rapidly at the beginning of its use. The tool crosses the first region occurs within the first few minutes of cutting. The break-in period is followed by gradual wear that occurs at a fairly uniform rate. This is called the **steady state wear** region. Finally, wear reaches a level at which the wear rate accelerates. This marks the beginning of the **failure** region, in which cutting temperature is higher, and the general efficiency of the machining process is reduced. If allowed to continue, the tool finally fails by temperature failure and many times attains unusable condition.

3.2   Tool life

A common way of quantifying the end of a tool life is to put a limit on the maximum acceptable flank wear, as shown in Table 3.1. Mathematically the tool life can be expressed by the following Taylor's tool life equation (3.1):
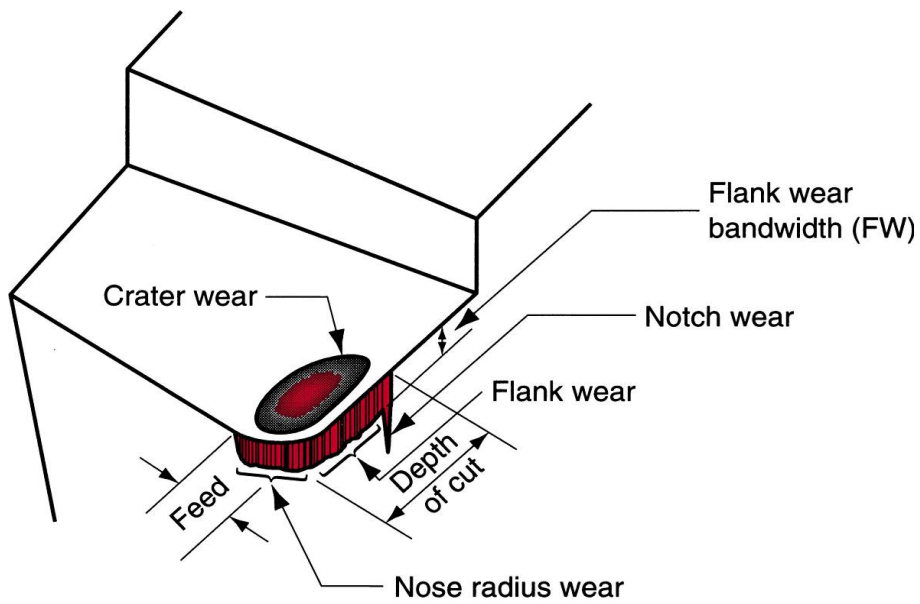
Figure 3.1: Cutting tool wear [54]
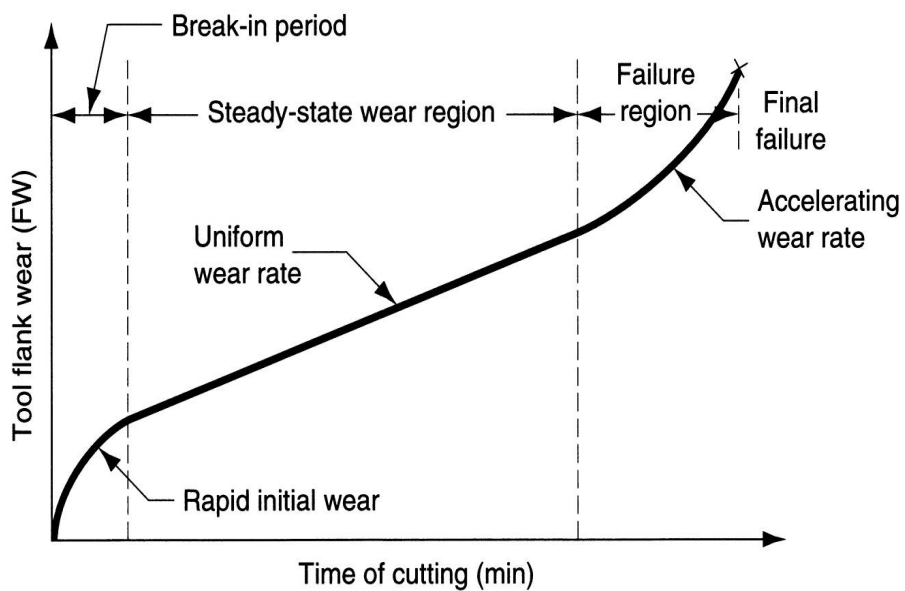
Figure 3.2: Tool wear as a function of cutting time [54]

$$VT^n = C \tag{3.1}$$

where V = cutting speed and T = tool life. The constants n and C depend upon the workpiece material and tool material [55]. This may be calculated from the experimental results.

3.3 Generalized Taylor's Tool Life Equation

Generalized Taylor's tool life equation 3.2 is given as follows

$$VT^n f^m d^p H^q = C \tag{3.2}$$

Where f = feed rate; d = depth of cut; H = work material hardness. The exponents, n, m, p, q and C are normally determined experimentally. The determination of these constants requires more number of experiments and valid for a particular set of machining conditions, workpiece materials and so on. However, there are several problems with these models (equations 3.1and 3.2). First, these do not take into account any imperfections in the process, such as tool vibration or chip adhesion and so on. Secondly, there are practical limitations to this model, as certain tools (such as CBN or carbide) require specific geometries to improve tool life. These models may not be useful to cutting tool condition monitoring systems because of stochastic nature of the machining process. The artificial neural network is a good tool to handle such type of non-linear and stochastic problems. But this neural network methods are costly in terms of training and testing the experimental data.

3.4 Selection of tool and workpiece materials

Selection of cutting tool material for a specific application is crucial to achieve efficient machining. It depends upon workpiece material, machining conditions

Table 3.1: Flank wear levels [7]

Tool Type	Maximum allowable Flank wear
HSS tools, roughing	1.5 mm
HSS tools, finishing	0.75 mm
Carbide tools	0.7 mm
Ceramic tools	0.6 mm

such as cutting speed, feed rate, depth of cut and so on. On the basis of experience and analysis, manufacturers and designers of cutting tools have recommended the selection criteria for cutting tool material with different workpiece materials as shown in Table 3.2. Selection of cutting tool materials mainly depends on workpiece material and its machining conditions.

In the past two decades, various researchers have attempted to analyze the cutting tool failure (flank wear, nose wear and crater wear) by applying the concepts of Artificial Neural Networks (ANN), Statistical methods, Fuzzy logic and so on. Almost all previous research has been focused on either flank wear prediction or crater wear prediction and so on. In the literature [7], Some methods and models are available in the area of cutting tool condition monitoring (TCM) system which is capable to predict all types of tool failure. In this work artificial flank wear and chipping failure are created externally using Electrical Discharge Machining (EDM) process. Using this worn out tool various experiments were conducted and the analysis has been made to create neural networks model in such a way that it is capable to predict both flank wear and chipping failure using back propagation algorithms. The next section deals with EDM process which is used to create flank wear and chipping failure.

Table 3.2: Tool materials and its applications [56]

Tool material	cutting speeds, m/min	applications
Carbon steel	-	Suitable only for soft materials like wood.
High speed steels	10 - 60	used for tougher materials in the form of drills, reamers, taps and small end mills.
Cobalt-chromium tungsten alloys	-	Can be used at speeds higher than those used in case of HSS.
Cemented carbides tools	30 - 250	Standard choice for machining steel with a hardness of 28-32 RC.
Cermets	150 - 350	This is used for machining the titanium based materials.
Ceramics	150 - 650	These are more stable than carbide tools at high temperatures which is suitable to operate at light loads and high speeds.
Cubic-boron nitride(CBN)	30 - 310	Second to diamond in hardness. Standard choice for machining steel with a hardness of 50 RC or higher.
Polycrystalline diamond (PCD)	200 - 2000	Used mainly for very high speed machining of aluminum silicon alloys/ composites

3.5 Creation of artificial flank wear

In the present work, the DNMG inserts are used which already have built-in chip breaking groove. So, during actual cutting, it is not possible to introduce crater wear. As mentioned earlier only two types of tool damage namely flank wear (nose wear also included in this case) and chipping were studied. In actual machining experiments, the wear generated geometry is not uniform hence its dimensions have to be averaged. However in the present case, uniform flank wear was artificially created having the desired dimension. It was done using EDM machine as discussed in the following paragraph. While creating artificial flank wear, the following important cutting tool geometrical parameters were taken into consideration namely, rake angle, clearance angle, length of the flank wear and radial wear length [55].

The relationship between flank wear and radial wear is given (Figure 3.3) as follows:

$$\boldsymbol{r_f} = \frac{h_f \tan \alpha_o}{1 - \tan \alpha_o \tan \gamma_o} \qquad (3.3)$$

where, r_f is the radial wear length, h_f is the flank wear length, α_o is clearance angle and γ_o is rake angle.

According to equation (3.3), the value of flank wear length (h_f) and radial wear length (r_f) are calculated to create flank wear in the range of 0.2 mm to 0.5 mm. EDM experimental set up as shown in Figure 3.4 is used to create artificial flank wear. For creating flank wear, the replica of the flank wear is first produced in the copper rod by turning operation and then this copper rod is used in the EDM process as a tool (cathode) to replicate the flank wear on the cutting tool(anode). The flank wear produced during actual machining is shown in Figure 3.5. The exact shape of the flank wear which is created through EDM process is as shown in Figure 3.6.
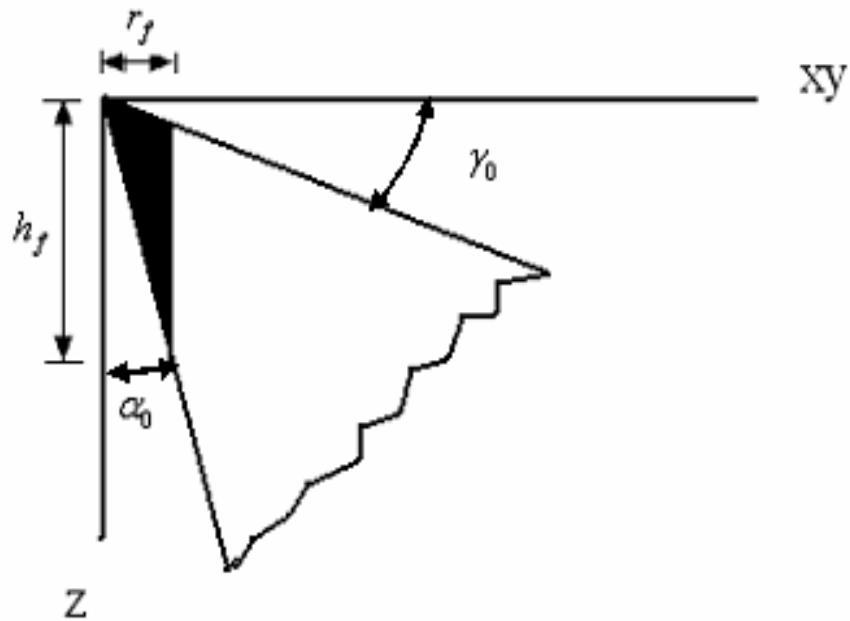
Figure 3.3: Schematic diagram of flank wear [55]
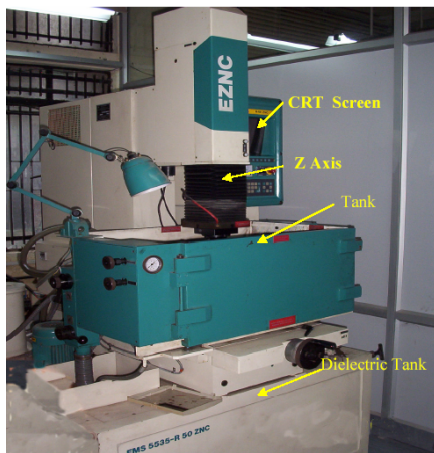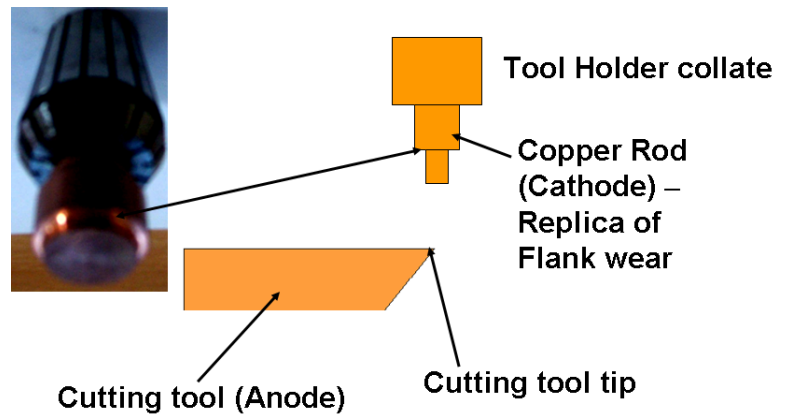
a   b

Figure 3.4: (a) EDM experimental setup (b) Schematic diagram of copper rod and DNMG cutting tool
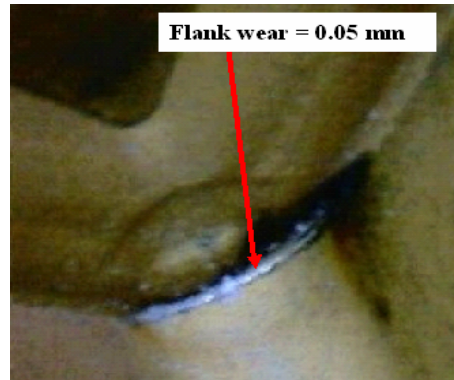
Figure 3.5: Flank wear produced during turning process
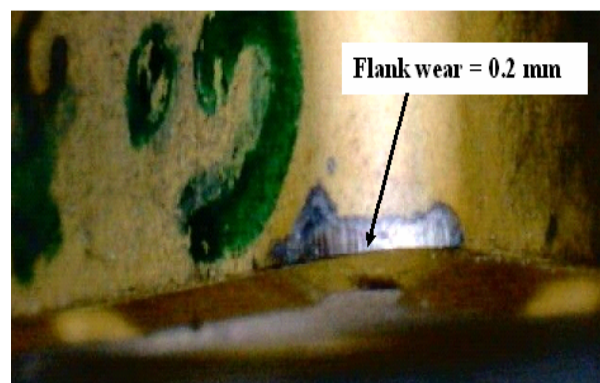
Figure 3.6: Artificial flank wear produced by EDM process

3.6 Creation of artificial chipping failure

To create chipping effect, the same procedure is used as in the above case except that in place of formation of flank wear, the cutting edge up to a certain depth and predetermined width is removed by EDM. A rectangular copper rod has been used in the EDM process as a tool (cathode) to create a chipped off tool (a small part of the cutting edge removed) on the DNMG cutting tool. During EDM, the DNMG cutting tool (used as a work piece in EDM operation) is made as an anode. Feed rate determines length of the cutting edge removed (say, 3 mm, 4 mm and so on) and depth of cut determines the depth of penetration of copper rod in to the cutting tool (like 0.2 mm, 0.3 mm and so on). However, there are some basic differences between the artificially created chipped off tool using EDM process and actually chipped off tool obtained during turning operation. Real life chipped off tool has undefined shape and size (Figure 3.7) and it is usually caused because of brittle fracture due to impact loading. The artificially created chipping is almost uniform and caused due to thermal erosion using EDM process. Hence, the artificially created chipped off tool may be having thermal effects like micro cracks and residual stresses as well [13]. However, this concept of artificially creating chipped off tool can be applied for producing non-uniform shape and size of a chipped off cutting edge also. Hence, while comparing the captured signals, this difference should be kept in mind. In this case, a rectangular copper rod (cathode) used for removing cutting edge in the cutting tool (anode) to a predefined value of r_f and a well defined length of cut (which is equal to experimental design value of depth of cut of machining parameters). The exact shape of chipping defect is as shown Figure 3.8.

The main objective of the present work is to standardize various tool failure measurements as well as to study the machining behavior for well defined failure levels. It is a well known fact that if the two tools work under the same

machining condition for the same period of time, the two flank wears will not be same hence it is a random process in this sense. By simulating wears on the tools using EDM process, the repeatable shape and size of the tool wear can be achieved to conduct many experiments of the similar worn out tools. In this analysis exactly 0.2, 0.3, 0.4 and 0.5 mm flank wear levels have been achieved for signals are captured. In the previous literature, Researchers have measured the flank wear by averaging the peaks of irregular shape. Further, all the three wears can be simultaneously created on the tool to study their effects.

In actual metal cutting experiments, the tool wear geometry generated is not uniform hence its dimensions have to be averaged out. Therefore, it was decided to artificially create the uniform wear (flank and chipping failure) of the desired averaged dimension on the tool using EDM machine as discussed in the following paragraph.

Real life flank wear on a cutting tool has undefined shape and size, while the artificially created flank wear is almost uniform and caused due to thermal erosion by sparking phenomenon in EDM process. Hence, the artificially created worn out tool may also have thermal defects like micro-cracks and thermal residual stresses. In actual machining, cutting tool tip is always subjected to high temperature. If cutting fluids is not used over this tip, there are good chances of development of micro cracks in the cutting edge. Hence, this tool wear can be considered as equivalent to artificially created tool wear. However, this concept of artificially creating flank wear on the tool can be applied for non-uniform shape and size also provided they are mathematically representable. Hence, while interpreting the captured signals, this difference should be kept in mind.

3.7 Tool wear measurement

The measurement of wear can be carried out using one of the three categories of sensors, namely proximity sensors, radioactive sensors and vision sensors. Most
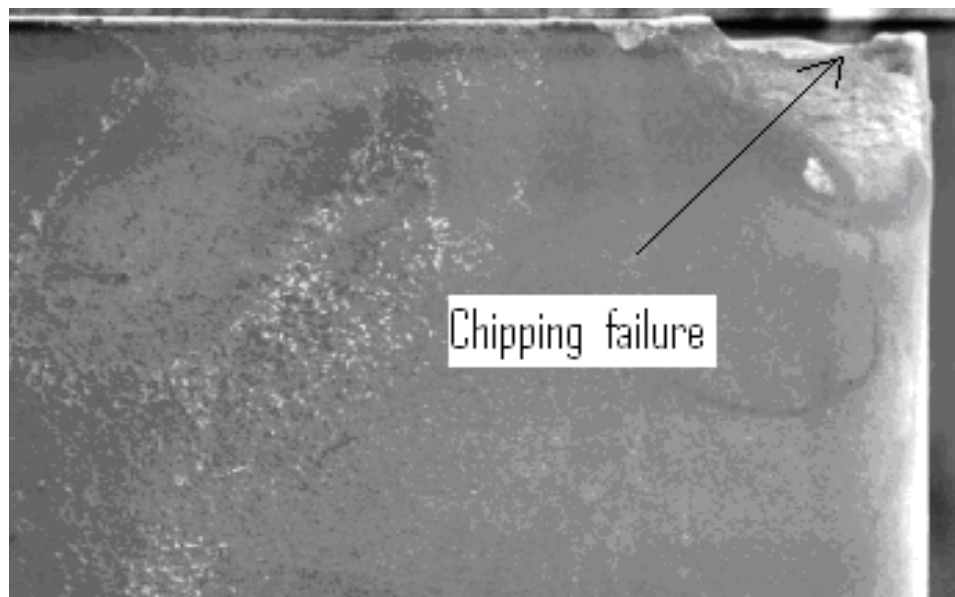
Figure 3.7: Cutting tool - Chipping Failure due to impact load
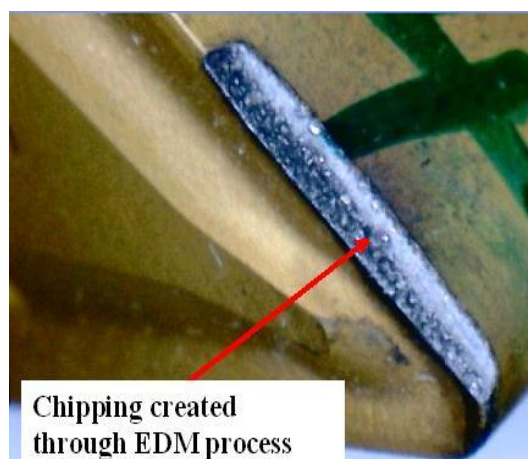
Figure 3.8: Chipping created by EDM process

of the researchers use optical microscope to determine worn out area, namely, flank wear length, crater wear length and so on.

In this study, optical USB port microscope (Scalar) is used to capture the image of worn out area with magnification factor of $50X$. Before measurements, insert is mounted on a stand, made of Perspex having included angle of 55^0 as shown in Figure 3.9. It covers entire portion of nose and flank face. Through out the measurements, position of the stand and focal distance are kept constant so that uniform measurements are achieved without any variation. In this microscope, built-in software (namely USB digital scale) is used to measure the flank wear as well as chipping depth.
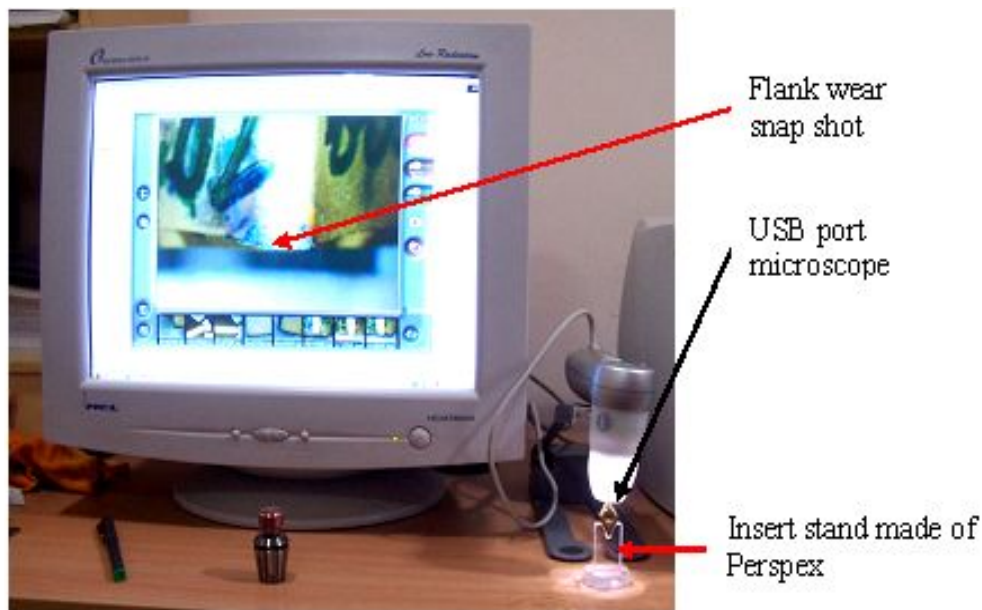
Figure 3.9: Flank wear measurements setup

Chapter 4

Experimental setup and Design of Experiments

4.1   Experimental setup

Now-a-days, high speed machining is popular to increase the production rate as well as to reduce the production cost. Selection of an appropriate machine is also an important task. All the experiments are carried out on a CNC GILDMEISTER CTX 400 Serie 2 turning center. One of the main objectives of the this research work is to monitor the condition / health of the cutting tool. While concentrating on cutting tool, it is assumed that the condition of the machine and its components is good in all other aspects such as foundation of the machine, rigidity of the machine components (such as bed, spindle, tail stock, etc.) and so on. All the components of the machine tool should function properly and should not vibrate by applying external dynamic load. Hence, the above said CNC turning center is chosen. The experimental set up is shown in Figure 4.1. The experiments are conducted on EN-8 steel (workpiece) using DNMG 150608 insert with Seco tool holder PDJNR 2020 K15 without cutting fluid (dry machining). Cutting fluid can not be applied during machining

process because the cutting tool is instrumented with resistance type strain gauge and accelerometer. It is possible to insulate the sensors from cutting fluids. In our experiments, strain gauge is pasted on the surface of the cutting tool by using adhesive. If pressurised cutting fluid is applied on the tool then there may be a chance of breakage of the electrical connections due to the simultaneous effect of high temperature and high pressure. For studying cutting fluid influence the strain gauge has to be hermetically seale. This could not be done in the present study.

4.1.1   Instrumentation system

There are two basic configurations of tool and process condition monitoring systems: compact and modular. Montronix, Brank-amp, Bruel and Kajer, Nordmann and Kistler produce the former. In such a system, the core element is the monitor. The monitors are universal, i.e. they can be fed with signals from different types of sensors. The signals generated by the sensors and conditioned by amplifiers are sent to the monitor, which is directly connected to the machine control (PLC/CNC). Only Kistler, which is basically a producer of excellent force, stress, vibration, AE sensors offer one universal monitor and also output of the sensor can be fed to the computer through DAQ card which is supplied by National Instruments (LabVIEW).

In this research work the cutting tool is instrumented with resistance type strain gauges ($TML - 120\Omega$) and two accelerometers (NP-3331 ONO-SOKKI). The PXI chassis is equipped with DAQ card, two connector blocks (SCXI 1314 and SCXI 1520), a Wheatstone bridge configuration and an amplifier (Figure 4.2). The magnitude of strain and amplitude of vibration depend upon various machining parameters, and it is observed that they increase with depth of cut and feed rate, and decrease with cutting speed. While machining, the cutting
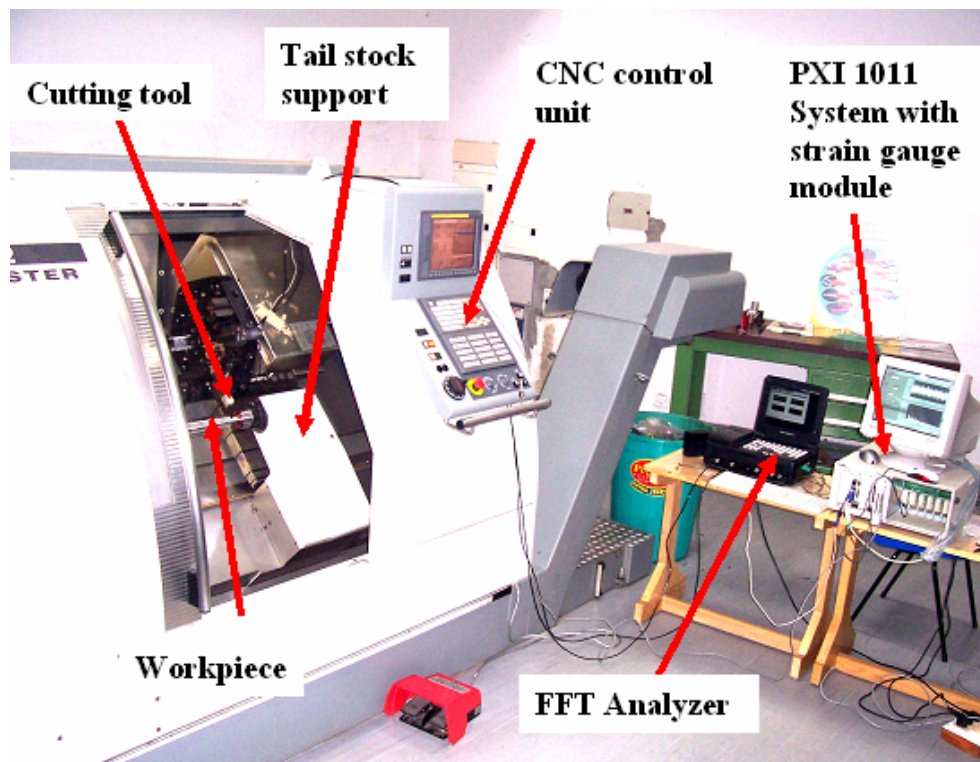
Figure 4.1: Experimental setup

tool is subjected to a state of stress. The resultant strain induces a voltage signal and it is measured with a half bridge configuration using LabVIEW. The experimental details including type of workpiece material and its sensors are shown in Table 4.1.
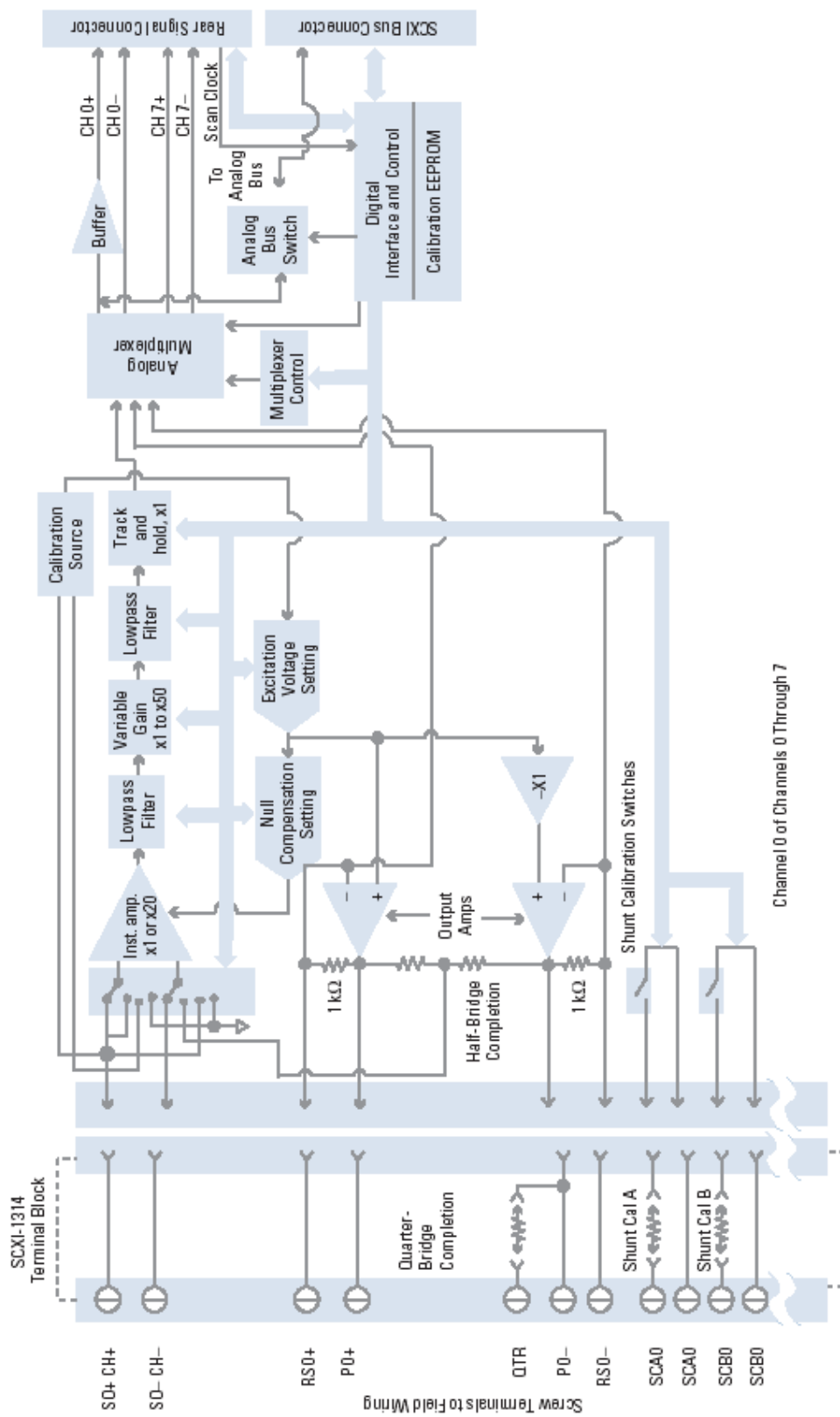
Figure 4.2: SCXI Universal strain gauge input module

Table 4.1: Experimental parameters

CNC turning center	GILDMEISTER CTX 400 Serie2
Work piece	EN 8 Steel
Holder type	PDJNR 2020 K15
Insert type	DNMG 150608 M3
Sensors	Accelerometer: NP-3331- ONO-SOKKI and Strain Gauges ($TML - 120\Omega$)
Data acquisition	PXI 1011System (National Instruments) and FFT analyzer (ONO-SOKKI)

Two accelerometers are placed in the turning center as shown in Figure 4.3. One is placed in the cutting direction on the tool holder and the other one is placed in the feed direction on the backside of the turret for measuring vibration amplitude in terms of accelerations (g-levels).

4.2   Design of Experiments

4.2.1   Flank wear experiments

3^k full factorial design [57] with three levels for each value of factors $'k'$ is used. The three levels of factors are low (-1), intermediate (0), high (1). It forms 3^3 factorial designs for three variables and it contains 27 experiments with degrees of freedom equal to 26. A full factorial design was selected to allow all the three level interactions between the independent variables to be effectively investigated. The independent variables in this study are cutting speed, feed rate and depth of cut. The artificial flank wear and chipping is the fourth and
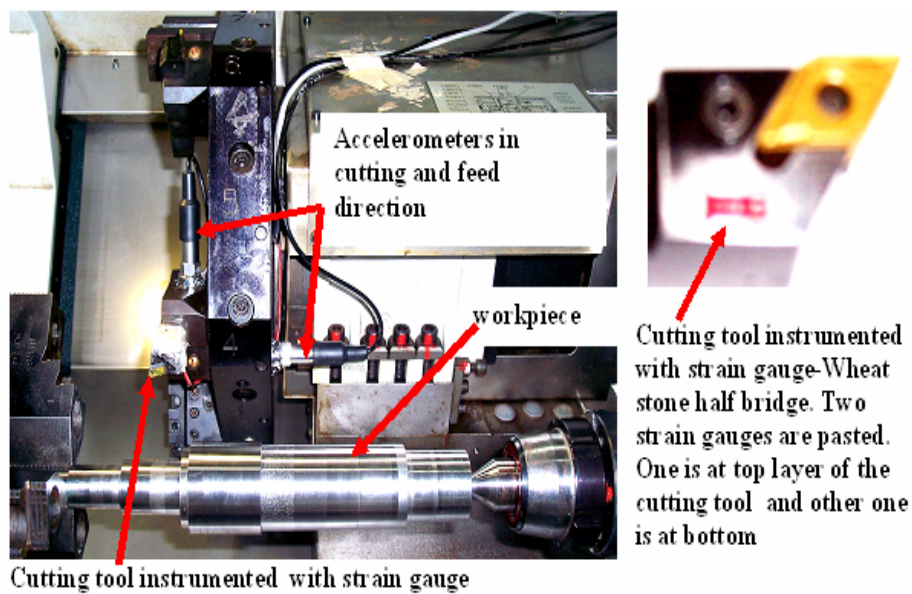
Figure 4.3: Accelerometers and Strain gauge locations

fifth independent variables respectively which is kept at five different levels ranging from 0 to 0.5 mm as shown in Table 4.2 and Table 4.3.

The three responses or dependent variables (namely, strain due to bending action of a cutting tool and two accelerometers responses in cutting direction and feed directions) are measured for various machining conditions. Tungsten carbide cutting tools equipped with throw-away inserts (DNMG 150608) were used in turning operation. Based on the previous study [58], flank wear level is minimum at the tool corner radius of 0.8 mm. So, in this study, the insert nose radius has been chosen as 0.8 mm with an angle of 55^0 diamond shape. The work piece material is EN8 steel and is supported by a tail stock to avoid excessive overhang. A total number of 135 experiments (Table 4.4 to Table 4.6) were performed to include all combinations of the four independent parameters.

Table 4.2: Levels and absolute values of Independent variables - Flank wear experiments

Variables	Units	Levels				
		-2	-1	0	1	2
Cutting speed	m/min	-	200	350	500	-
Feed rate	mm/min	-	100	300	500	-
Depth of cut	mm	-	3	4	5	-
Flank wear	mm	0	0.2	0.3	0.4	0.5

Table 4.3: Levels and absolute values of Independent variables - Chipping failure experiments

Levels	Cutting speed in m/min	Feed rate in mm/min	Depth of cut in mm	Chipped off depth in mm
-2	200	100	3.0	0.0
-1	275	200	3.5	0.2
0	350	300	4.0	0.3
1	425	400	4.5	0.4
2	500	500	5.0	0.5

Table 4.4: Dynamic response of accelerometer (*channel 1*) in cutting direction

Experimental conditions			Acceleration, g for different levels of flank wear(mm)				
Ex No	CS	FR	DOC	0.5	0.4	0.3	0.2	0.0
1	500	500	5	0.2330	0.1580	0.0298	0.0091	0.0107
2	500	500	4	0.0528	0.0079	0.0131	0.0043	0.0026
3	500	500	3	0.0456	0.0196	0.0026	0.0009	0.0020
4	500	300	5	0.0759	0.0298	0.0132	0.0113	0.0070
5	500	300	4	0.0389	0.0079	0.0050	0.0058	0.0012
6	500	300	3	0.0348	0.0035	0.0047	0.0023	0.0014
7	500	100	5	0.0492	0.0033	0.0019	0.0028	0.0061
8	500	100	4	0.0310	0.0029	0.0019	0.0020	0.0031
9	500	100	3	0.0238	0.0013	0.0003	0.0006	0.0005
10	350	500	5	0.2750	0.2330	0.1050	0.0199	0.0111
11	350	500	4	0.2000	0.0200	0.0219	0.0053	0.0036
12	350	500	3	0.0316	0.0111	0.0038	0.0030	0.0034
13	350	300	5	0.2530	0.0456	0.0247	0.0128	0.0083
14	350	300	4	0.1540	0.0187	0.0090	0.0085	0.0061
15	350	300	3	0.0275	0.0052	0.0074	0.0043	0.0016
16	350	100	5	0.1890	0.0348	0.0105	0.0066	0.0064
17	350	100	4	0.0691	0.0115	0.0097	0.0009	0.0039
18	350	100	3	0.0107	0.0008	0.0026	0.0011	0.0009
19	200	500	5	0.2650	0.2650	0.2320	0.0345	0.0153
20	200	500	4	0.2320	0.0585	0.0241	0.0090	0.0095
21	200	500	3	0.1760	0.0065	0.0092	0.0087	0.0052
22	200	300	5	0.2410	0.0621	0.0261	0.0442	0.0132
23	200	300	4	0.1630	0.0389	0.0110	0.0098	0.0091
24	200	300	3	0.1580	0.0076	0.0058	0.0045	0.0019
25	200	100	5	0.1060	0.0613	0.0145	0.0129	0.0112
26	200	100	4	0.0613	0.0186	0.0098	0.0092	0.0053
27	200	100	3	0.0186	0.0042	0.0077	0.0051	0.0037
CS=Cutting speed, m/min			FR=Feed rate, mm/min		DOC=Depth of cut, mm			

Table 4.5: Dynamic response of accelerometer (*channel 2*) in feed direction

	Experimental conditions			Acceleration, g for different levels of flank wear(mm)				
Ex No	**CS**	**FR**	**DOC**	**0.5**	**0.4**	**0.3**	**0.2**	**0.0**
1	500	500	5	0.2670	0.2450	0.0103	0.0089	0.0068
2	500	500	4	0.2370	0.0883	0.0065	0.0058	0.0037
3	500	500	3	0.1570	0.0277	0.0035	0.0025	0.0017
4	500	300	5	0.0939	0.0638	0.0071	0.0061	0.0040
5	500	300	4	0.0448	0.0191	0.0049	0.0051	0.0031
6	500	300	3	0.0239	0.0087	0.0024	0.0017	0.0025
7	500	100	5	0.0457	0.0229	0.0040	0.0033	0.0033
8	500	100	4	0.0408	0.0059	0.0028	0.0028	0.0024
9	500	100	3	0.0191	0.0065	0.0015	0.0007	0.0019
10	350	500	5	0.2480	0.2370	0.0210	0.0136	0.0077
11	350	500	4	0.2450	0.0389	0.0086	0.0061	0.0054
12	350	500	3	0.1640	0.0110	0.0054	0.0033	0.0044
13	350	300	5	0.2490	0.0627	0.0100	0.0070	0.0054
14	350	300	4	0.1900	0.0122	0.0066	0.0058	0.0034
15	350	300	3	0.1430	0.0057	0.0033	0.0021	0.0027
16	350	100	5	0.0929	0.0264	0.0050	0.0053	0.0037
17	350	100	4	0.0264	0.0055	0.0036	0.0029	0.0028
18	350	100	3	0.0249	0.0045	0.0031	0.0007	0.0025
19	200	500	5	0.2710	0.1210	0.0226	0.0194	0.0083
20	200	500	4	0.2640	0.0239	0.0123	0.0094	0.0067
21	200	500	3	0.1690	0.0017	0.0085	0.0037	0.0051
22	200	300	5	0.2330	0.0408	0.0159	0.0125	0.0061
23	200	300	4	0.1470	0.0063	0.0120	0.0084	0.0041
24	200	300	3	0.1310	0.0039	0.0062	0.0045	0.0034
25	200	100	5	0.1920	0.0167	0.0127	0.0064	0.0049
26	200	100	4	0.1330	0.0249	0.0089	0.0033	0.0032
27	200	100	3	0.0601	0.0044	0.0081	0.0010	0.0028
CS=Cutting speed, m/min				FR=Feed rate, mm/min		DOC=Depth of cut, mm		

Table 4.6: Dynamic response of Strain gauge (*channel 3*)

Experimental conditions			Micro strain for different levels of flank wear(mm)				
Ex No	CS	FR	DOC	0.5	0.4	0.3	0.2	0.0
1	500	500	5	7.4488	4.2373	0.0141	0.02108	0.001350
2	500	500	4	0.0274	0.1118	0.0013	0.00566	0.000378
3	500	500	3	0.0100	0.0017	0.0006	0.00229	0.000234
4	500	300	5	0.8566	0.0210	0.0025	0.00736	0.001245
5	500	300	4	0.0224	0.0031	0.0011	0.00174	0.000166
6	500	300	3	0.0017	0.0011	0.0002	0.00053	0.000020
7	500	100	5	0.0500	0.3906	0.0007	0.00004	0.000749
8	500	100	4	0.0141	0.0079	0.0003	0.00056	0.000148
9	500	100	3	0.0015	0.0010	0.0003	0.00009	0.000138
10	350	500	5	13.9720	5.7864	0.3940	0.02123	0.269500
11	350	500	4	0.5940	0.0141	0.0727	0.01852	0.001401
12	350	500	3	0.1176	0.0045	0.0061	0.01562	0.000265
13	350	300	5	1.0856	1.8221	0.1274	0.01791	0.013886
14	350	300	4	0.3371	0.0104	0.0241	0.00196	0.000343
15	350	300	3	0.0727	0.0017	0.0159	0.00108	0.000159
16	350	100	5	0.0637	0.0797	0.0014	0.00014	0.000803
17	350	100	4	0.0485	0.0100	0.0012	0.00064	0.000286
18	350	100	3	0.0270	0.0012	0.0007	0.00096	0.000002
19	200	500	5	14.1680	13.9720	12.8480	0.65594	0.367030
20	200	500	4	4.2373	0.3184	5.6611	0.01325	0.015560
21	200	500	3	0.3217	0.0727	0.0168	0.00064	0.006222
22	200	300	5	2.4882	2.4882	0.4354	0.02416	0.019056
23	200	300	4	0.4334	0.0141	0.0322	0.00437	0.012440
24	200	300	3	0.1361	0.0036	0.0199	0.00038	0.004686
25	200	100	5	0.1450	0.0985	0.0110	0.00303	0.000729
26	200	100	4	0.0943	0.0284	0.0011	0.00080	0.001429
27	200	100	3	0.0286	0.0017	0.0009	0.00049	0.000128
CS=Cutting speed, m/min			FR=Feed rate, mm/min		DOC=Depth of cut, mm			

4.2.2 Chipping failure experiments

Chipping failure normally occurs due to improper selection of machining conditions or due to hard spots in the workpiece material, which lead to chipping failure of the cutting edge. To study about input and output response of machining, a four factors central composite rotatable design [57] with five levels (-2, -1, 0, 1, and 2) has been chosen to minimize the number of experiments. It contains 31 experiments (Table 4.7) with degrees of freedom equal to 30. The independent variables in this study are cutting speed, feed rate, depth of cut and chipped off depth. The independent variables were kept at five different levels as shown in Table 4.3.

Two responses or dependent variables (namely, strain due to bending action of a cutting tool and acceleration, g in cutting direction) are measured for various machining conditions. Tungsten carbide cutting tools [58] (throw - away inserts DNMG 150608) were used in turning operation. The work piece material is EN-8 alloy steel and it is supported by a tail stock to avoid excessive overhang.

Dynamometers can measure the static and dynamic forces accurately, and they can be used [59] as a part of cutting tool condition monitoring system. But, their frequency range is usually limited by the natural frequency f_0 of piezoelectric components of about 3 kHz. In order to avoid amplitude distortion, the usable frequency of a piezoelectric transducer is restricted to about 0.6 times of f_0. In view of this, an attempt has been made to measure both static and dynamic components of cutting force using resistance type strain gauges ($TML - 120\Omega$ - 3 mm gauge length). Such gauges can follow the static and dynamic response of a system up to 350 kHz. These strain gauges are economical and get easily pasted on the surface of the tool. Also, they do not affect the stiffness of the tool holder.

Channel 0 to 7

Channel 2 Strain Gauges are connected with half bridge configuration. It consists of three wires. One is common to both strain gauges and connected with S+ and other two wires were connected with P+ and P- respectively in SCXI 1314 connecting box.
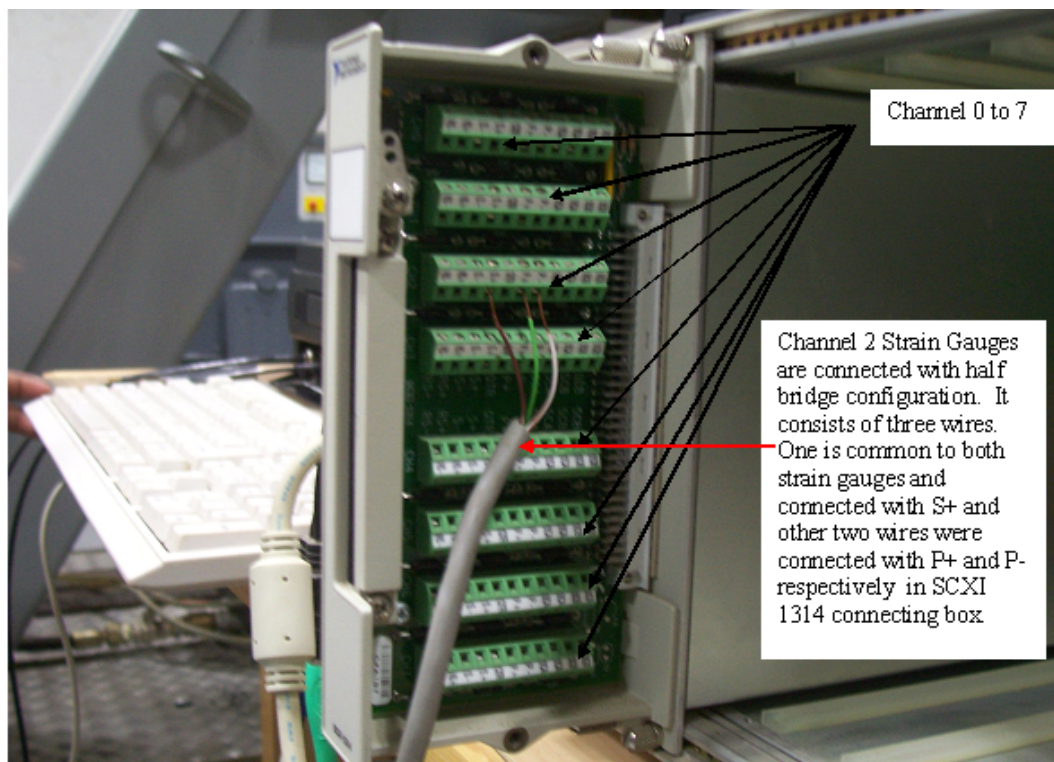
Figure 4.4: Diagram of SCXI-1314 connecting channel

Several references are available [60] on vibrations in the low frequency range, close to the natural frequency of vibration of spindle work piece (up to 300 Hz). Various authors have found that the frequencies relevant for TCM can be as high as 8 kHz, and usually above 1 kHz. This means that the signal essentially, consists of low frequency components that are indicators of static cutting force.

In this chapter 4 experimental designs and their responses are repoted . The analysis part will be carried out in the subsequent Chapter 5 (Parametric analysis).

Table 4.7: Chipping failure experimental parameters and its sensor responses

No	Cutting speed, m/min	Feed rate, mm/min	Depth of cut, mm	Chipped off depth, mm	Acceleration, g	Micro strain
1	200	300	4.0	0.4	0.155	60.520
2	275	200	3.5	0.3	0.042	15.200
3	275	400	3.5	0.3	0.067	37.290
4	275	200	4.5	0.3	0.042	40.390
5	275	400	4.5	0.3	0.066	49.272
6	275	200	3.5	0.5	0.047	14.678
7	275	400	3.5	0.5	0.082	46.000
8	275	200	4.5	0.5	0.088	40.000
9	275	400	4.5	0.5	0.106	49.000
10	350	100	4.0	0.4	0.022	14.468
11	350	500	4.0	0.4	0.065	39.807
12	350	300	3.0	0.4	0.043	11.687
13	350	300	5.0	0.4	0.059	39.468
14	350	300	4.0	0.2	0.028	7.844
15	350	300	4.0	0.6	0.069	40.472
16	350	300	4.0	0.4	0.034	28.793
17	350	300	4.0	0.4	0.038	26.176
18	350	300	4.0	0.4	0.037	25.059
19	350	300	4.0	0.4	0.036	24.401
20	350	300	4.0	0.4	0.036	23.104
21	350	300	4.0	0.4	0.033	22.224
22	350	300	4.0	0.4	0.035	22.690
23	425	200	3.5	0.3	0.012	11.687
24	425	400	3.5	0.3	0.027	25.700
25	425	200	4.5	0.3	0.014	0.250
26	425	400	4.5	0.3	0.046	9.468
27	425	200	3.5	0.5	0.023	24.342
28	425	400	3.5	0.5	0.040	30.338
29	425	200	4.5	0.5	0.040	31.492
30	425	400	4.5	0.5	0.050	40.724
31	500	300	4.0	0.4	0.003	0.005

Chapter 5

Parametric Analysis

5.1 Response surface methodology

Response surface methodology (RSM) is a structured, organized method that is used to determine the relationship between the different input factors (Xs) affecting a process and the output of that process (Y). It involves designing a set of experiments, in which all relevant factors are varied systematically [29]. When the results of these experiments are analyzed, they help to identify optimal conditions, the factors that most influence the results, and those that do not, as well as details such as the existence of interactions and synergies between factors.

Building a design means, carefully choosing a small number of experiments that are to be performed under controlled conditions. There are four interrelated following steps in building a design:

- Define an objective to the investigation, e.g. better understand or sort out important variables or find optimum.

- Define the variables that will be controlled during the experiment (design variables), and their levels or ranges of variation.

- Define the variables that will be measured to describe the outcome of the experimental runs (response variables), and examine their precision.

- Among the available standard designs, choose the one that is compatible with the objective, number of design variables and precision of measurements, and has a reasonable cost.

In this thesis, cutting phenomenon has been analyzed by using power spectrum of vibration and strain gauge signals. Typical power spectral plots are shown in Figures 5.1 and 5.2. It is seen that 3.91 kHz is the predominant frequency in the response signals. At this particular frequency the cutting tool is subject to higher amplitude of vibration because of its own natural frequency. In the higher frequency range, natural frequencies of the tool holder are observed. The forces in this range (higher frequency) are called as dynamic cutting forces. In the present work, the fundamental natural frequency of the cutting tool was found to be 3.91 kHz, by conducting a rap test as shown in Figure 5.3. Experiments have been carried out for various machining conditions. Strain gauge and vibration signals are measured from 0 to 10 kHz with a sampling rate of 25.6 kHz. Sample size is 4096 data points. Programming is done in LabVIEW to acquire the strain gauge signals and store them continuously frame by frame to monitor the condition of the cutting tool at every stage in on-line.

Input parameters (amplitude of acceleration, g and strain) to the **ANOVA** are obtained from the three sensors output using a

5.2   Flank wear model and validation

5.2.1   Model Development

Input parameters (amplitude of acceleration, g and strain) to the **ANOVA** are obtained from the three sensors output using MatLab code as shown in the
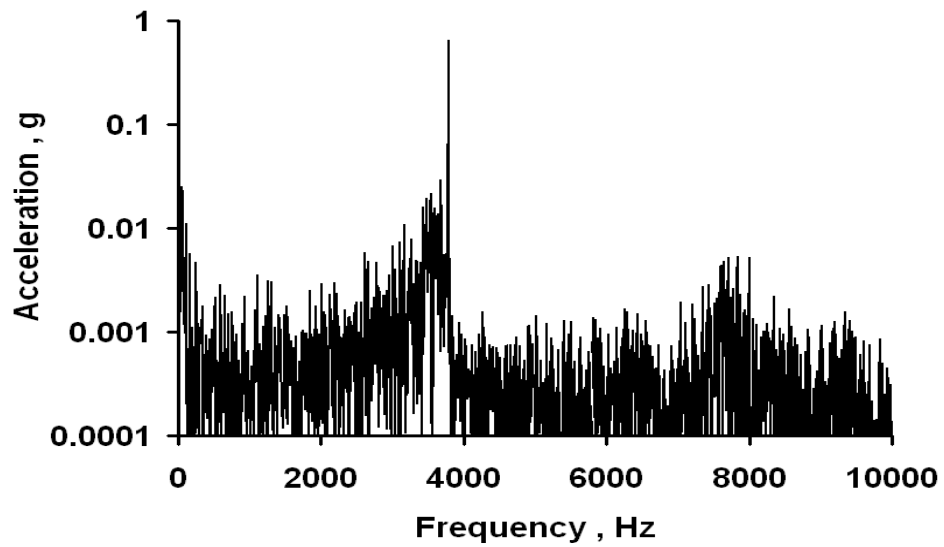
Figure 5.1: Response of the accelerometer in cutting direction. Cutting speed = 200 m/min, feed = 500 mm/min and depth of cut = 3mm for flank wear of 0.3 mm.
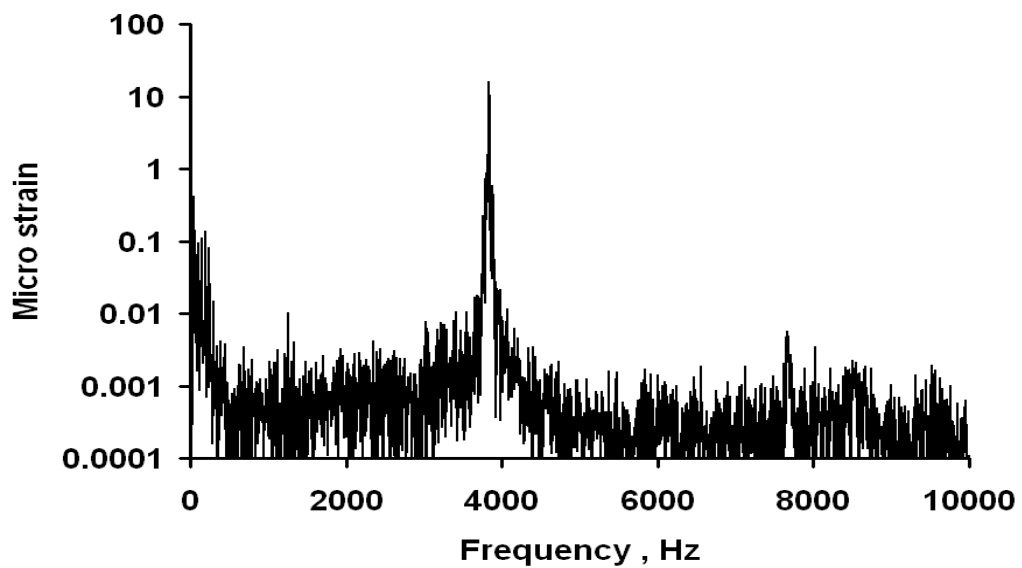
Figure 5.2: Response of the strain gauge.Cutting speed = 200 m/min, feed = 500 mm/min and depth of cut = 3 mm for flank wear of 0.3 mm.
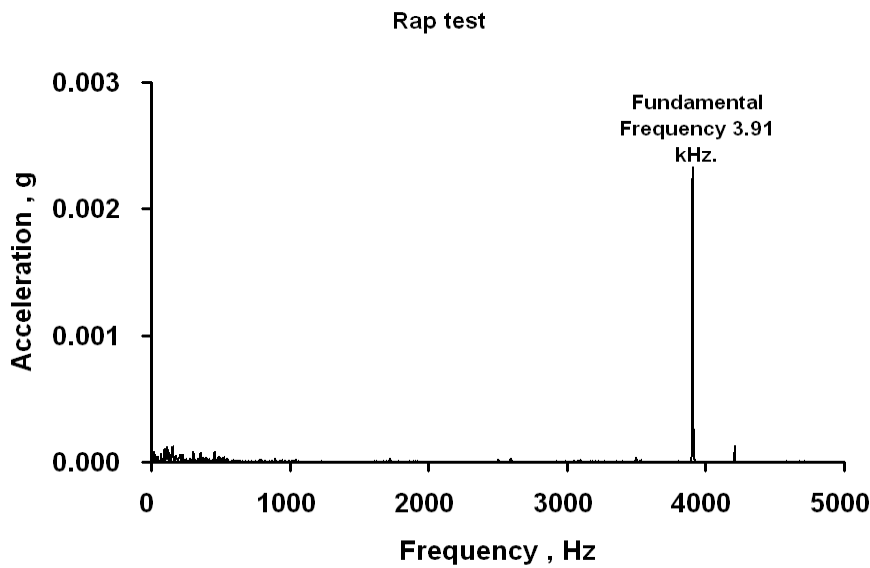
Figure 5.3: Fundamental Frequency - Rap test

Tables 4.4, 4.5 and 4.6. Using Data fit statistical software various models have been developed (say, polynomial (R^2 = 0.5171), power (R^2 = 0.6712)and exponential models (R^2 = 0.8973)). Out of all these models, the exponential model yields highest R^2 value and these models are shown in equations 5.1, 5.2 and 5.3. From the ANOVA (Table 5.1) all the values of $P \leq 0.01$ which indicates that all the machining parameters are effective and also significant indicates at 99% confidence level. The detailed ANOVA has been made with respect to machining input parameters and their significance of cutting parameters are shown in Table 5.1 for channel 1 (Response of accelerometer in cutting direction). From the results of ANOVA (Tables 5.2 and 5.3), it is observed that F Ratios were large enough and indicate that the developed models are appropriate [57].

Out of five levels of flank wear, three levels (0.2, 0.3 and 0.4 mm) were selected for the analysis of variance (ANOVA) to develop the regression models (equations 5.1, 5.2 and 5.3) to show the relationship between output response and machining input parameters. A model has four independent parameters (as

shown in Table 5.4) for three dependent responses . The selected models for channel 1, channel 2 and channel 3 are given by the equations 5.1, 5.2 and 5.3, respectively. These models gave higher value of F-ratio as compared to the tabulated F-ratio value which demonstrates that the selected models are appropriate. According to ANOVA response (F ratio, P and R^2 values) the best regression model has been chosen.

$$\beta_1 = \exp(a_1 x_1 + b_1 x_2 + c_1 x_3 + d_1 x_4 + e_1) \tag{5.1}$$

$$\beta_2 = \exp(a_2 x_1 + b_2 x_2 + c_2 x_3 + d_2 x_4 + e_2) \tag{5.2}$$

$$\delta = \exp(a_3 x_1 + b_3 x_2 + c_3 x_3 + d_3 x_4 + e_3) \tag{5.3}$$

where, x_1 = cutting speed, x_2 = feed rate, x_3 = depth of cut, x_4 = flank wear, β_1 = Acceleration, g in cutting direction, β_2 = Acceleration, g in feed direction, δ= Micro strain. Following values of the various coefficients of equations (5.1-5.3) have been obtained.

$a_1 = 2.565 \times 10^{-3}, a_2 = 1.939 \times 10^{-3}, a_3 = 7.054 \times 10^{-3}, b_1 = 6.379 \times 10^{-3}$,
$b_2 = 6.137 \times 10^{-3}, b_3 = 9.878 \times 10^{-3}, c_1 = 1.706, c_2 = 1.296, c_3 = 2.006,$
$d_1 = 7.066, d_2 = 22.169, d_3 = 6.538, e_1 = 15.233, e_2 = 20.734, e_3 = 13.444$

5.2.2 Model Validation

To compare experimental and theoretical results, the error between the regression model values and experimental values are calculated as (equation 5.4):

$$\delta = \frac{A_m - A_i}{A_m} \times 100 \tag{5.4}$$

where δ = error rate between experimental data and regression model data,A_i = the experimentally measured acceleration, g or micro strain, A_m= the predicted

Table 5.1: ANOVA for the effect of machining parameters on dynamic response of accelerometer in cutting direction (channel 1)

Source	DF	SS	MS	F	P
Regression	4	0.174	4.348E-02	166.045	0
Residual Error	76	1.990E-02	2.618E-04		
total	80	0.194			
Predictor	**Coef**	**SE Coef**	**T**	**P**	
Constant	-15.233	0.988	-15.427	0.004	
Cutting speed	-2.560E-03	3.219E-04	-7.970	0.008	
Feed rate	6.370E-03	5.802E-04	10.996	0.002	
Depth of cut	1.707	0.184	9.294	0.004	
Flank wear	7.063	0.635	11.121	0.006	
Source	**DF**				
Cutting speed	1				
Feed rate	1			$R^2 = 0.897$	
Depth of cut	1				
Flank wear	1				

Table 5.2: ANOVA for the effect of machining parameters on dynamic response of accelerometer in feed direction (channel 2)

Source	DF	SS	MS	F	P
Regression	4	0.123	3.086E-02	352.031	0
Residual Error	76	6.662E-03	8.7662E-05		
total	80	0.130			
Predictor	**Coef**	**SE Coef**	**T**	**P**	
Constant	-20.734	0.984	-21.074	0.001	
Cutting speed	1.939E-03	2.131E-04	9.099	0.006	
Feed rate	6.137E-03	3.862E-04	15.891	0.003	
Depth of cut	1.297	8.325E-02	15.577	0.001	
Flank wear	22.163	2.183	10.155	0.005	
Source	**DF**				
Cutting speed	1				
Feed rate	1			$R^2 = 0.949$	
Depth of cut	1				
Flank wear	1				

Table 5.3: ANOVA for the effect of machining parameters on dynamic response of strain gauge bridge (channel 3)

Source	DF	SS	MS	F	P
Regression	4	343.347	85.837	81.396	0
Residual Error	76	80.147	1.055		
total	80	423.494			
Predictor	**Coef**	**SE Coef**	**T**	**P**	
Constant	-13.444	2.185	-6.152	0.004	
Cutting speed	-7.054E-03	9.450E-04	-7.457	0.001	
Feed rate	9.878E-03	1.880E-03	5.254	0.001	
Depth of cut	2.006	0.388	5.168	0.007	
Flank wear	6.538	0.934	6.998	0.008	
Source	**DF**				
Cutting speed	1				
Feed rate	1			$R^2 = 0.811$	
Depth of cut	1				
Flank wear	1				

Table 5.4: Levels of Independent variables

Variables	Units	Levels				
Cutting speed	m/min	200	350	500		
Feed rate	mm/min	100	300	500		
Depth of cut	mm	3	4	5		
Flank wear	mm	0	0.2	0.3	0.4	0.5
Chipping depth	mm	0.2	0.3	0.4	0.5	0.6
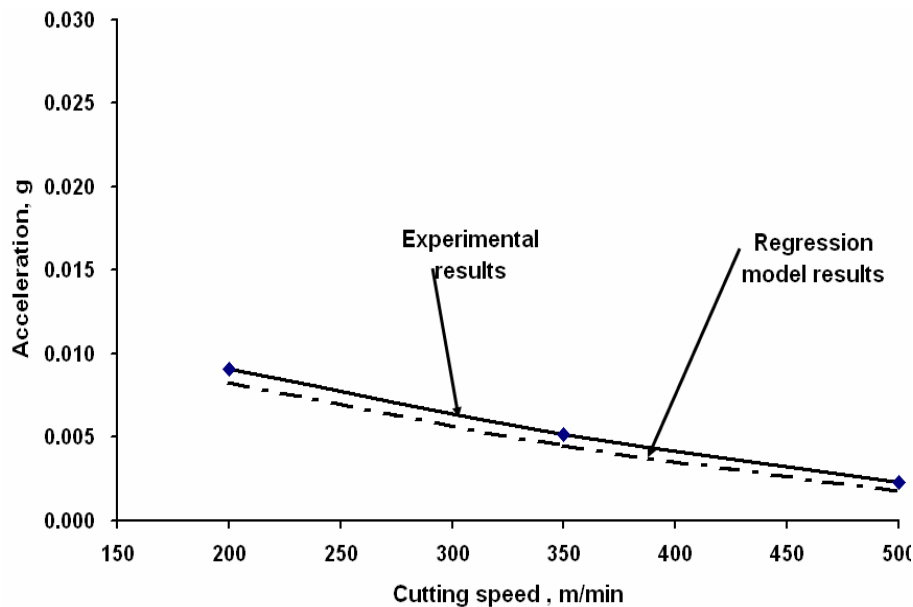
Figure 5.4: Response of accelerometer in feed direction. Variation of Vibration levels, g Vs Cutting speed for feed rate = 300 mm/min, depth of cut = 4 mm and flank wear = 0.3 mm

acceleration, g or micro strain from regression equations (5.1, 5.2 and 5.3).

Figures 5.4, and 5.5 show that the developed regression models can accurately predict (interms of g and micro strain) tool condition to some extent. The error rate of channel 1 (β_1) of this model is calculated by using equation (5.4). The calculated values are 4.82% for the cutting speed 200 m/min, 11.41% for the cutting speed 350 m/min and 22.6% for the cutting speed 500 m/min. The deviation (or percentage of error) marginally increases with increase in cutting speed as shown in Figure 5.6. This increasing error may be due to measurements errors in the sensors at high cutting speed.

The error rate or deviation rate increases with increase in feed rate as shown in Figures 5.7, 5.8 and 5.9 which is due to variation in dynamic cutting conditions and increase in cutting force. If cutting force increases, the distortion of amplitude also increases in both accelerometer and strain gauge bridge.

Similarly, error values increase with increase in depth of cut (shown in Figures

Figure 5.5: Response of strain gauge. Variation of Micro strain Vs Cutting speed for feed rate = 300 mm/min, depth of cut = 4 mm and flank wear = 0.3 mm

Figure 5.6: Response of accelerometer in cutting direction. Variation of Vibration levels, g Vs Cutting speed for feed rate = 300 mm/min, depth of cut = 4 mm and flank wear = 0.3 mm
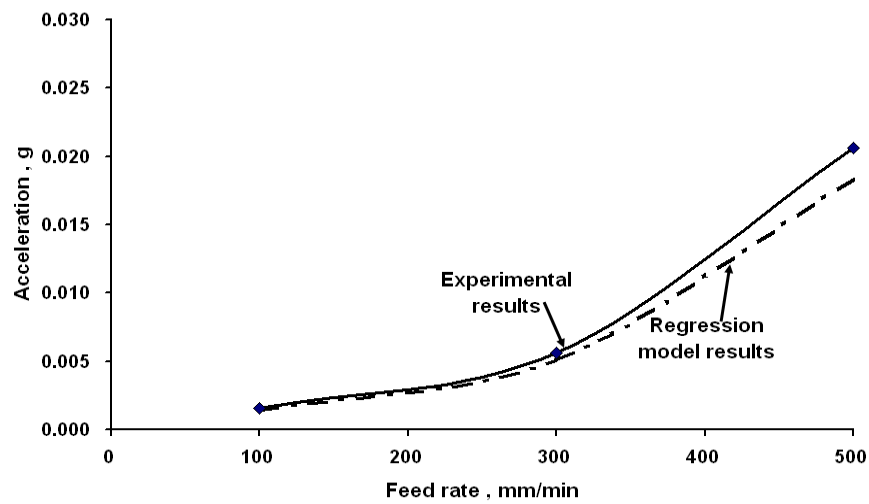
Figure 5.7: Response of accelerometer in cutting direction. Variation of Vibration levels, g Vs Feed rate in cutting direction for cutting speed = 350 mm/min , depth of cut = 4 mm and flank wear = 0.3 mm
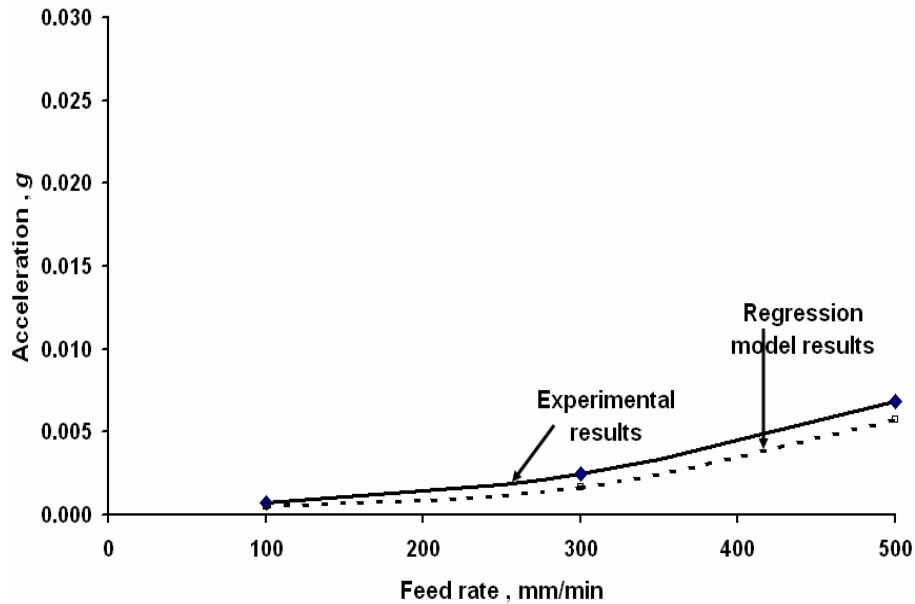
Figure 5.8: Response of accelerometer in feed direction. Variation of Vibration levels, g Vs Feed rate for cutting speed = 350 mm/min , depth of cut = 4 mm and flank wear = 0.3 mm
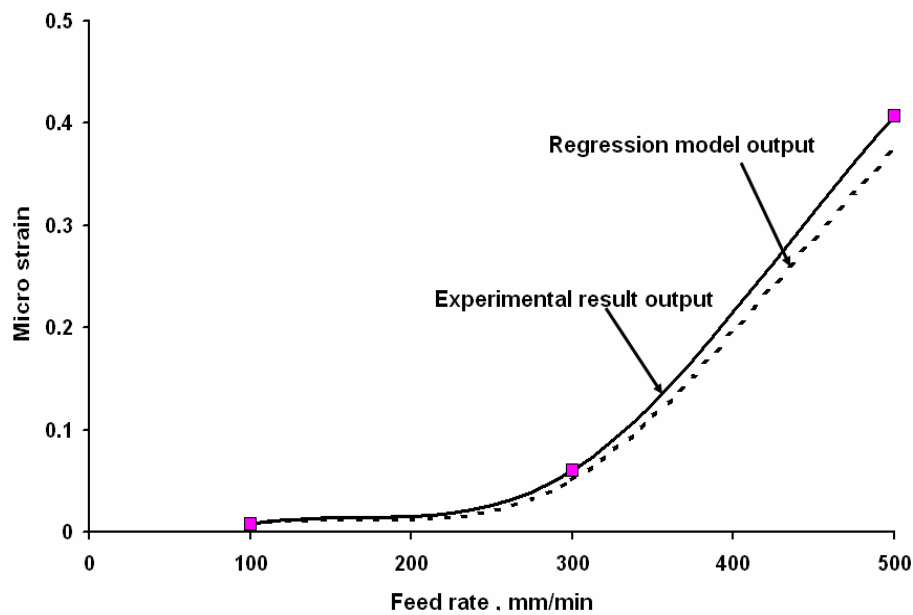
Figure 5.9: Response of strain gauge. Variation of Micro strain Vs Feed rate for cutting speed = 350 mm/min , depth of cut = 4 mm and flank wear = 0.3 mm

5.10, 5.11 and 5.12) as well as increase in flank wear (Figures 5.13, 5.14 and 5.15). This is due to increase in cutting force as discussed above.

5.2.3 Parametric Analysis

Based on the developed model (equations 5.1, 5.2 and 5.1) the effects of operating parameters (namely, cutting speed, feed rate, depth of cut and flank wear) on the magnitudes of vibration and micro strain have been calculated. To perform the parametric study using these regression models, the relationships have been drawn between the machining conditions and responses as shown in Figures 5.16 - 5.24.

Effect of depth of cut on cutting tool vibration and Strain

The relation between acceleration, g and depth of cut for various flank wear levels are as shown in Figures 5.16 and 5.17. The tool vibration increases with increase in depth of cut as well as increase in flank wear. This is due to an increase in cutting force which reduces
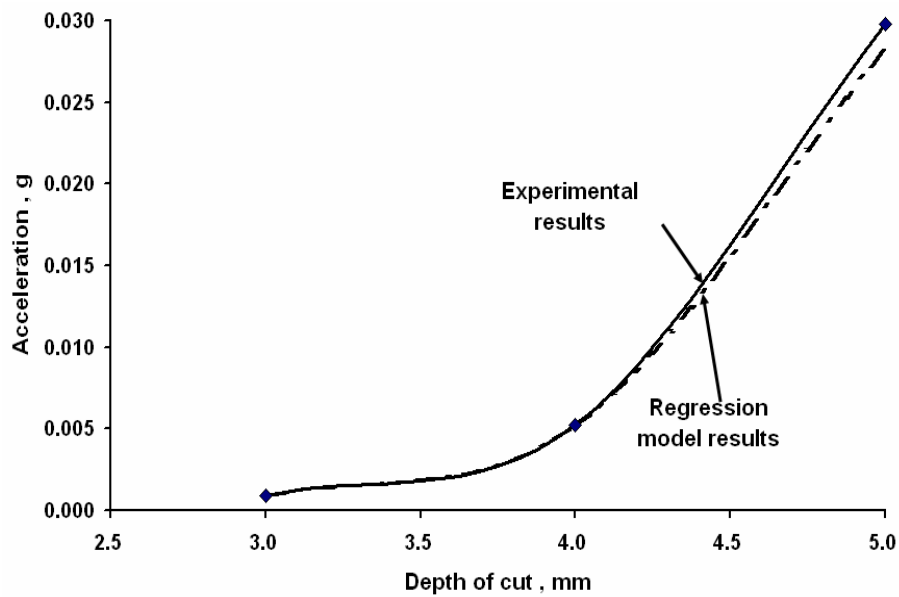
Figure 5.10: Response of accelerometer in cutting direction. Variation of Vibration levels, g Vs Depth of cut for cutting speed = 350 m/min, feed rate = 300 mm/min and flank wear = 0.3 mm
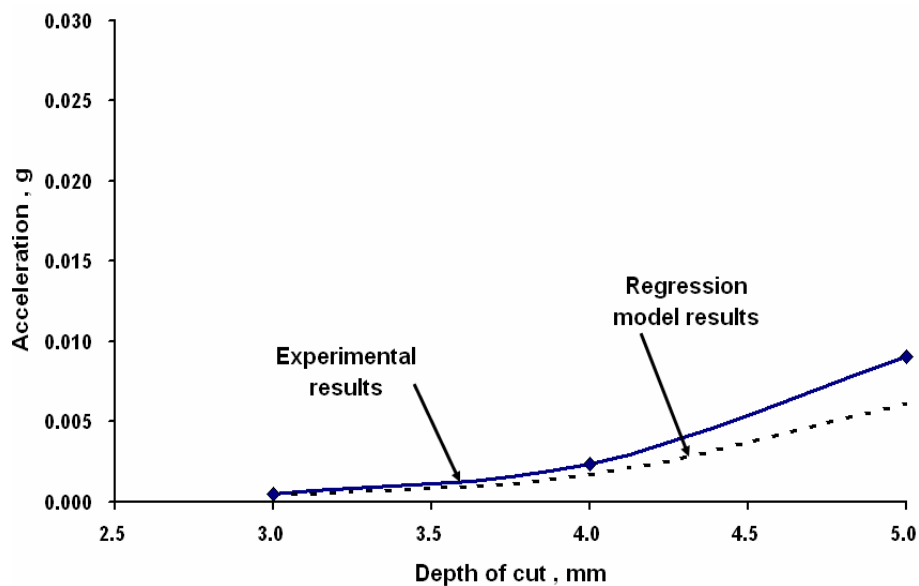
Figure 5.11: Response of accelerometer in feed direction. Variation of Vibration levels, g Vs Depth of cut for cutting speed = 350 m/min, feed rate = 300 mm/min and flank wear = 0.3 mm
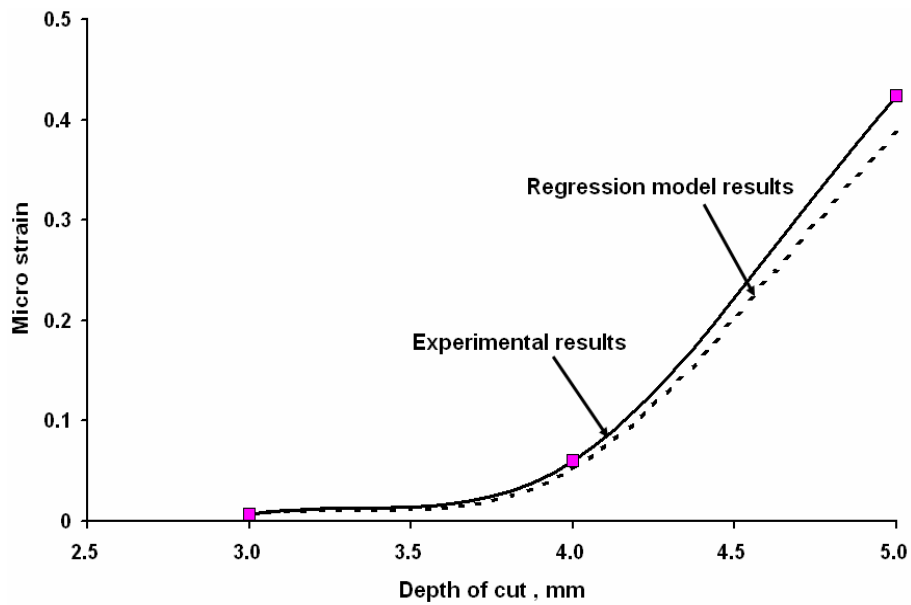
Figure 5.12: Response of strain gauge. Variation of Micro strain Vs Depth of cut for cutting speed = 350 m/min, feed rate = 300 mm/min and flank wear = 0.3 mm
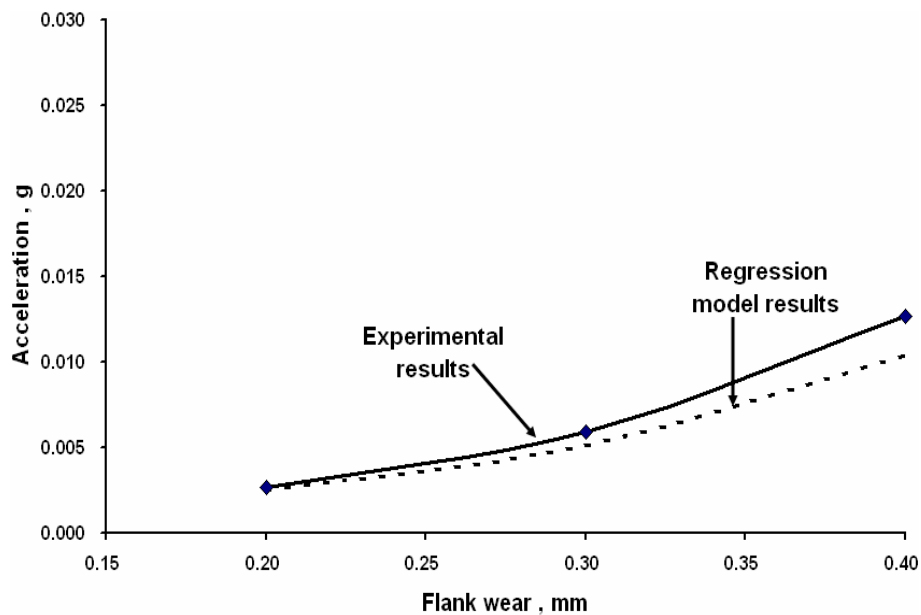
Figure 5.13: Response of accelerometer in cutting direction. Acceleration, g Vs Flank wear for cutting speed = 350 m/min , depth of cut = 4 mm and flank wear = 0.3 mm
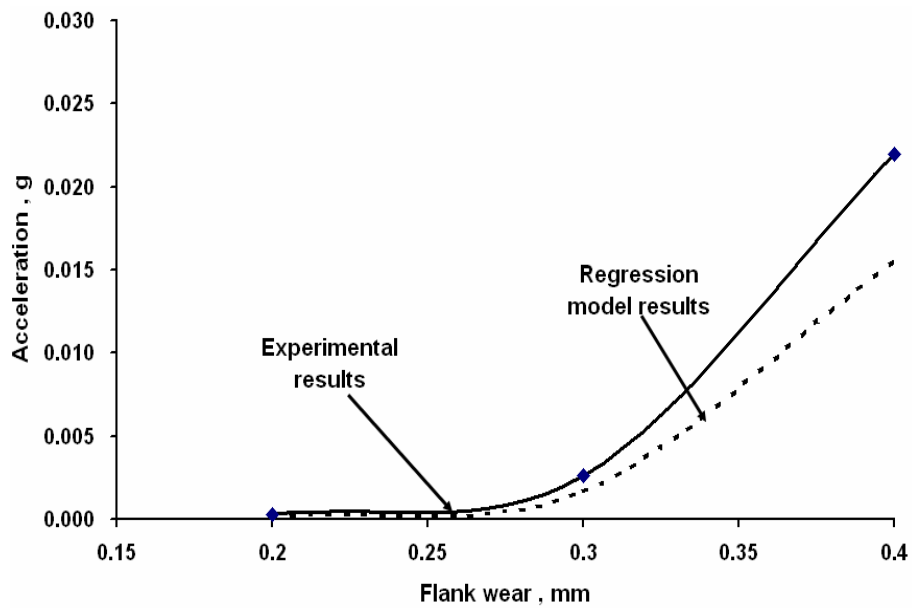
Figure 5.14: Response of accelerometer in feed direction. Acceleration, g Vs Flank wear for cutting speed = 350 m/min , depth of cut = 4 mm and flank wear = 0.3 mm
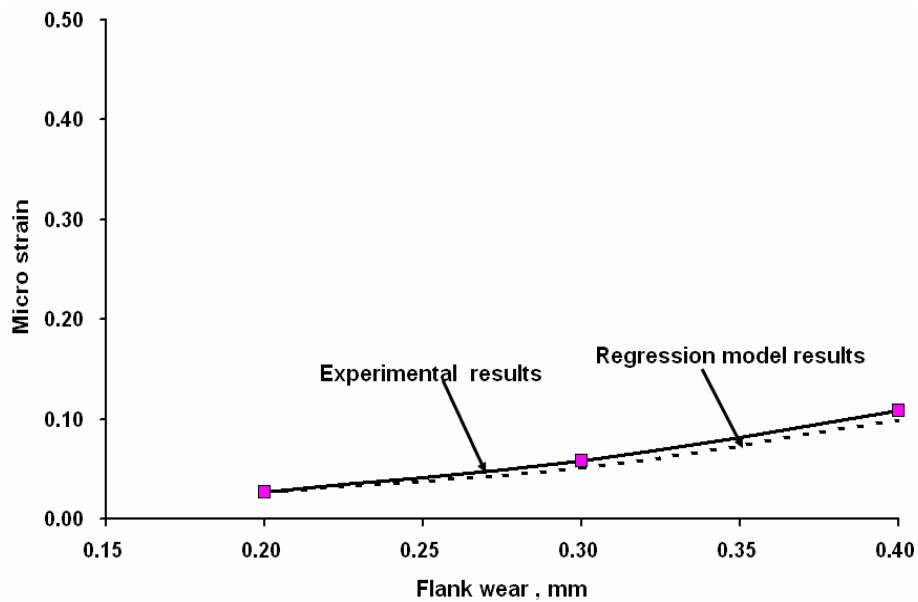
Figure 5.15: Response of strain gauge. Variation of Micro strain Vs Feed rate for cutting speed = 350 mm/min , depth of cut = 4 mm and flank wear = 0.3 mm
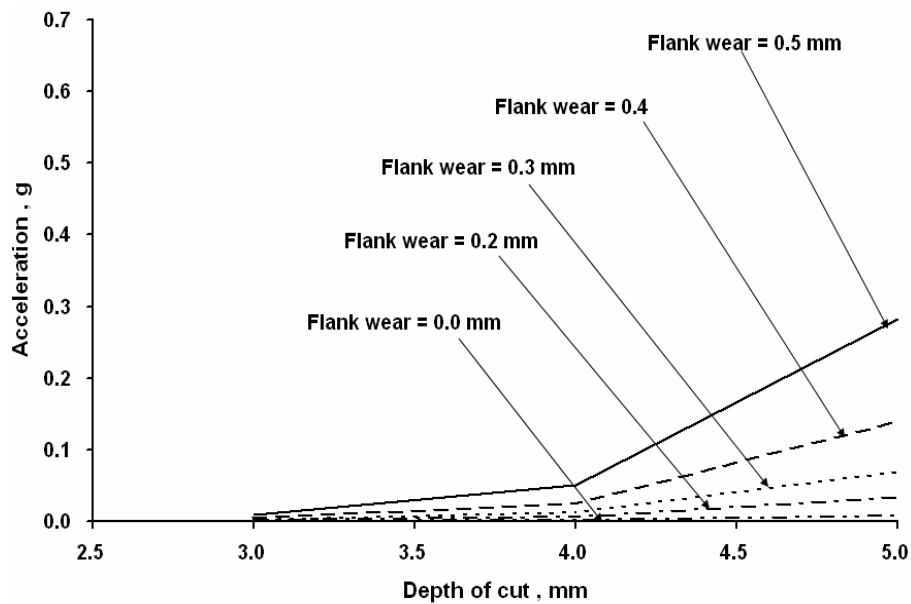
Figure 5.16: Response of accelerometer in cutting direction. Acceleration, g Vs Depth of cut for cutting speed = 500 m/min, feed rate = 500 mm/min

stiffness of the cutting tool. It is observed that, in all cases the amplitude of vibration in terms of acceleration, g is small up to 0.3 mm flank wear level due to small variation in cutting force. In case of strain as a response, the variation in strain level is also low up to 0.3 mm flank wear level due to small variation (Figure 5.18) in cutting force, but there is a sudden rise in strain beyond 0.3 mm flank wear due to increase in cutting force.

Effect of Feed rate, Cutting speed on cutting tool vibration and Strain

The relationships between machining parameter feed rate and acceleration, g for various flank wear levels are shown in Figures 5.19 (channel 1) and 5.20 (channel 2). The amplitude of vibration g, increases with increase in feed rate which results in increased dynamic cutting force. The increase in dynamic cutting force is associated with reduction in the stiffness of the cutting tool. The variation in strain level is low (Figure 5.21) up to 0.2 mm flank wear level due to small variation in cutting force. Similarly the effects of cutting speed for various flank wear levels are shown in Figures 5.22 and 5.23. Increase in cutting speed marginally reduces the cutting force and hence it will reduce
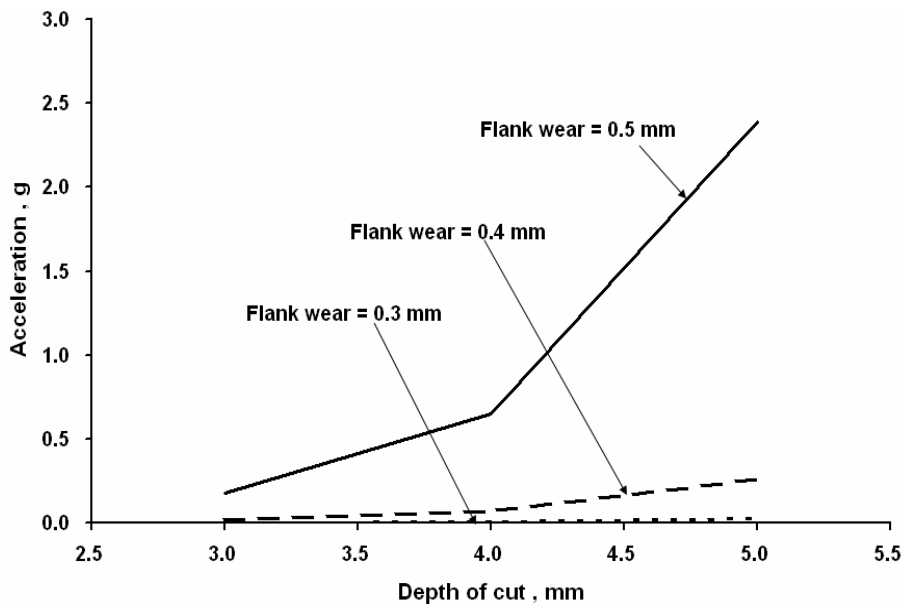
Figure 5.17: Response of accelerometer in feed direction. Acceleration, g Vs Depth of cut for cutting speed = 500 m/min, feed = 500 mm/min
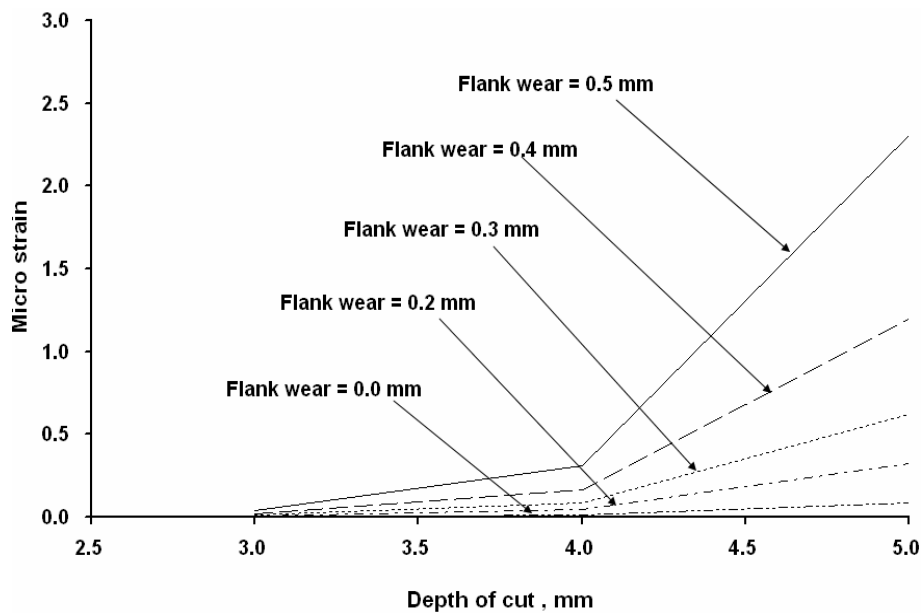
Figure 5.18: Response of strain gauge. Micro strain Vs Depth of cut for Cutting speed = 500 m/min, feed = 500 mm/min
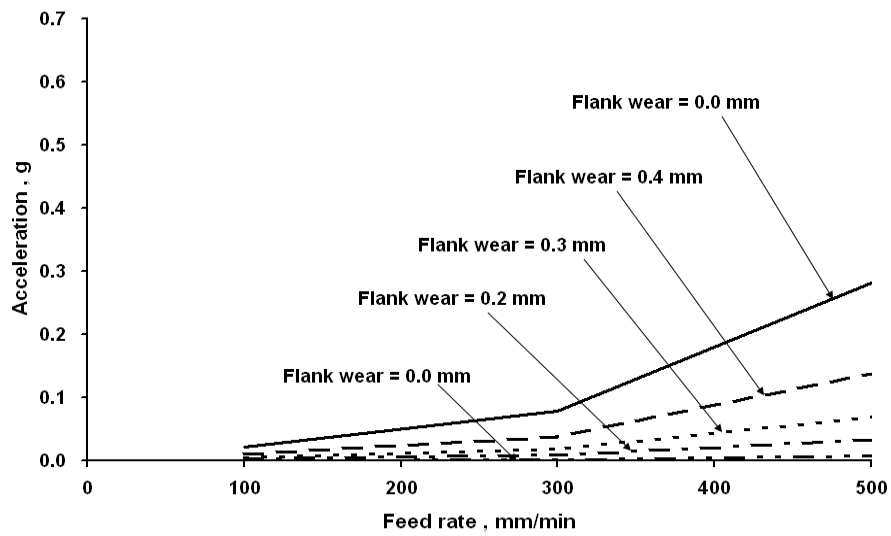
Figure 5.19: Response of accelerometer in cutting direction. Acceleration, g Vs Feed rate for cutting speed = 500 m/min, depth of cut = 5 mm

the vibration and strain levels. The variation in strain level is low up to 0.2 mm flank wear level due to very small variation (Figure 5.24) in cutting force.
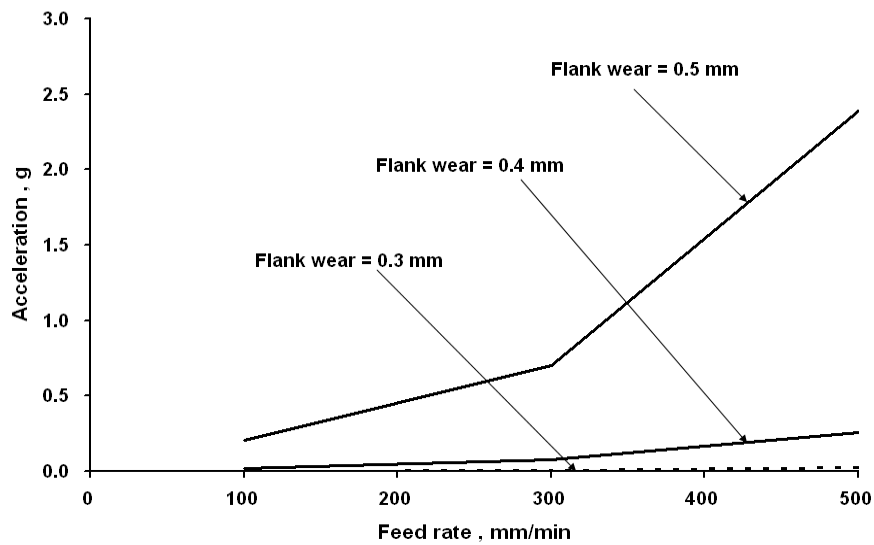
Figure 5.20: Response of accelerometer in feed direction. Acceleration, g Vs Feed rate for cutting speed = 500 m/min, depth of cut = 5 mm
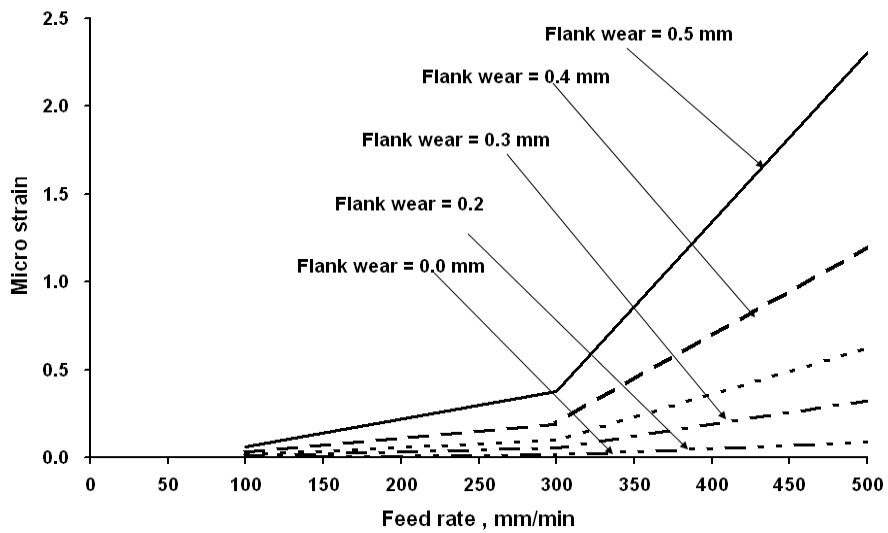
Figure 5.21: Response of strain gauge. Micro strain Vs Feed rate for cutting speed = 500 m/min, depth of cut = 5 mm
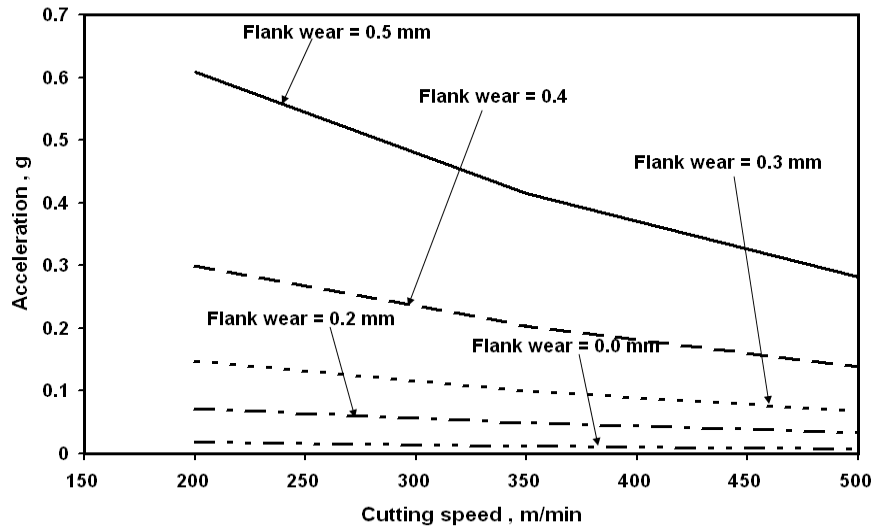
Figure 5.22: Response of accelerometer in cutting direction. Acceleration, g Vs Cutting speed for feed rate = 500 mm/min, depth of cut = 5 mm

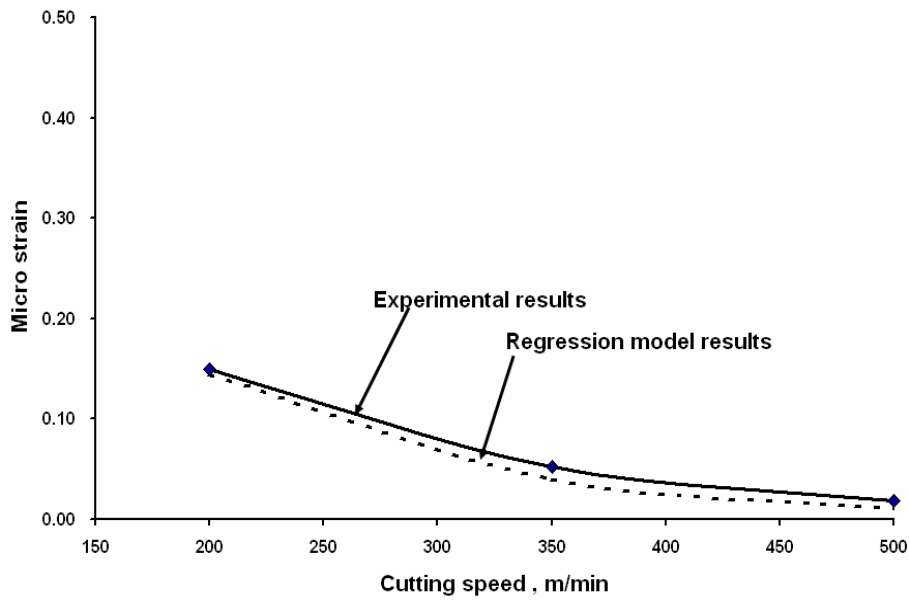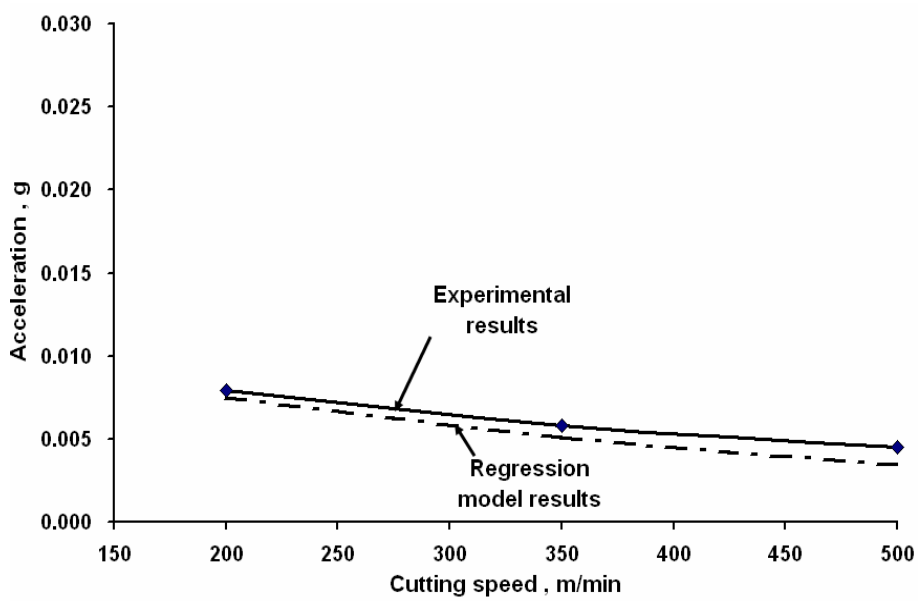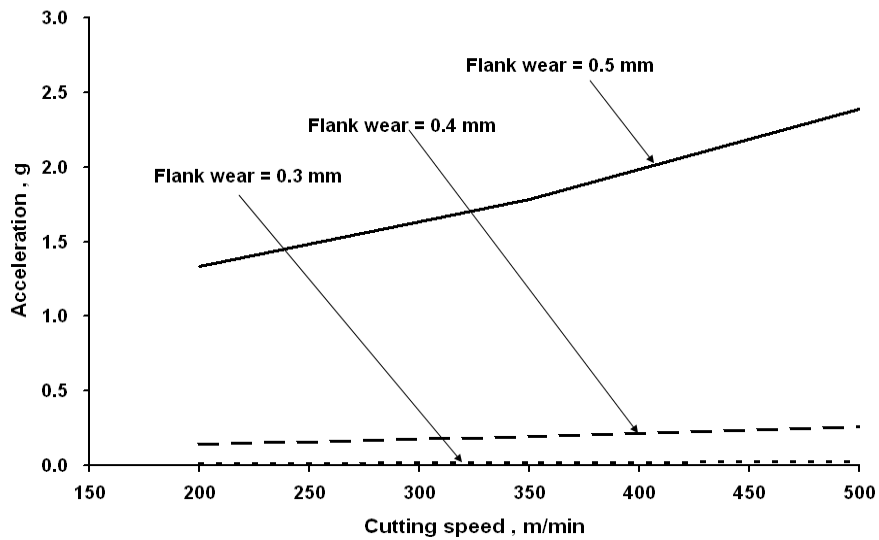Figure 5.23: Response of accelerometer in feed direction. Acceleration, g Vs Cutting speed for feed rate = 500 mm/min, depth of cut = 5 mm
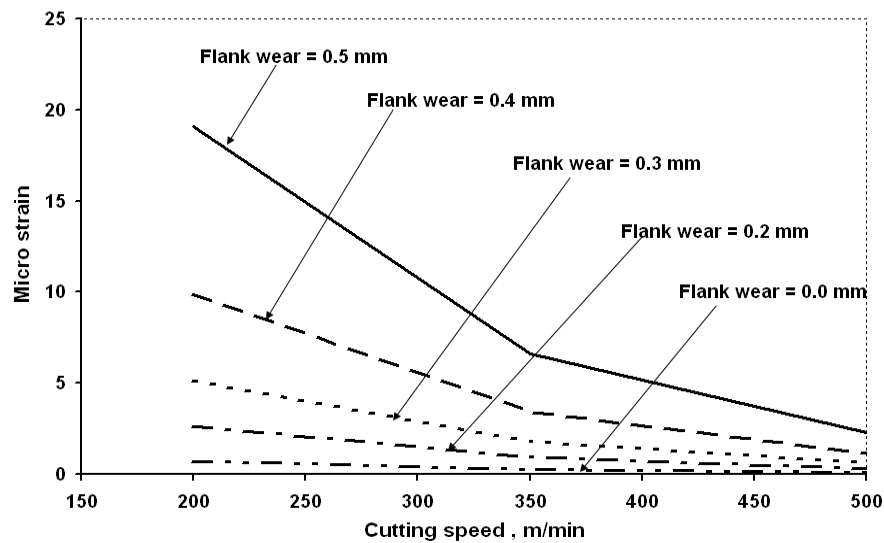
Figure 5.24: Response of strain gauge. Micro strain Vs Cutting speed for feed rate = 500 mm/min, depth of cut = 5 mm

5.3   Cutting edge chipping Failure

Health monitoring of a cutting tool during the machining process is an important issue especially from the quality of the product point of view. Health monitoring of a cutting tool deals with one or more of the following tasks [75]:

- Detection of collisions, i.e. unwanted movements between workpiece and cutting tool or machine tool,

- Detection or identification of tool fracture (cutting edge breakage), and

- Identification of gradual wear (flank, crater, nose wear etc) caused by abrasion or other influences.

Out of the above three tasks, first two are difficult tasks to control in a systematic manner. The detection of collision and cutting edge breakage at micro/macro level should be monitored in real time to avoid any major damage to the

machine tool as well as workpiece. Most of the literature [7] deals with gradual wear which is caused by friction between cutting tool and workpiece, and cutting tool and chip and it depends on various cutting conditions such as cutting speed, feed rate, depth of cut, condition of coolant, cutting tool position and so on. In any machining process the growth of gradual tool wear [30] is slow, and the cutting tool should be replaced or reconditioned after its life period is over. In contrast to the gradual wear, the chipping (cutting edge breakage) failure occurs instantaneously due to a sudden impact to the cutting tool. If it is possible to identify its occurrence, then the system should have provision to take a corrective action almost instantaneously to save the workpiece and the machine tool from any further damage. For identification of the cutting edge breakage, this chapter focuses on the two issues of the research problem: (i) to create an artificially chipped off tool (or cutting edge broken tool) in a controlled manner using EDM process, and (ii) to capture the signals when the chipped off cutting tool continues to machine a workpiece under different machining conditions using accelerometers and strain gauges.

Cutting tool health (gradually worn-out as well as chipped off(micro/macro) cutting tool condition) monitoring techniques [23, 30] can be useful especially in an automated cutting process and unmanned factory to prevent any damage to the cutting tool, machine tool and workpiece. In any metal cutting operation, one of the major hurdles in realizing its complete automation is the prediction of the state of the cutting tool. Cutting tool condition monitoring can help in on-line realization of the tool wear, tool breakage, and workpiece surface roughness.

Vibration and cutting force monitoring techniques applied to the detection of tool wear have been reported in reference [81].The failure mechanism called "chipping" occurs when small pieces of the carbide insert (or any other tool) are

separated away from the cutting edge during the machining process(Figure 3.7). Eventually, increased cutting force at the chipped off cutting edge causes the cutting edge to become inefficient and leading quickly to catastrophic failure. Chipping may not always be obvious. Some chipping occurs microscopically, where appearance may be confused with normal flank wear unless examined closely. Chipping may result due to a variety of conditions, namely, poor rigidity in the tooling set-up, weak cutting edge, deflecting workpiece, inadequate machine tool and varying cutting load due to various reasons. A chipped off cutting tool has been created using EDM process, as shown in Figures 5.25 a and 5.25b.

(a)   (b)
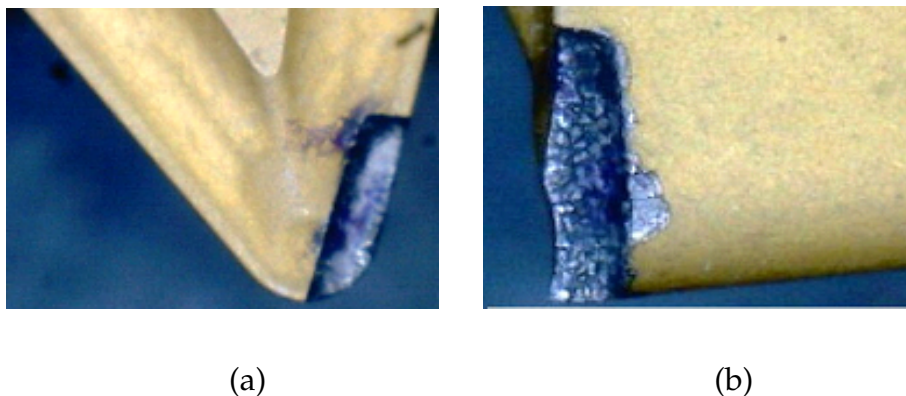
Figure 5.25: Chipped off cutting edge of the tool produced by EDM process (a) Top view of chipped off portion (b) Side view of chipped off portion

Four factors central composite rotatable design [57] with five levels (-2, -1, 0, 1, and 2) has been chosen to minimize the number of experiments. It contains 31 experiments with degrees of freedom equal to 30. The independent variables in this study are cutting speed, feed rate, depth of cut and chipped off depth. The independent variables were kept at five different levels as shown in Table 5.5.

Table 5.5: Levels of Independent variables

Levels	Cutting speed in m/min	Feed rate in mm/min	Depth of cut in mm	Chipped off depth in mm
-2	200	100	3.0	0.0
-1	275	200	3.5	0.2
0	350	300	4.0	0.3
1	425	400	4.5	0.4
2	500	500	5.0	0.5

Two responses or dependent variables (strain due to bending action of a cutting tool and acceleration, g in cutting direction) are measured for various machining conditions. Tungsten carbide cutting tools [58] (throw - away inserts DNMG 150608) were used in turning operation. The work piece material is EN-8 alloy steel and it is supported by a tail stock to avoid excessive overhang.

The cutting phenomenon has been analyzed by using power spectrum of vibration and strain gauge signals. Typical power spectral plots are shown in Figures 5.26 and 5.27. It is noted that in power spectral curves the amplitude of vibration values and micro strain values are dominated at the tool's natural frequency (Figure 5.3). It is observed that the peaks of vibration and strain gauge signals exhibit response in dynamic frequency range especially at the cutting tool natural frequency (3.91 kHz as shown in Figure 5.26) with respect to various machining conditions. In this analysis, the effects of four cutting parameters have been analyzed with respect to response parameters in-terms of vibration and strain.

Input parameters (amplitude of acceleration, g and strain) to the ANOVA are
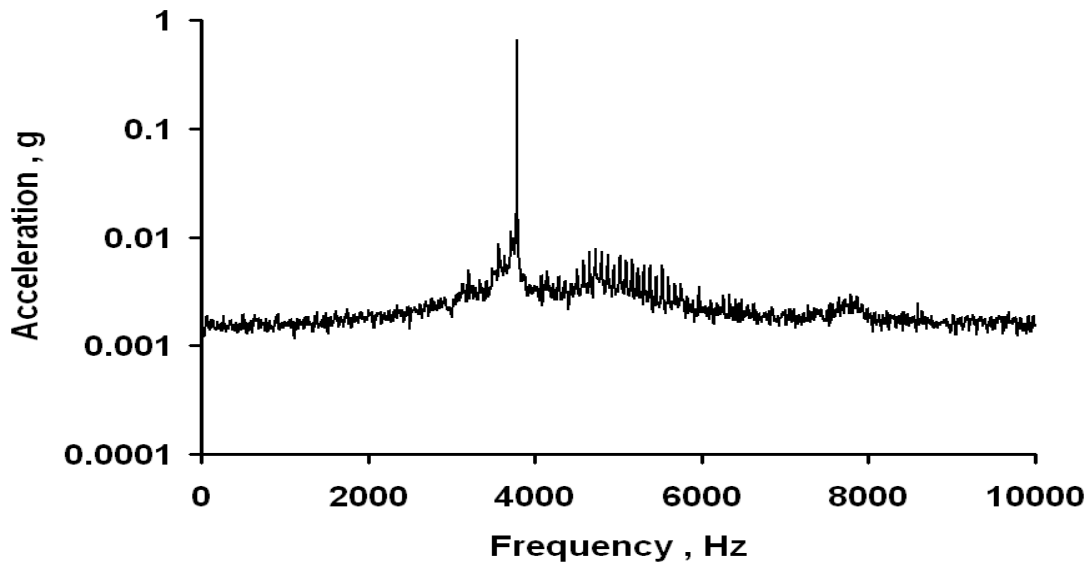
Figure 5.26: Response of accelerometer in cutting direction (Cutting speed = 350 m/min, Feed = 400 mm/min, depth of cut = 4 mm and chipped off depth = 0.3 mm)

obtained from the sensors output and the models are described in the later part of this section. In order to develop an empirical model, statistical analysis is performed on the experimental data to determine the most significant input machining parameters with respect to output responses (acceleration, *g* and strain).

Regression models have been developed using 31 experimental conditions as per desired central composite rotatable experimental design shown in Table 4.7. In central rotatable [57] composite design, the response of the system and input parameters are taken to have the following relationships (equation 5.5)

$$Y_u = b_0 + \sum b_i x_{iu} + \sum b_{ii} x_{iu}^2 + \sum b_{ij} x_{iu} x_{ju} \qquad (5.5)$$

where, Y_u = output response of the system , x_{iu} = known as input parameters to the system, and b_0, b_i, b_{ii}, b_{ij} are coefficients.
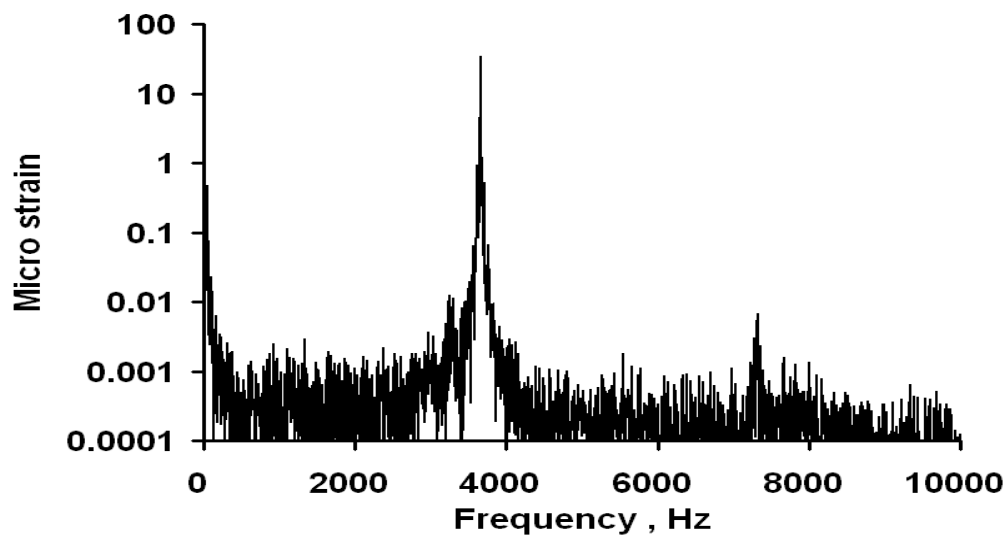
Figure 5.27: Response of strain gauge (Cutting speed = 350 m/min, Feed = 400 mm/min, depth of cut = 4 mm and chipped off depth = 0.3 mm)

The regression models (equations 5.6 and 5.7) have been developed using equation (5.5) to predict the output responses (acceleration and strain). The developed models are significant with confidence limit of 99% and as can be seen in ANOVA in Tables 5.6 and 5.7. The value of F-ratio in both the cases is higher than the tabulated value. Further if P≤0.05 indicates that the parameter is significant at 99% confidence level. The coefficients of cutting speed in both the models are negative while for feed rate and depth of cut are positive.

From the ANOVA, all the values of $P \leq 0.01$ indicate that the effect of the parameter is significant. The detailed ANOVA (Tables 5.6 and 5.7) has been performed for each level of chipped off depth with respect to machining input parameters as shown in Tables 5.6 and 5.7. In Table 5.6, the value of $P \geq 0.01(0.039)$ for the machining parameter depth of cut which is not significant. This may be due chipped off cutting edge at desired depth of cut. From the results of ANOVA, it is observed that F ratios were large enough and

indicate that the developed models are appropriate.

$$\beta = 0.475 - 0.12 \times 10^{-2}x_1 + 0.207 \times 10^{-3}x_2 - 0.11x_3 - 0.255x_4 + 0.2 \times 10^{-5}x_1^2$$
$$-0.1 \times 10^{-6}x_2^2 + 0.117 \times 10^{-1}x_3^2 - 0.22x_4^2 - 0.1 \times 10^{-7}x_1x_2 - 0.27 \times 10^{-4}x_1x_3$$
$$-0.44 \times 10^{-3}x_1x_4 - 0.8 \times 10^{-5}x_2x_3 - 0.93 \times 10^{-4}x_2x_4 + 0.96 \times 10^{-1}x_3x_4$$

$$(5.6)$$

where β = Acceleration, g in cutting direction, x_1 = cutting speed, x_2 = feed rate, x_3 = depth of cut, x_4 = chipped off depth.

$$\kappa = -21.7104 - 0.11 \times 10^{-2}x_1 + 0.283x_2 + 29.122x_3 - 353.029x_4 + 0.32 \times 10^{-3}x_1^2$$
$$+0.1 \times 10^{-3}x_2^2 + 2.496x_3^2 + 26.910x_4^2 - 0.27 \times 10^{-3}x_1x_2 - 0.126x_1x_3 + 0.602x_1x_4$$
$$-0.464 \times 10^{-1}x_2x_3 + 0.8 \times 10^{-2}x_2x_4 + 45.444x_3x_4$$

$$(5.7)$$

where, κ = Micro strain.

5.3.1 Comparison of experimental and model value for chipped off cutting tool

The percent difference (Δ) between experimental (E) and the model value (R) has been calculated by using following equation (5.8)

$$\Delta = \frac{R - E}{R} \times 100 \qquad (5.8)$$

where Δ = Percentage of error rate, R = Calculated value from regression equations, E = Experimental value. The calculated percentage of error rate values are 24.69% for the cutting speed 200 m/min, 8.14% for the cutting speed 300 m/min and 7.89% for the cutting speed 500 m/min. The deviations (or percentage of errors) increased with decrease in cutting speed as shown in Figure 5.28. This indicates that the model is more appropriate at higher cutting

Table 5.6: ANOVA for effect of machining parameters with respect to dynamic response of accelerometer in cutting direction(*channel 1*)

Source	DF	SS	MS	F	P
Regression	14	0.0242976	0.0017355	9.94	0
Residual Error	16	0.0027941	0.0001746		
Total	30	0.0270917			
Predictor	**Coef**	**SE Coef**	**T**	**P**	
Constant	0.03552	0.004995	7.112	0	
Cutting speed	-0.04939	0.005395	-9.156	0	
Feed rate	0.02171	0.004751	4.025	0.001	
Depth of cut	0.0121	0.002147	2.243	0.039	
Chipped off depth	0.02022	0.008618	3.748	0.002	
Source	**DF**				
Cutting speed	1				
Feed rate	1		$R^2 = 0.897$		
Depth of cut	1				
Chipped off depth	1				

Table 5.7: ANOVA for effect of machining parameters with respect to dynamic response of strain gauge bridge (*channel 3*)

Source	DF	SS	MS	F	P
Regression	4	4932.3	1233.1	17.67	0
Residual Error	26	1814.8	69.8		
Total	30	6747.1			
Predictor	**Coef**	**SE Coef**	**T**	**P**	
Constant	-8.51	18.01	-0.47	0.641	
Cutting speed	-0.1327	0.02274	-5.84	0	
Feed rate	0.06685	0.01705	3.92	0.001	
Depth of cut	9.244	3.411	2.71	0.012	
Chipped off depth	63.57	17.05	3.73	0.001	
Source	**DF**				
Cutting speed	1				
Feed rate	1		$R^2 = 0.884$		
Depth of cut	1				
Flank wear	1				

speed compared to the lower cutting speed. Similarly the percentage of error rate has been calculated for micro strain. The calculated percentage of error rate values are 17.01% for the cutting speed 200 m/min, 16.87% for the cutting speed 300 m/min and 7.92% for the cutting speed 500 m/min. The deviations (or percentage of errors) increased with decrease in cutting speed as shown in Figure 5.29. This again indicates that the model is more appropriate at higher cutting speed as compared to the lower cutting speed as discussed above.
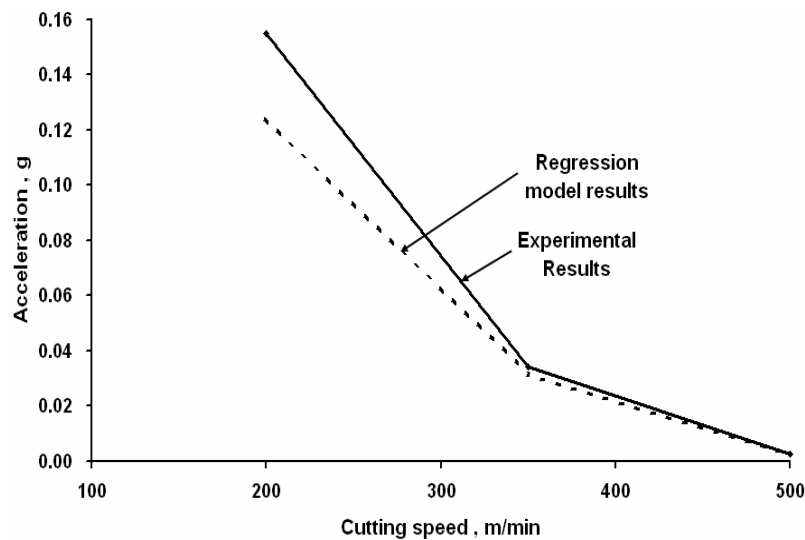
Figure 5.28: Response of accelerometer in cutting direction. Acceleration , g Vs Cutting speed for feed rate = 300 mm/min, depth of cut = 4 mm and chipped off depth = 0.4 mm

5.3.2 Comparison of chipped off tool and gradual flank wear tool

For automated industries and otherwise, it is important to differentiate between the signals obtained in case for gradual worn out (in flank) tool and the chipped off tool. It is observed (Figure 5.30) that acceleration, g value for a chipped off tool is substantially more when compared with gradual worn out (flank wear)
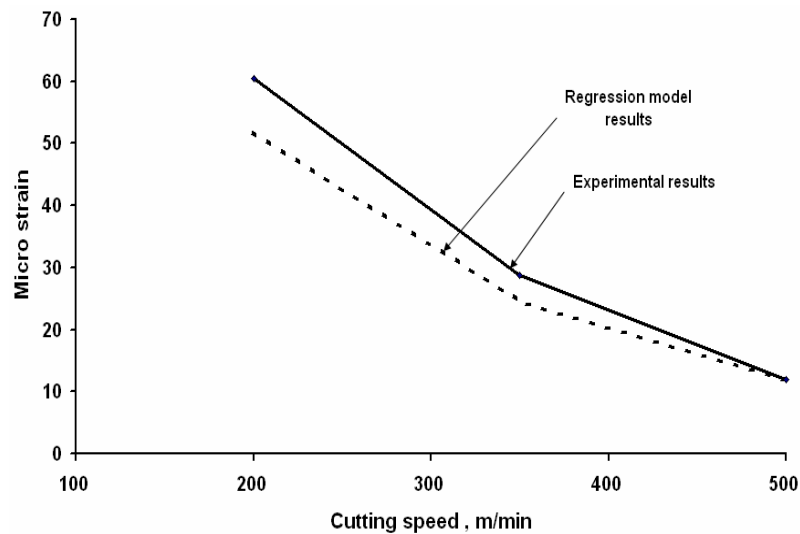
Figure 5.29: Response of strain gauge. Micro strain Vs Cutting speed for feed rate = 300 mm/min, depth of cut = 4 mm and chipping depth = 0.4 mm

cutting tool. Similarly, the amplitude of strain decreases with increase in cutting speed (Figure 5.31) and it is observed that the strain value is more for a chipped off cutting tool as compared to a gradual worn out tool. This is due to fractured cutting edge which obviously increases the cutting force.

Similarly for different machining conditions (cutting speed, feed rate, depth of cut and chipped off depth), the out response are analyzed and various graph have been plotted like acceleration, g vs feed rate (Figure 5.30), g vs depth of cut (Figure 5.31), g vs chipped off depth (Figure 5.32), micro strain vs feed rate (Figure 5.33), micro strain vs depth of cut (Figure 5.34), micro strain vs chipped off depth (Figure 5.35) and so on.

It is observed that in all the above cases the amplitude of acceleration, g as well as amplitude of strain values are more for a chipped off cutting tool when compared with a gradual worn out (flank wear) cutting tool. This is because of fractured cutting edge which obviously increases the cutting force (rubbing action between cutting tool and workpiece).
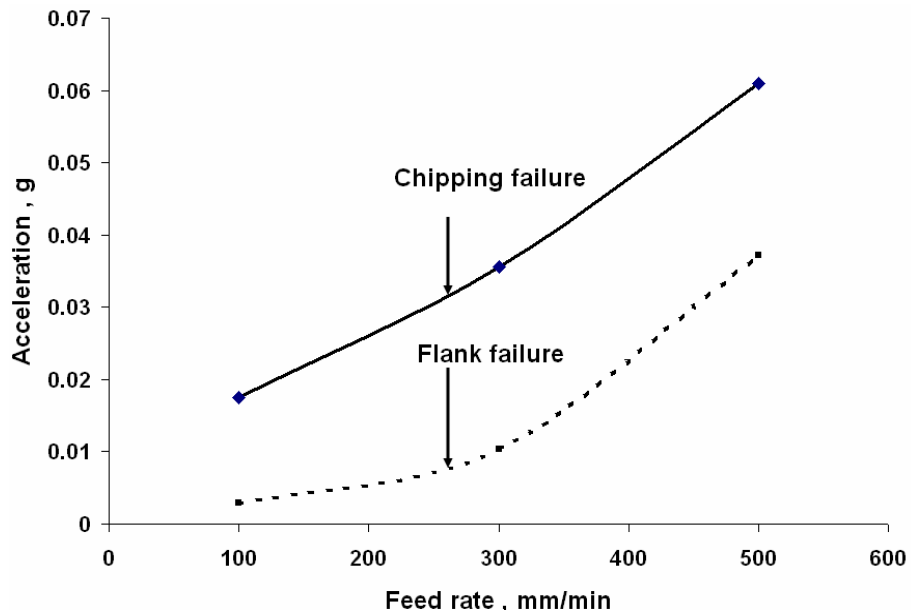
Figure 5.30: Response of accelerometer in cutting direction. Acceleration, g Vs Feed rate (Cutting speed = 350 m/min, depth of cut = 4 mm for chipped off depth = 0.5 mm and flank wear = 0.5 mm tool
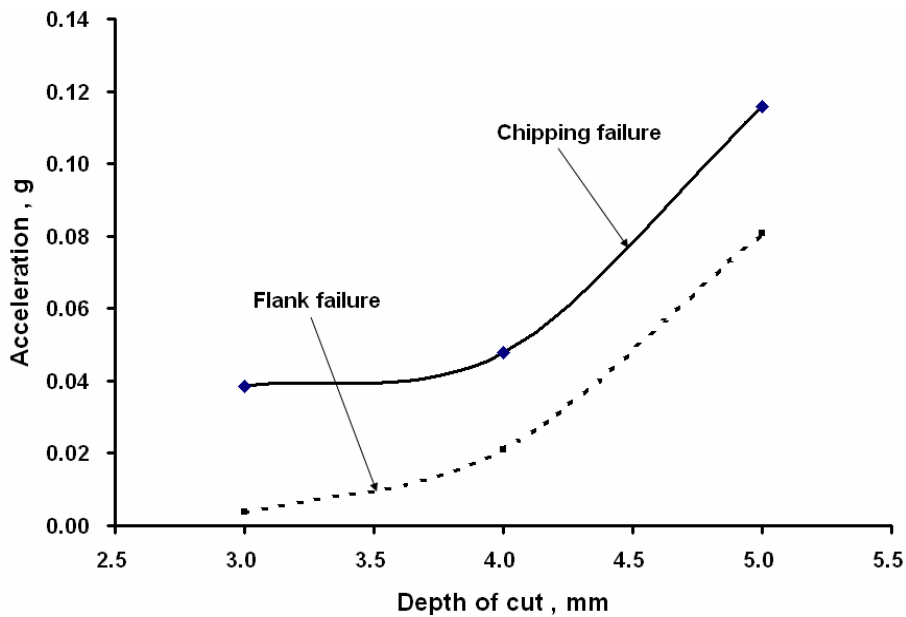
Figure 5.31: Response of accelerometer in cutting direction. Acceleration, g Vs Depth of cut for cutting speed = 350 m/min, feed rate = 300 mm/min for chipped off depth = 0.5 mm and flank wear = 0.5 mm tool
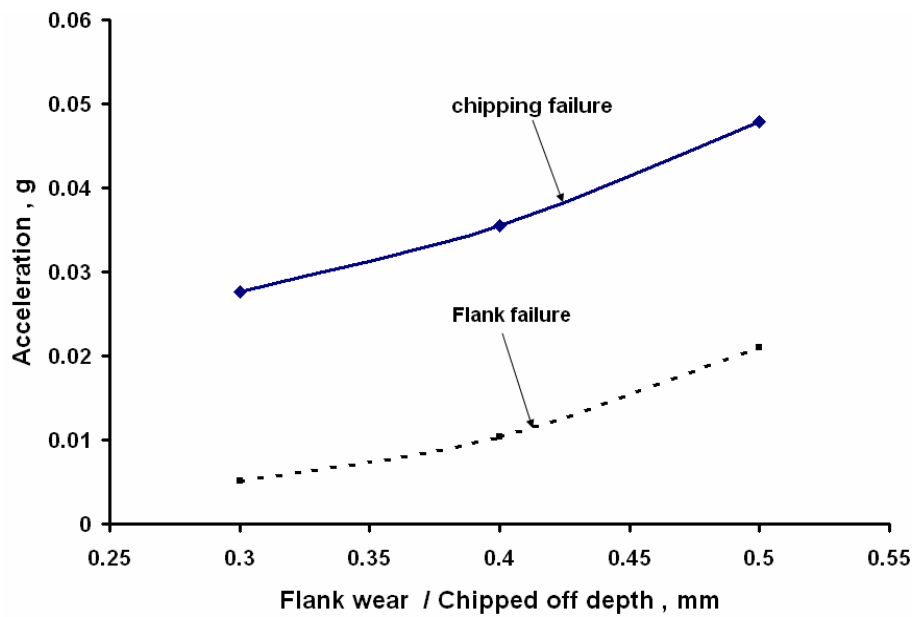
Figure 5.32: Response of accelerometer in cutting direction. Acceleration, g Vs Chipped off depth for cutting speed = 350 m/min, feed rate = 300 mm/min and depth of cut = 4mm
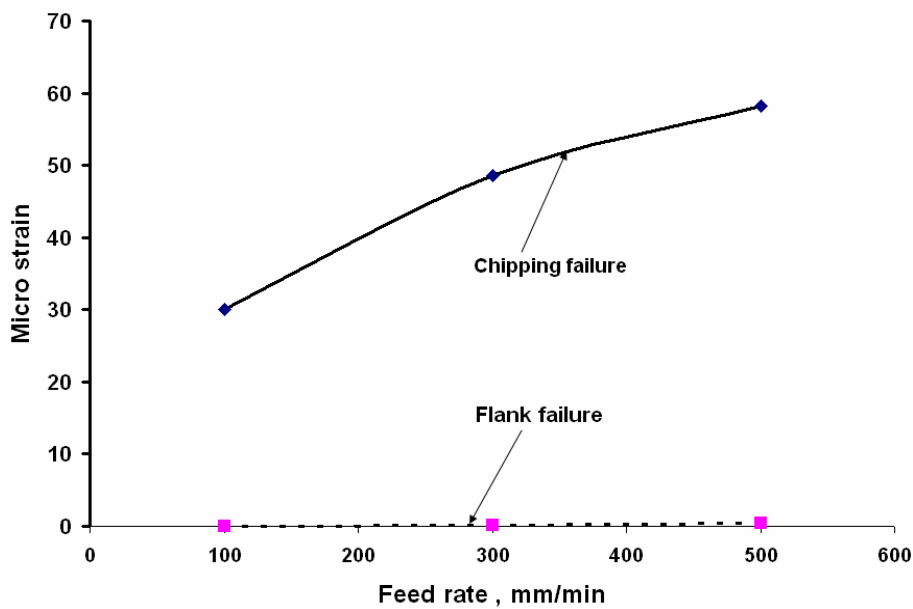
Figure 5.33: Response of strain gauge. Micro strain Vs Feed rate for cutting speed = 350 m/min, depth of cut = 4 mm, chipped off depth = 0.5 mm and flank wear = 0.5 mm tool
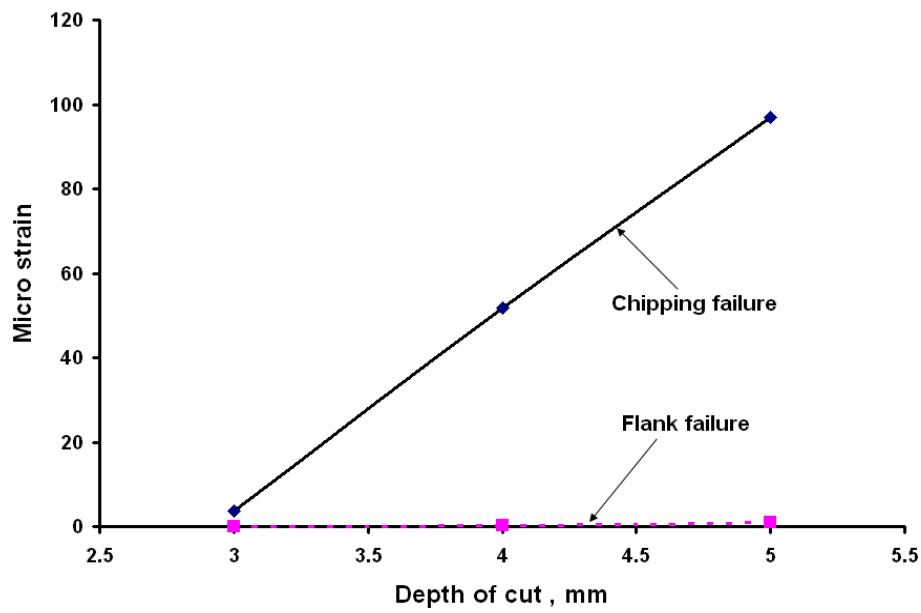
Figure 5.34: Response of strain gauge. Micro strain Vs Depth of cut for cutting speed = 350 m/min, feed rate = 300 mm/min, chipped off depth = 0.5 mm and flank wear = 0.5 mm tool)
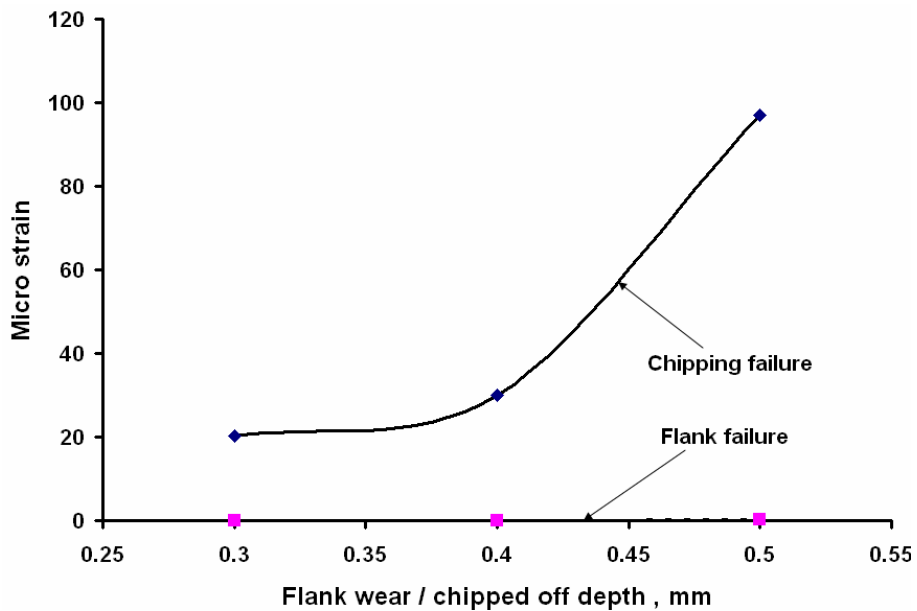
Figure 5.35: Response of strain gauge. Micro strain Vs Chipped off depth for cutting speed = 350 m/min, feed rate = 300 mm/min and depth of cut = 4mm)

5.4 Remarks

Regression/empirical models for flank wear and chipping failure were developed based on experimental results. The match between the regression and experimental curves indicates the validity of the regression model, and the ability of the system to measure the gradual flank wear and chipping failure of cutting tools during the process. Applications of the current system are limited to turning operations with negative inserts. However, in order to be utilize the system commercially, a more versatile tool/transducer coupling system needs to be developed to accommodate various tool holder designs and insert geometries. This empirical model may be used to develop a feed back system to monitor the cutting tool by fixing lower and higher range of acceleration, g and/or micro strain values.

Chapter 6

Artificial Neural Network Design

6.1   Artificial Neural Network Design

An Artificial Neural Network (ANN) is an interconnected group of artificial neurons that uses a mathematical or computational model for information processing based on a connectionist approach to computation. In most cases an ANN is an adaptive system that changes its structure based on external or internal information that flows through the network.

In the present work, Neural Networks based diagnosis has been divided into four phases. (i) Instrumentation and Data acquisition, (ii) Data analysis and Signal processing (iii) Neural Network Architecture Design (iv) Network training and Validation.

The experimental setup and data acquisition has already been discussed in previous chapters.

Here, the salient features of Network Design and Network Training and validation are described first.

6.1.1 Artificial Neuron

The artificial neuron was developed to mimic the first order characteristics of the biological neuron. An artificial neuron is an information processing unit that is fundamental to the operation of a neural network. A set of inputs is applied, each representing the output of another neuron. Each input is multiplied by a corresponding weight, analogous to synaptic strength, and all the weighted inputs are then summed to determine the activation level of the neuron. Figure 6.1 shows a typical model of neuron.

The three basic elements of the neuron model are described below.
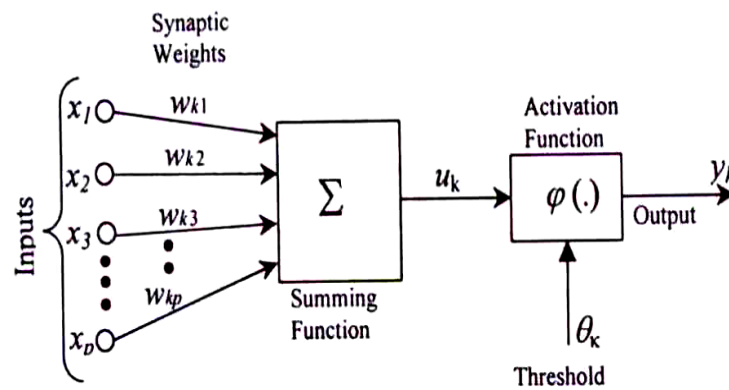
Figure 6.1: Nonlinear Model of Neuron

a) Synapses

These are connecting links each of which is characterized by a weight or strength of its own. w_{kj} represents weighting factor between a signal x_j at the input of the sample j, and a neuron k.

b) Adder

It sums up the input signals weighted by the respective synapses of the neuron. The operation is similar to that of linear adder.

c) Activation function

It defines the output of a neuron in terms of activity level at its input. It limits the amplitude of output of the neuron and introduces non-linearity in the network. These are sometimes referred to as squashing functions as they are used to limit the output in the definite small range irrespective of values of the input. Activation functions for the hidden units are required to introduce non-linearity into the network. Without non-linearity, hidden units would not make nets more powerful than just plain perceptrons (which do not have any hidden units, just input and output units). Almost any nonlinear function does the job, although for back propagation learning, it must be differentiable and it helps if the function is bounded; the sigmoidal functions such as *logistic* and *tanh* are the most common choices. Some of the common transfer functions are described in the Table 6.1.

The neuron also includes an externally applied threshold function, θ_k which has the effect of lowering the net input of the activation function. On the other hand, employing a bias term rather than threshold may increase the net input to the activation function.

Table 6.1: Activation Functions

Function name	**Mathematical expression**
Linear Activation Function	$\varphi(x) = x$
Positive Linear Activation Function	$\varphi(x) = x$; for $x \geq 0$ and
	$\varphi(x) = 0$; for $x \leq 0$
Hyperbolic Linear Tangent Sigmoid	$\varphi(x) = \frac{2}{1+\exp(-\rho x)} - 1$
Logistic Sigmoid Activation Function	$\varphi(x) = \frac{1}{1+\exp(-\rho x)}$

In the expressions above, ρ is a constant, and $\varphi(.)$ is the activation function. These four activation functions are represented graphically in Figure 6.2.
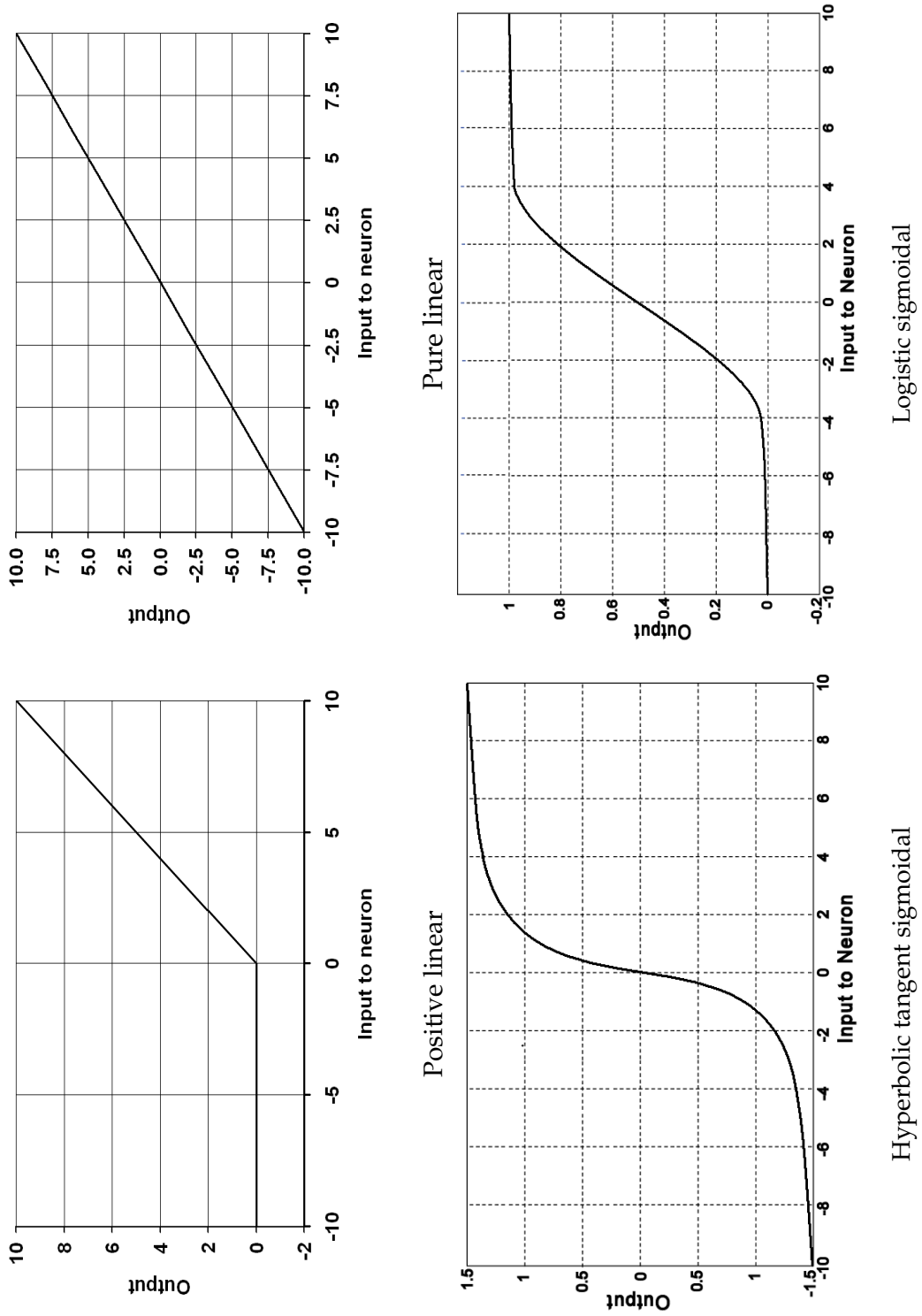
Figure 6.2: Activation functions

6.1.2 Network Architectures

The manner in which the neurons in a neural network are structured is intimately linked with the learning algorithm used to train the network. Four general classes of network architectures are:

a) Single Layer Feed Forward Network

This is a network of neurons organized in the form of layers. The simplest form of a network consists of an input layer of source nodes that project on to an output layer of neurons, but not vice versa. This is of feed forward type (Figure 6.3 a).

b) Multi-layer Feed Forward Network

It is similar to the one described above, except that it has one or more hidden layers of neurons. Hidden layers of neurons are interfaces between the input and output layers. It is observed that some problems converge better when these hidden layers are used (Figure 6.3 b).

c) Recurrent Networks

A recurrent network distinguishes itself from the feed-forward network as it has at least one feedback loop. For example, a recurrent network may consist of single layer of neurons, with each neuron feeding its output signal back to the input of all other neurons (Figure 6.3 c). A time delay may be introduced in the feedback path. Recurrent networks typically operate with a discrete representation of data and employ neurons with a hard-limiting activation function.

d) Lattice Structure

A lattice consists of a one or more multi-dimensional array of neurons with a corresponding set of source nodes that supply the input signals to the arrays

(Figure 6.3 d). The dimension of the lattice refers to the number of dimensions in which the graph lies.
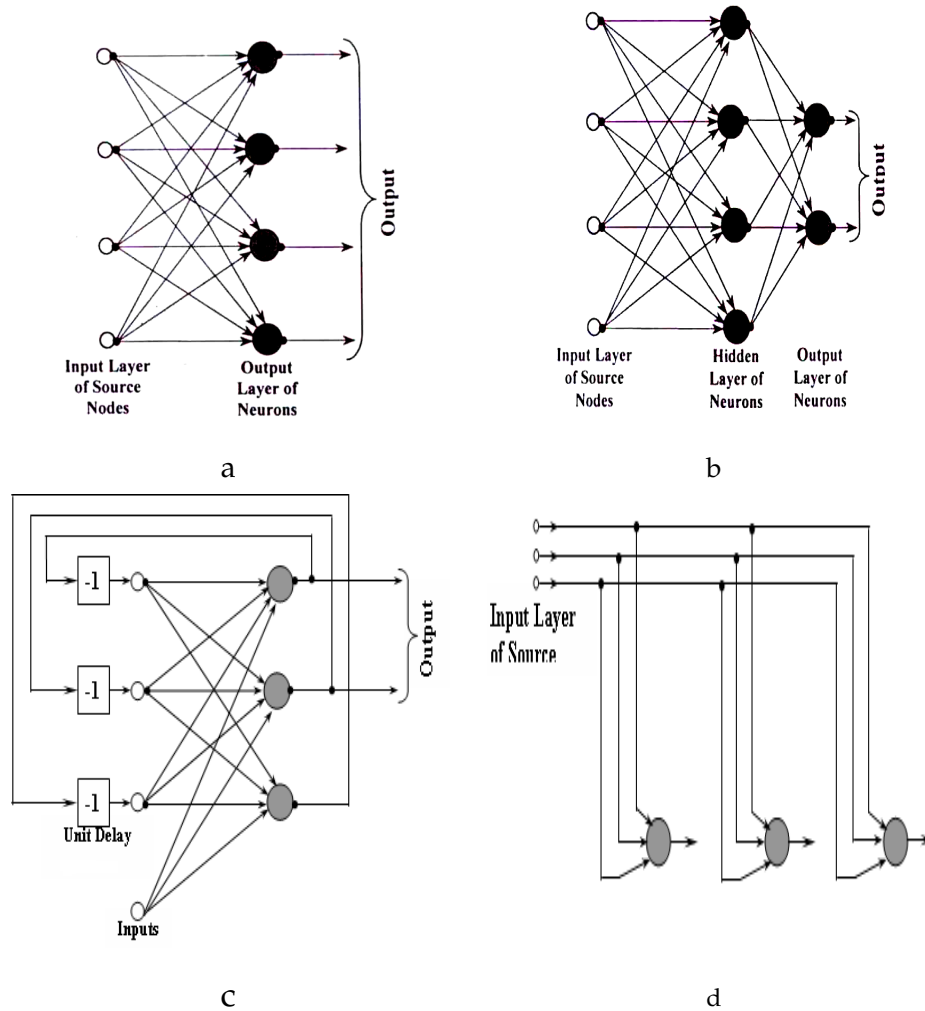
Figure 6.3: Network Architectures (a) Single layer feed forward neural network (b) Feed forward neural network with one hidden layer (c) Recurrent Network (d) One-Dimensional Lattice of 3-Neurons.

6.1.3 The Back-propagation Training Algorithm

The Back-propagation Training Algorithm (BPA) is a popular training algorithm. Its major attraction is its suitability to a large number of applications and high

rate of convergence. It is designed to solve the problems of choosing weight values for layered artificial neural networks with feed forward connections from input layer to hidden layer and then to the output layer. The algorithm performs the input to output mapping by minimizing a cost function using a gradient search technique. The cost function, which is equal to the mean squared difference between the desired and the actual net output, is minimized by making wide connection adjustments according to the error between the computed and target output processing element values. There are two stages in the development of a backpropagation algorithm, namely forward-pass and backward-pass. During the forward pass all the weights of the network are initialized randomly and the network outputs and the difference between the actual and target output (i.e. the error) is calculated for the initialized weights. During the backward step, the initialized weights are adjusted to minimize the error by propagating the error backwards. The network outputs and error are calculated again with the updated weights and the process repeats till the error is acceptably small. These two steps are described below and the whole algorithm can be represented schematically as shown in Figure 6.4.

Forward-Pass

Referring to Figure 6.4 the input vector p to the network is

$$x_p = (x_{p1}. \ldots . x_{pN})'. \tag{6.1}$$

where x_{pi} represents the input attribute i for the vector p.
The net input to the hidden layer becomes

$$net_{pj}^h = \sum_{i=1}^{N} w_{ji}^h x_{pi} + \theta_j^h \tag{6.2}$$

where w_{ji}^h represents the weight of the layer h from node i to node j and θ_L^h represents the threshold for the node L of the layer h.
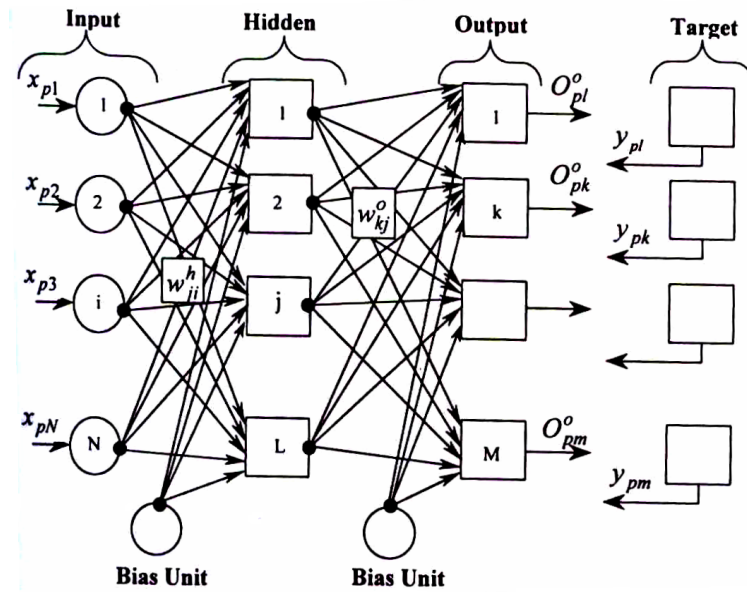
Figure 6.4: The three layer back propagation network architecture

The outputs from the hidden layer (which is input to the output layer) are

$$O_{pj}^h = i_{pj} = f_j^h(net_{pj}^h) \tag{6.3}$$

O_{pj}^h is the output from the node j of the hidden layer h, f_j^h is the activation function at node j of the hidden layer h. The equations 6.2 and 6.3 are represented graphically in Figure 6.5.
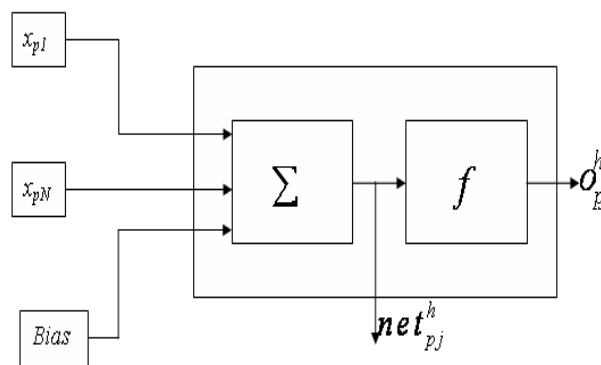
Figure 6.5: Output calculation at each node in the forward-pass

In the above the net-input values at output layer unit are

$$net^o_{pk} = \sum_{j=1}^{L} w^o_{kj} i_{pj} + \theta^o_k \tag{6.4}$$

while the outputs at output units are

$$O^o_{pk} = f^o_k(net^o_{pk}) \tag{6.5}$$

Individual error at each output unit is

$$\delta_{pk} = y_{pk} - O^o_{pk} \tag{6.6}$$

from which the overall mean square error can be computed as

$$E_p = \frac{1}{2} \sum_{k=1}^{M} \delta^2_{pk} \tag{6.7}$$

Backward-Pass

Weight adjustment is carried out at the output layer through the following procedure. Using equations 6.6 and 6.7, the mean square error, E_p can be expressed as

$$E_p = \frac{1}{2} \sum (y_{pk} - O^o_{pk})^2 = \frac{1}{2} \sum \left[y^o_{pk} - f^o_k(net^o_{pk}) \right]^2 \tag{6.8}$$

The weight change of an output layer weight is the negative gradient of E_p with respect to output layer weights w^o_{kj} and can be written as

$$\frac{\partial E_p}{\partial w^o_{kj}} = -(y_{pk} - O^o_{pk}) \frac{\partial f^o_k}{\partial (net^o_{pk})} \frac{\partial (net^o_{pk})}{\partial w^o_{kj}} \tag{6.9}$$

However, using equation (6.4)

$$\frac{\partial (net^o_{pk})}{\partial w^o_{kj}} = \left(\frac{\partial}{\partial w^o_{kj}} \sum w^o_{kj} i_{pj} + \theta^o_k \right) = i_{pj} \tag{6.10}$$

and using equation (6.5)

$$\frac{\partial f_k^o}{\partial (net_{pk}^o)} = f_k^o(net_{pk}^o) = O_{pk}^o(1 - o_{pk}^o) \tag{6.11}$$

Therefore, the weight change at the output layer weight is

$$\Delta_p^o w = \frac{-\partial E_p}{\partial w_{kj}^o} = (y_{pk} - O_{pk}^o)f_k^o(net_{pk}^o)i_{pj} \tag{6.12}$$

Now denoting

$$\delta_{pk}^o = (y_{pk} - O_{pk}^o)f_k^o(net_{pk}^o) \tag{6.13}$$

the weight change at the output layer weights can be written as

$$\Delta_p^o w = \delta_{pk}^o i_{pj} \tag{6.14}$$

To make the learning process smooth and to ensure that the weight changes take place in the same direction, two network parameters - learning rate coefficient η and momentum α - are introduced in lieu of direct application of the above mentioned weights, so that

$$w_{kj}^o(t+1) = w_{kj}^o(t) + \eta(y_{pk} - O_{pk}^o)f_k^o(net_{pk}^o)i_{pj} + \alpha w_{kj}^o(t-1) \tag{6.15}$$

A small value of η implies that the network will have to make a large number of iterations. Its value is normally kept between 0.05 and 0.9. It is often possible to increase its value as the network error decreases, thereby increasing the speed of convergence. Another way to increase convergence speed is by adopting an extra momentum term while updating the weights. This additional term tends to keep the weight changes in the same direction. The entire weight updating process at the output layer can be represented schematically as shown in Figure 6.6.

While updating the weights for the hidden layers it should be noted that there is no target output and therefore the adjustment of weights is proportional to their initial contribution. From equations 6.4 and 6.5 one gets

$$E_p = \frac{1}{2}\sum_k \left[y_{pk} - f_k^o\left(\sum w_{kj}^o i_{pj} + \theta_k^o\right)\right]^2 \tag{6.16}$$
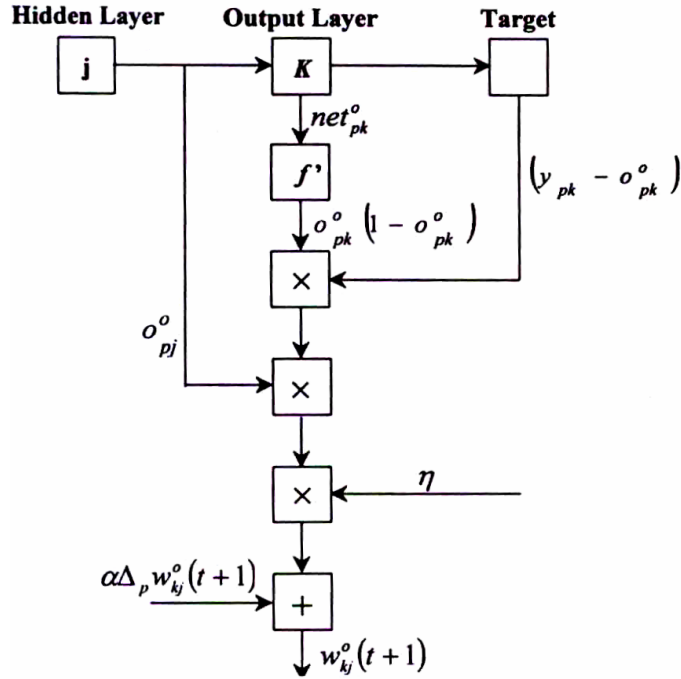
Figure 6.6: Output layer weight updating

The weight change of a hidden layer weights is the negative gradient of E_p with respect to hidden layer weights w_{ji}^h and is given by

$$\frac{\partial E_p}{\partial w_{ji}^h} = -\sum_k (y_{pk} - O_{pk}^o) \frac{\partial O_{pk}^o}{\partial(net_{pk}^o)} \frac{\partial(net_{pk}^o)}{\partial i_{pj}} \frac{\partial i_{pj}}{\partial(net_{pj}^h)} \frac{\partial(net_{pj}^h)}{\partial w_{ji}^h} \tag{6.17}$$

and the individual terms on the right hand side of the above equation can be expanded as

$$\frac{\partial O_{pk}^o}{\partial(net_{pk}^o)} = \frac{\partial(f_k^o(net_{pk}^o))}{\partial(net_{pk}^o)} = f_k^o(net_{pk}^o) = O_{pk}^o(1 - O_{pk}^o) \tag{6.18}$$

$$\frac{\partial(net_{pk}^o)}{\partial i_{pj}} = \frac{\partial \sum_{j=1}^L w_{kj}^o i_{pj} + \theta_k^o)}{\partial i_{pj}} = w_{kj}^o \tag{6.19}$$

$$\frac{\partial i_{pj}}{\partial(net_{pj}^h)} = \frac{\partial(f_j^h(net_{pj}^h))}{\partial(net_{pj}^h)} = f_j^h(net_{pj}^h) = o_{pj}^h(1 - o_{pj}^h \tag{6.20}$$

$$\frac{\partial(net_{pj}^h)}{\partial w_{ji}^h} = \frac{\partial(\sum_{i=1}^N w_{ji}^h x_{pi} + \theta_j^h)}{\partial w_{ji}^h} = x_{pi} \tag{6.21}$$

Substituting the above equations (6.18)to (6.21) in equation 6.17 one gets

$$\Delta_p w_{ji}^h = -\frac{\partial E_p}{\partial w_{ji}^h} = x_{pi} O_{pj}^h (1 - O_{pj}^h) \sum_k (y_{pk} - O_{pk}^o) O_{pk}^o (1 - O_{pk}^o) w_{kj}^o \qquad (6.22)$$

Network parameters η, α can be introduced in a manner similar to that in the case of the output layer, to express the final weight change at the hidden layer as

$$w_{ji}^h(t+1) = w_{ji}^h(t) + \eta x_{pi} O_{pj}^h (1 - o_{pj}^h) \sum (y_{pk} - O_{pk}^o) O_{pk}^o (1 - O_{pk}^o) w_{kj}^o + \alpha w_{ji}^h(t-1).$$

$$(6.23)$$

The entire weight updating process at hidden layer can be schematically represented as shown in Figure 6.7.
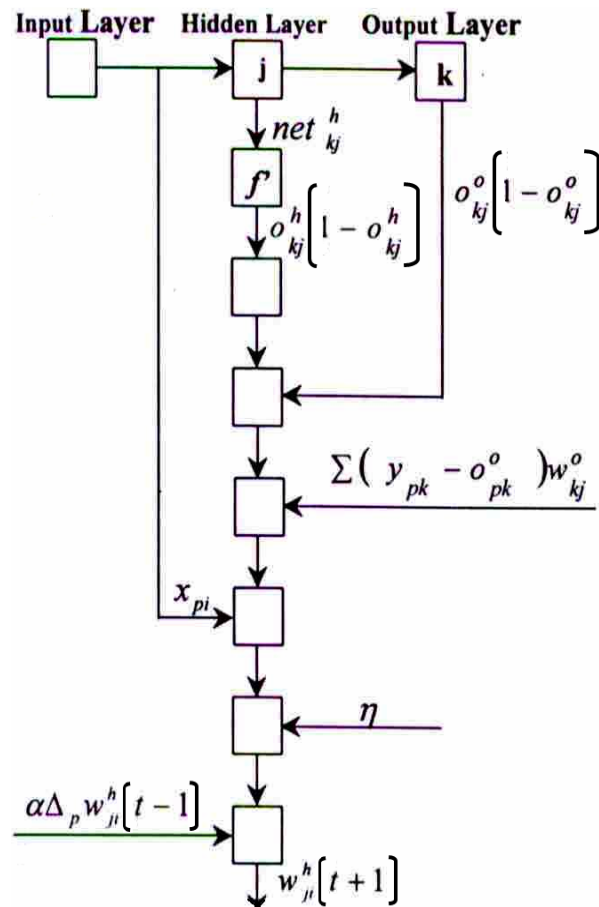
Figure 6.7: Hidden layer weight updating

6.1.4 Training Algorithms

Training is accomplished in a network by sequentially applying input vector, while adjusting network weights according to a predetermined procedure. During training, the network weights gradually converge to values such that each input vector produces the desired output vector. Neural network toolbox in MATLAB provides fifteen different learning functions. Those used in present study are briefly described below. Gradient Descent Back-propagation *(TRAINGD)*: updates the weight and bias values according to gradient descent as follows.

$$dw = \eta \times \frac{dE_p}{dw}, \tag{6.24}$$

where w is the weight/bias variable, η is the learning rate, and E_p is the performance. Resilient Back-propagation *(TRAINRP)*: This training algorithm updates weights and bias according to the following relationship

$$dw = \Delta w \times sign(gw), \tag{6.25}$$

where Δw are all initialized and gw is the gradient. At each iteration the elements of Δw are modified. If an element of gw changes sign between two successive iterations then the corresponding Δw is decreased by certain value. If it maintains its sign then corresponding Δw is increased by certain value. This continuous change in the value of Δw ensures gradual but faster convergence.

6.1.5 Probabilistic Neural Network (PNN)

Investigations were also carried out, during the present study, on the suitability of probabilistic neural networks for fault identification. Probabilistic Neural Networks (PNNs) find their application mainly in classification problems [72]. Some of the salient features of such networks are briefly described here.

A Probabilistic Neural Network bases itself on Bayes' Rule which describes the probability of the presence of a particular fault conditional to the observation of a

certain symptom as

$$P(H_i/E) = \frac{P(E/H_i)P(H_i)}{\sum P(E/H_n)P(H_n)} \tag{6.26}$$

where

$P(H_i/E)$ the probability that fault H_i is present, given the symptom E.

$P(E/H_i)$ probability that symptom E will be observed when fault H_i.

$P(H_i)$ the apriori probability that fault H_i is present

in absence of any specific symptom.

The following computational procedure can be followed.

$P(H_i)$ Information generally obtained from Machine History, or

otherwise taken as unity for all possible faults

$\sum P(E/H_n)P(H_n)$ this term in the denominator is constant for all i.

Given a symptom E, the network computes the conditional probability $P(H_i/E)$, of the presence of faults $(i = 1, 2, ..k)$. A comparison is then made

if $P(H_i/E) > P(H_j/E)$ for all $j \neq i$,   then the fault is H_i

or $P(E/H_i) > P(E/H_j)$ for all $j \neq i$,   then the fault is H_i .

$P(E/H_i)$ is computed using the following

$$P(E/H_i) = \frac{1}{(2\pi)^{m/2}\sigma_i^m n_i} \sum_{j=1}^{n_i} \left[\frac{-(E - E_j^i)^T (E - E_j^i)}{2\sigma_i^2} \right] \tag{6.27}$$

where

m number of observations e in every training symptom pattern E

n_i number of training symptom patterns pertaining to the ith fault H_i.

σ_i smoothing parameter computed using radial basis functions.

The probabilistic neural network, in addition to the input layer, has two hidden Layers and an output layer (Figure 6.8). Its major difference with a Backpropagation network is that it can be constructed after only a single pass of the training data sets. Also, the activation function is statistically derived from estimates of the probability density functions based on training patterns.
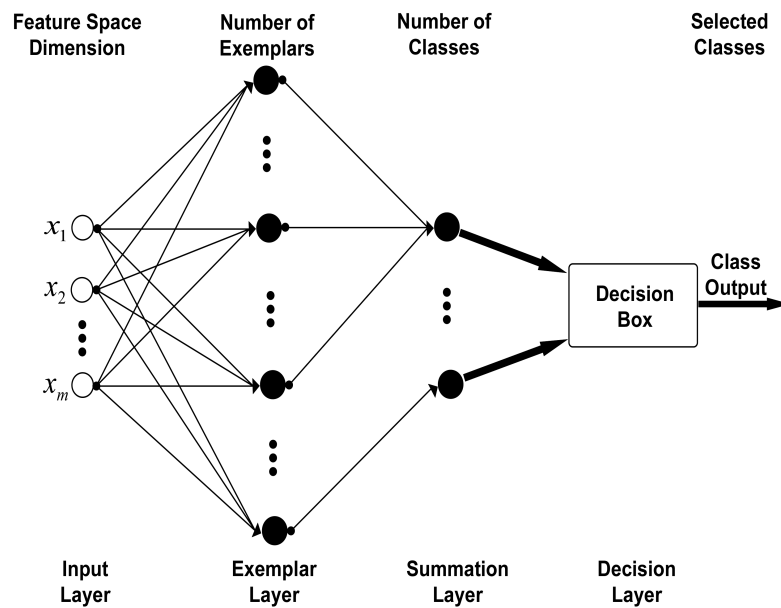
Figure 6.8: Probabilistic Neural Network Architecture

6.2 Data Acquisition, Storage and Display

A computer code has been developed in LabVIEW for data acquisition, data storage and display. This program has the following adjustable features:

(i) Scan rate (set at 25000 samples/s).

(ii) Number of data points to be read before each display (set at 4096 data points).

(iii) Device and Channel numbers from which to acquire data

(set at Device No. 1 and Channel No. 1).

(iv) Frequency range (set at 10000 Hz).

A Hanning window is then applied to the acquired time domain signal. Fast Fourier Transform (FFT) of the time signal is carried out and the FFT is displayed in 'real' time along with the time domain signal on the front panel. Provision is also made on the front panel for the user to select the desired frequency range for FFT display.

Option is provided for logging the time domain data and frequency domain data into the hard disc at any desired instant of time.

Figure 6.9 and Figure 6.10 show *front panel* and *block diagram* respectively of VI for data acquisition.
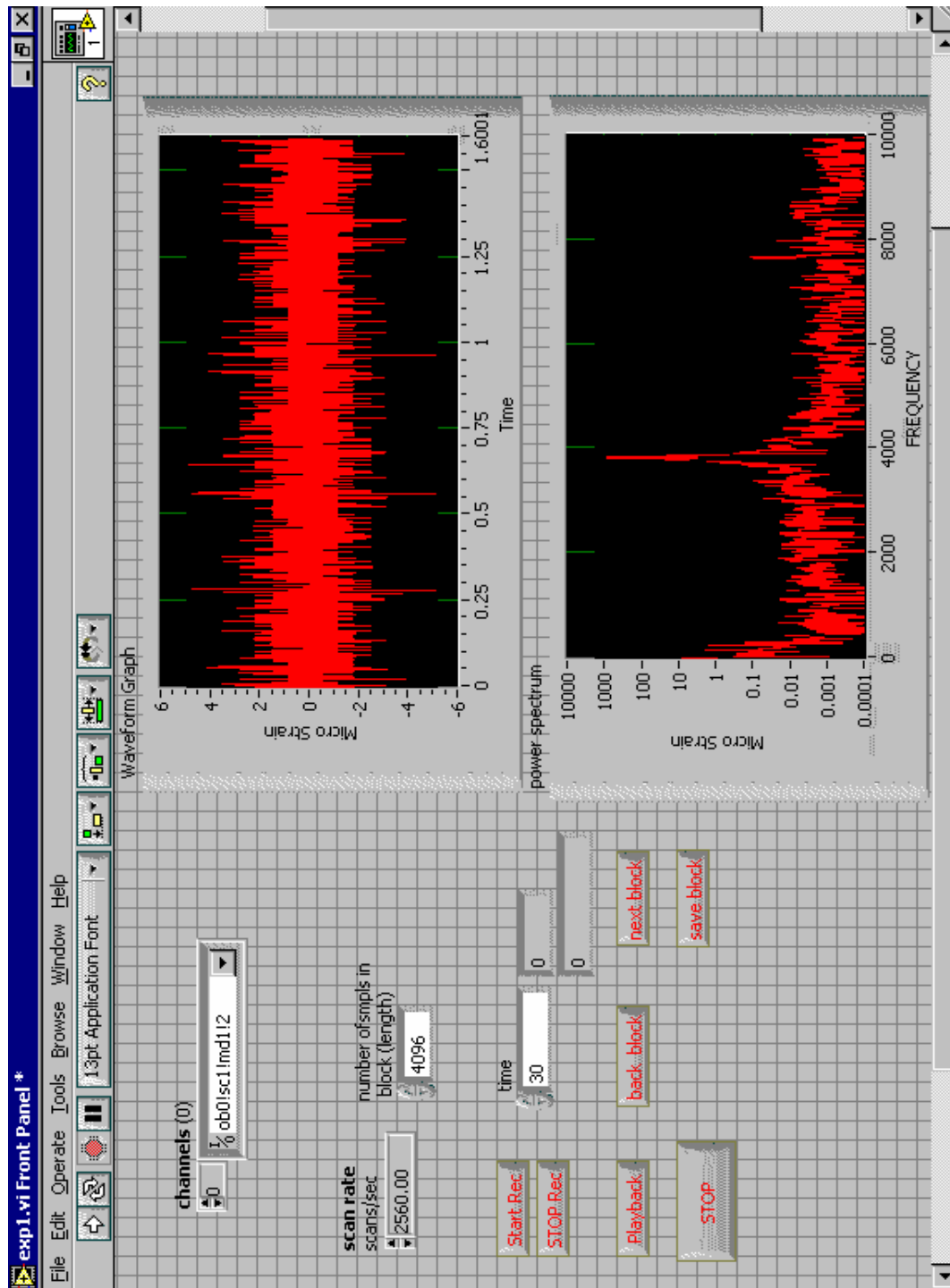
Figure 6.9: Front panel of VI to acquire Strain gauge signal
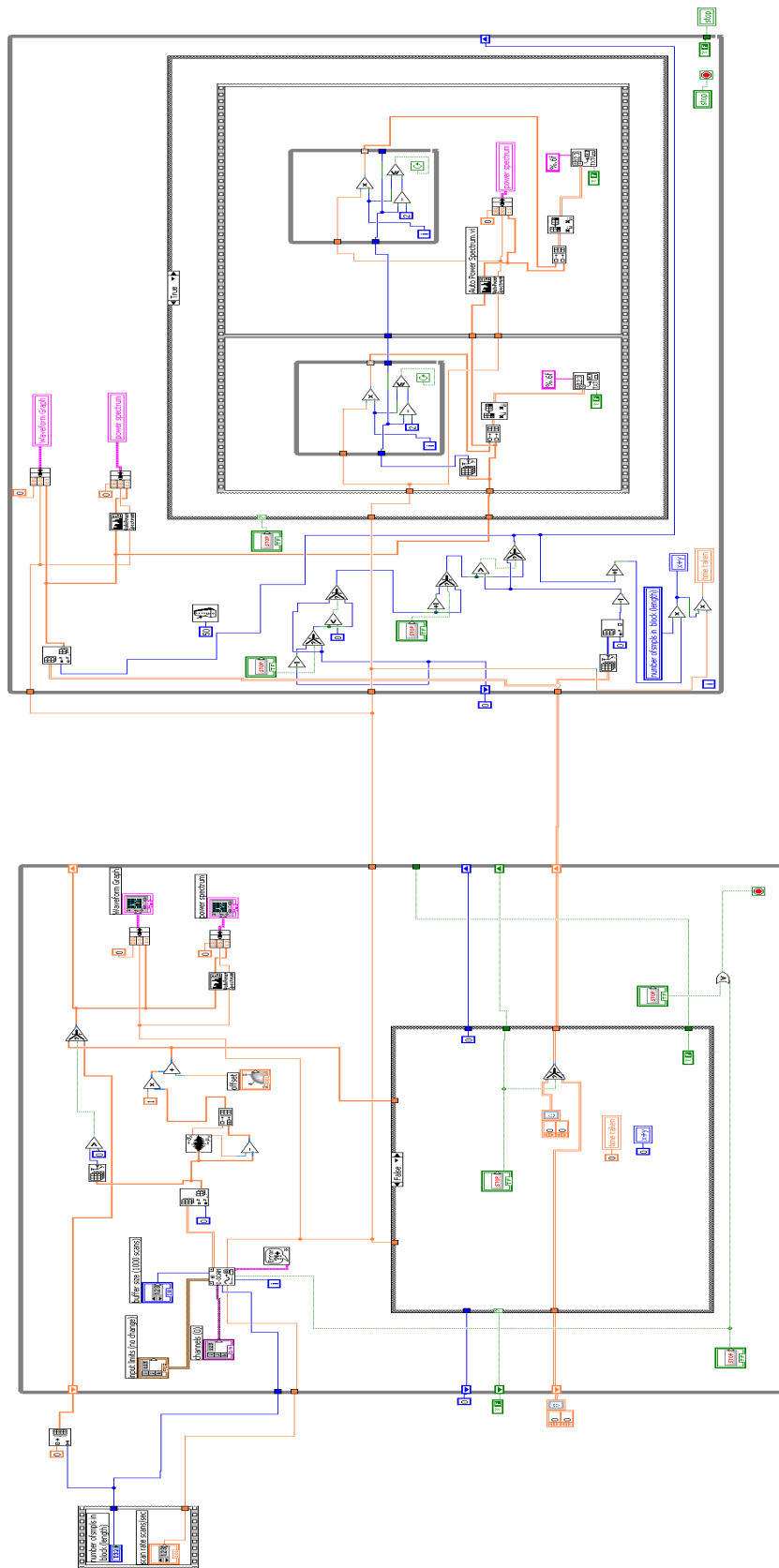
Figure 6.10: Block diagram of VI to acquire Strain gauge signal

6.3   Fault Simulation

A variety of faults were simulated on the set-up. As a first step, the machine was run without introduction of any fault. Signatures for such no-fault operation establish the baseline data. This baseline data can then be used for comparison with signatures obtained under faulty conditions.

Fault generation was carried out in the following steps.

6.3.1   Flank Wear

Flank wear	Severity level I	0.0 mm
	Severity level II	0.2 mm
	Severity level III	0.3 mm
	Severity level IV	0.4 mm
	Severity level V	0.5 mm

Data was acquired for each of the above cases for each of the following machining conditions.

Cutting speed	a	200 m/min
	b	350 m/min
	c	500 m/min
Feed Rate	a	100 mm/min.
	b	300 mm/min.
	c	500 mm/min.
Depth of cut	a	3 mm.
	b	4 mm.
	c	5 mm.

6.3.2 Chipping Failure

Chipping failure Severity level I   0.0 mm

Severity level II   0.2 mm

Severity level III   0.3 mm

Severity level IV   0.4 mm

Severity level V   0.5 mm

Data was acquired for each of the above cases for the following machining conditions.

Cutting speed	a	200 m/min.
	b	275 m/min.
	c	350 m/min.
	d	425 m/min.
	e	500 m/min.
Feed Rate	a	100 mm/min.
	b	200 mm/min.
	c	300 mm/min.
	d	400 mm/min.
	e	500 mm/min.
Depth of cut	a	3.0 mm.
	b	3.5 mm.
	c	4.0 mm.
	d	4.5 mm.
	e	5.0 mm.

Typical time domain signals for the Flank Wear cases (for severity levels 0.0 mm - 0.5 mm) for fixed operating conditions (Cutting speed = 500 m/min, feed rate = 500 mm/min and depth of cut = 5 mm) are given in Figures 6.11, 6.12 and 6.13. Typical time domain signals for another set of operating conditions (Cutting speed = 350 m/min, feed rate = 300 mm/min and depth of cut = 4 mm.) are

given in Figures 6.14, 6.15 and 6.16.

Similarly, for Chipping failure cases the corresponding time domain Signals are given in Figures 6.17, and 6.18. Typical time domain signals for another set of operating conditions for chipping failure cases (Cutting speed = 350 m/min, feed rate = 500 mm/min and depth of cut = 4 mm.) are given in Figures 6.19 and 6.20.

It can be readily seen from the time domain signatures that it is difficult to tell one fault condition or severity level from another. The need for processing of the raw time domain data is obvious.

In the present work (i) Frequency Domain Analysis and (ii) Statistical Analysis is carried out to further process these signals. The processed (i) FFT data and (ii) the statistical data are then fed as input to the Neural Networks developed for diagnosis.

6.4   Finite Element Analysis of cutting tools

Finite element modeling and analysis have been carried out to study the dynamic behavior of the cutting tool. It has been used to validate the experimentally obtained natural frequency of the tool. From the FE analysis and experimental results (Rap test), it is found that first natural frequency of the cutting tool is 3.91 kHz. This analysis is useful to extract the information from the sensors output in particular frequency domain analysis. These extracted data are used to train and test the artificial neural networks.

The finite element method (FEM) model used as an explicit method, which is more suitable for events with large nonlinear deformations at high strain rate with complex contacts between surfaces, conditions typically expected in metal
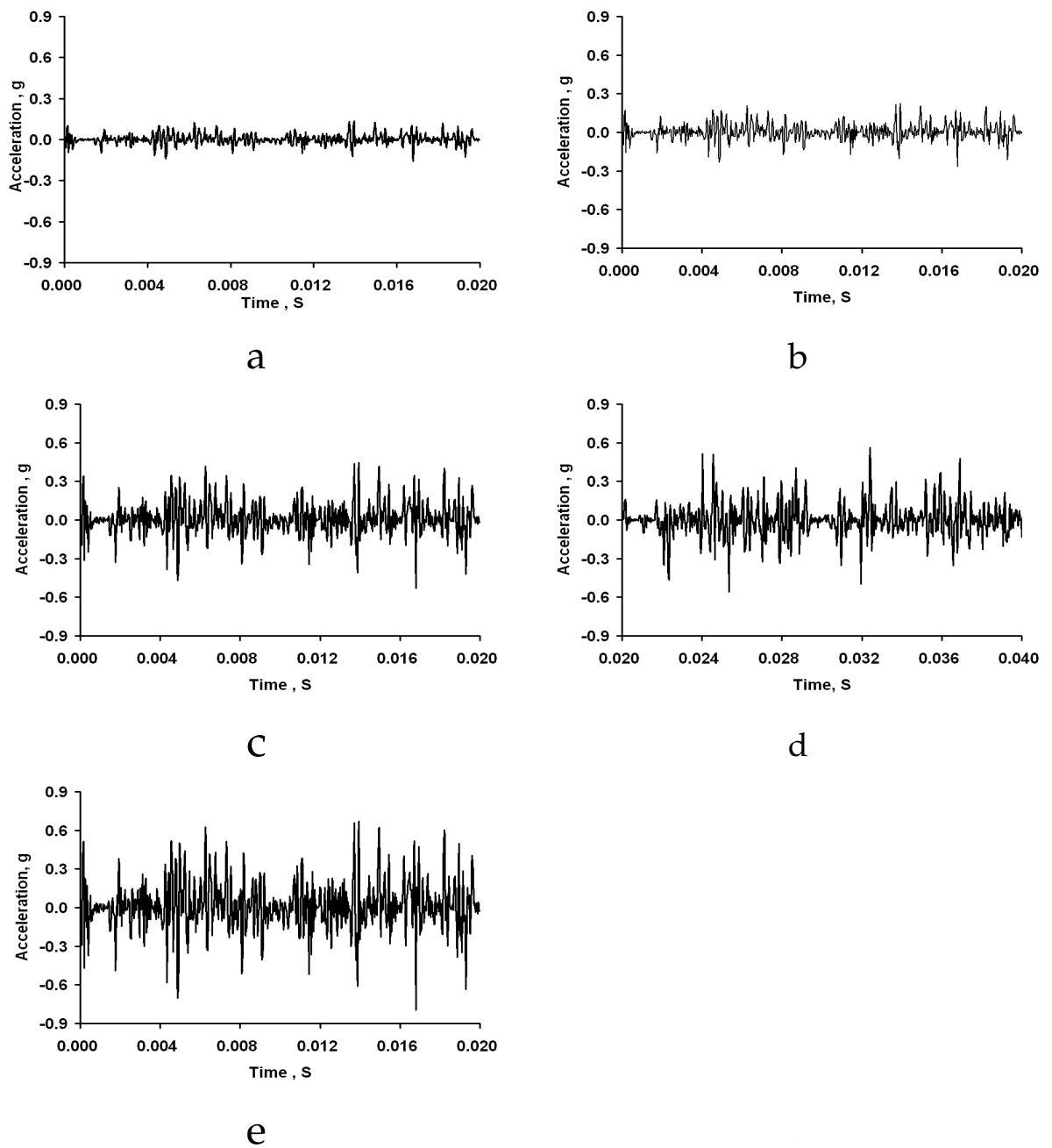
Figure 6.11: Typical accelerometer time domain signal in cutting direction for (a) new cutting tool (b) 0.2 mm flank wear cutting tool (c) 0.3 mm flank wear cutting tool (d) 0.4 mm flank wear cutting tool (e) 0.5 mm flank wear cutting tool. Cutting speed = 500 m/min, feed rate = 500 mm/min and depth of cut = 5 mm.
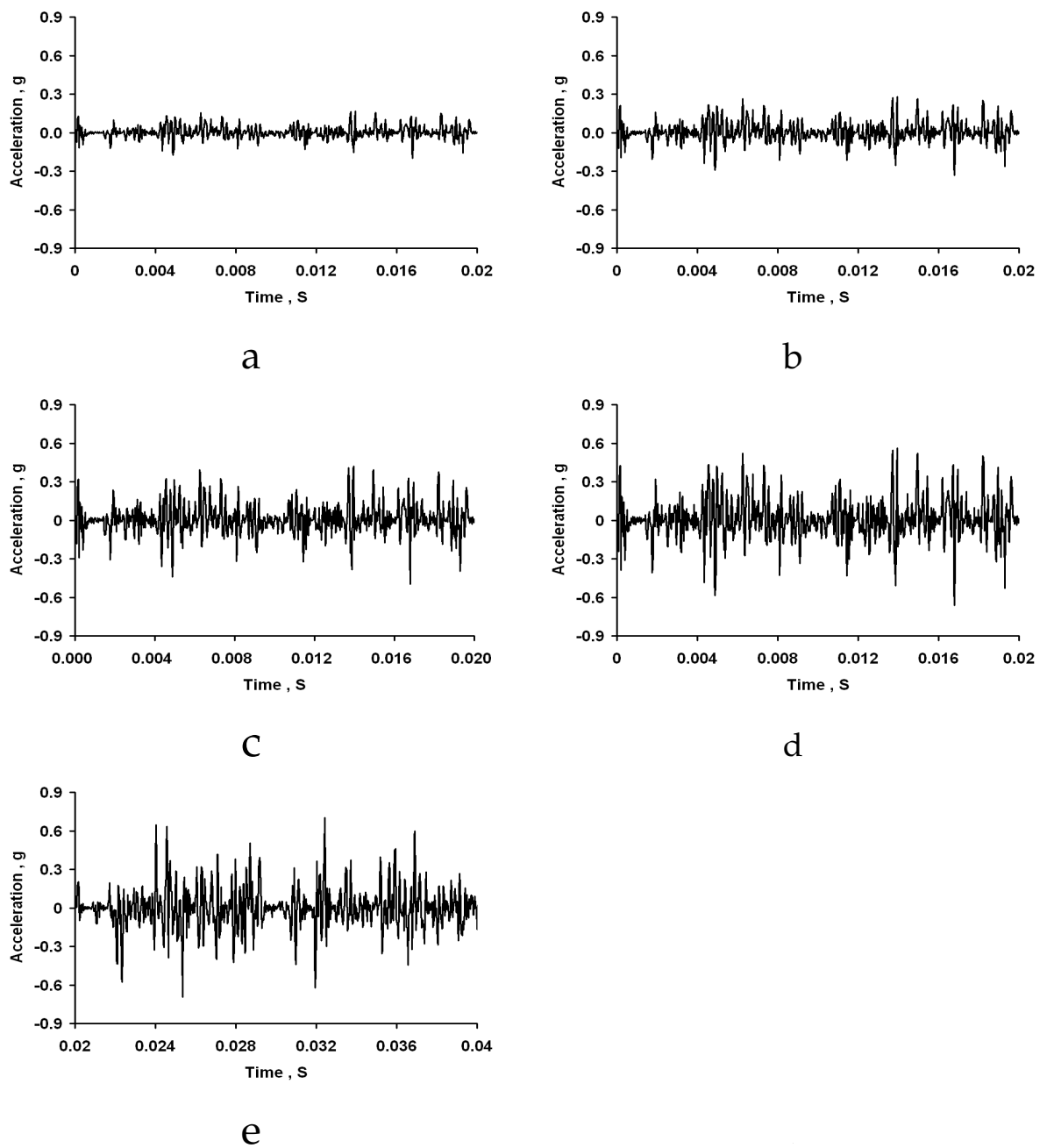
Figure 6.12: Typical accelerometer time domain signal in feed direction for (a) new cutting tool (b) 0.2 mm flank wear cutting tool (c) 0.3 mm flank wear cutting tool (d) 0.4 mm flank wear cutting tool (e) 0.5 mm flank wear cutting tool. Cutting speed = 500 m/min, feed rate = 500 mm/min and depth of cut = 5 mm.
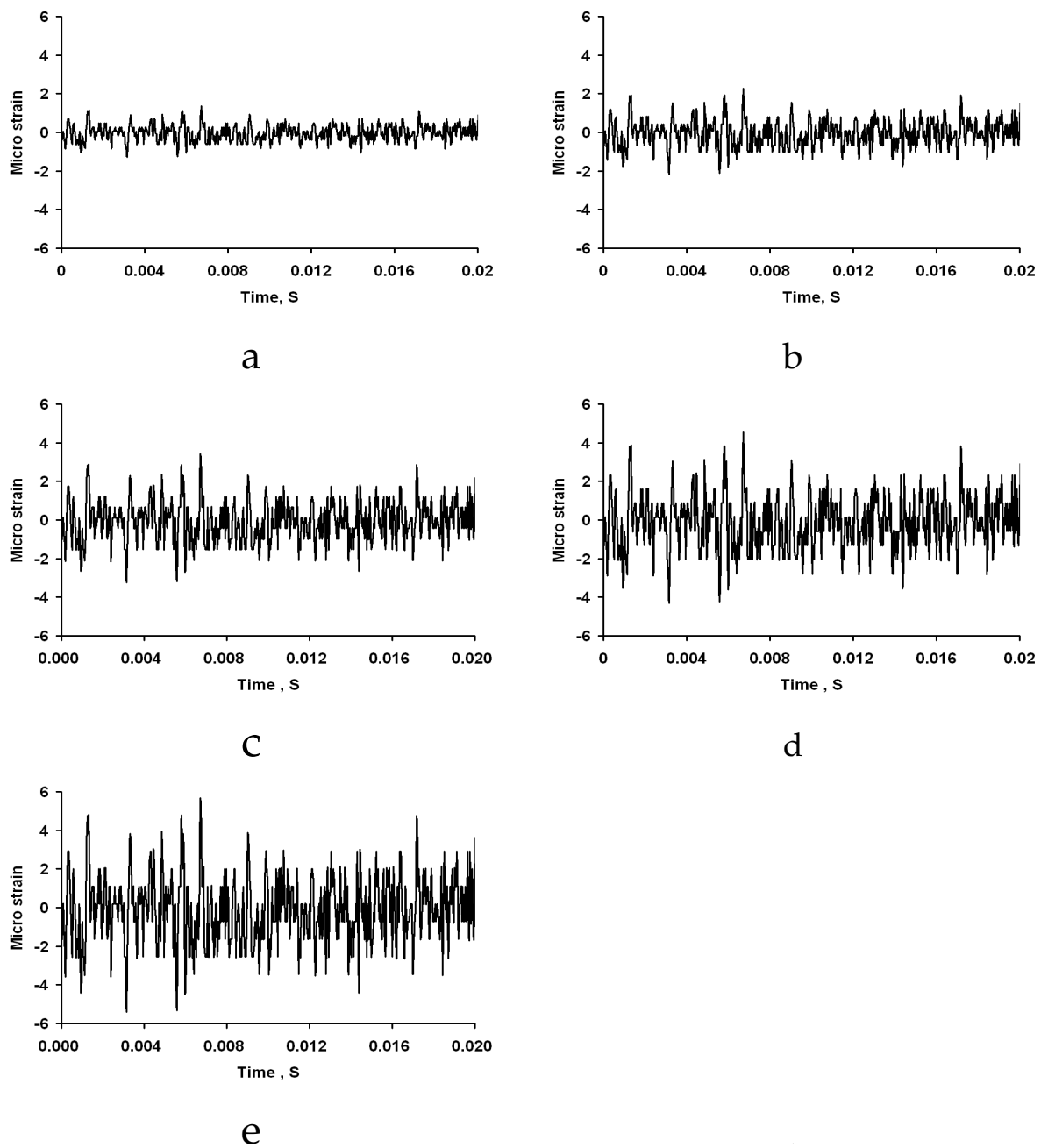
Figure 6.13: Typical strain gauge time domain signal for (a) new cutting tool (b) 0.2 mm flank wear cutting tool (c) 0.3 mm flank wear cutting tool (d) 0.4 mm flank wear cutting tool (e) 0.5 mm flank wear cutting tool. Cutting speed = 500 m/min, feed rate = 500 mm/min and depth of cut = 5 mm.
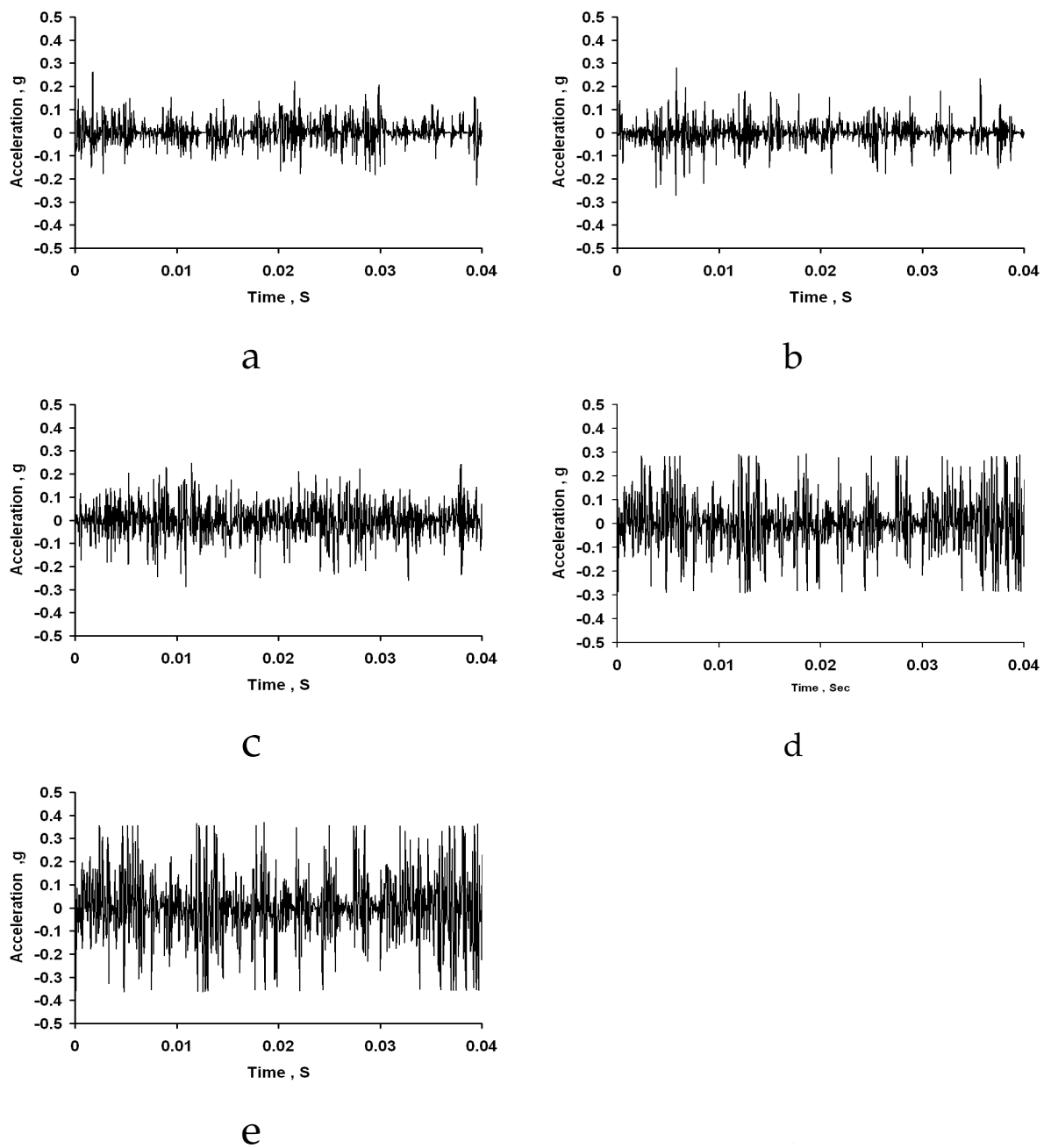
Figure 6.14: Typical accelerometer time domain signal in cutting direction for (a) new cutting tool (b) 0.2 mm flank wear cutting tool (c) 0.3 mm flank wear cutting tool (d) 0.4 mm flank wear cutting tool (e) 0.5 mm flank wear cutting tool. Cutting speed = 350 m/min, feed rate = 300 mm/min and depth of cut = 4 mm.
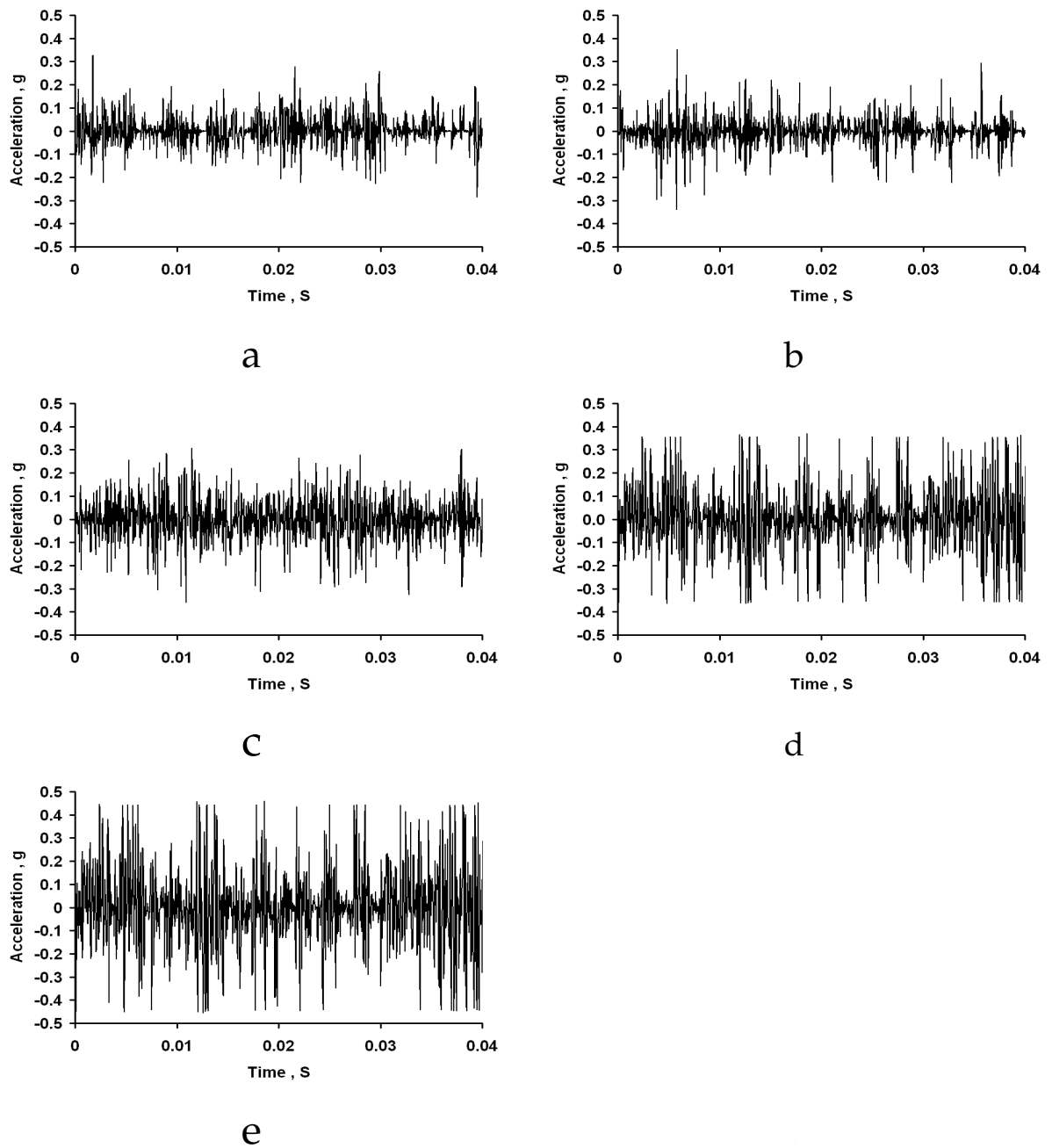
Figure 6.15: Typical accelerometer time domain signal in feed direction for (a) new cutting tool (b) 0.2 mm flank wear cutting tool (c) 0.3 mm flank wear cutting tool (d) 0.4 mm flank wear cutting tool (e) 0.5 mm flank wear cutting tool. Cutting speed = 350 m/min, feed rate = 300 mm/min and depth of cut = 4 mm.
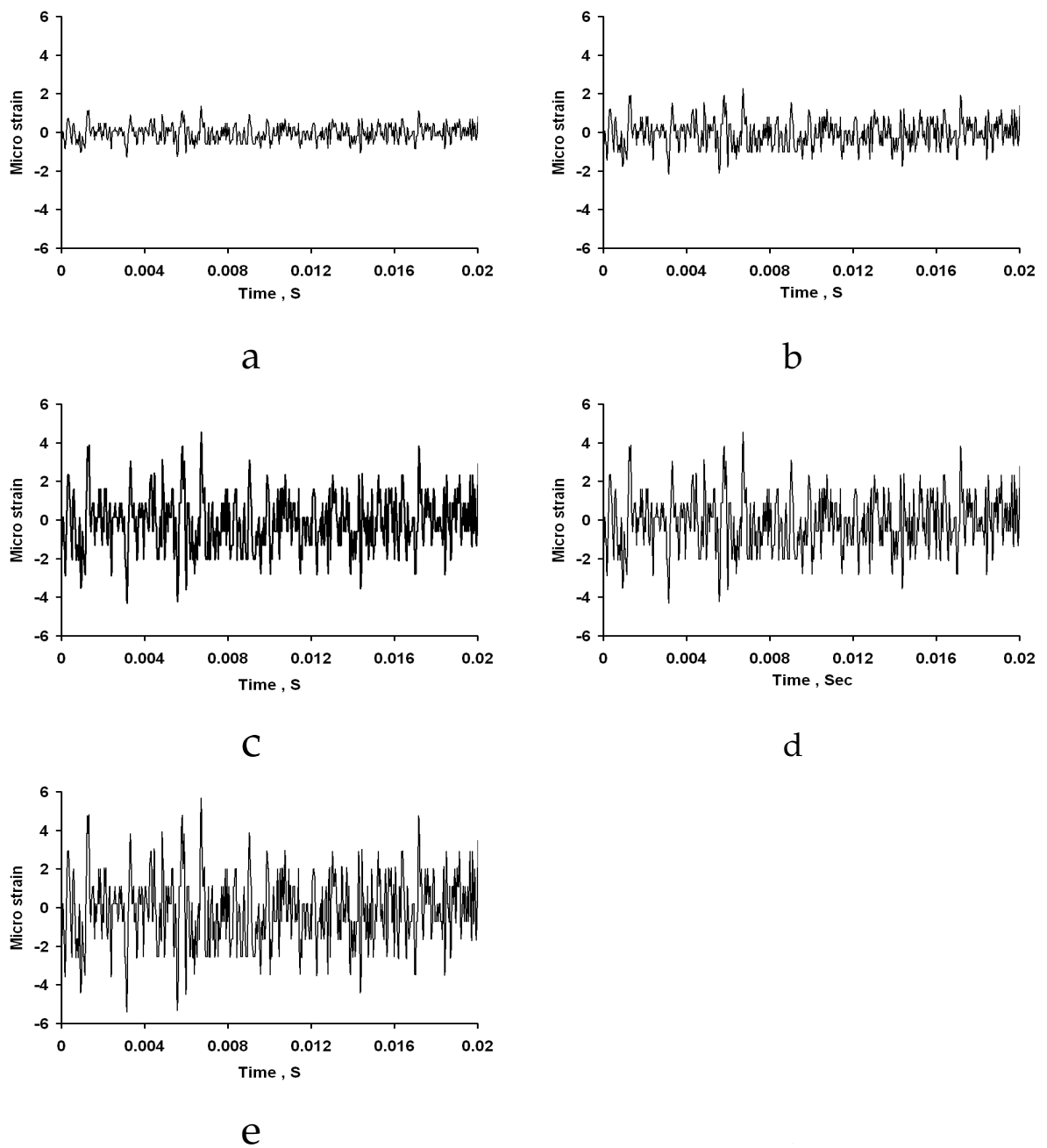
Figure 6.16: Typical strain gauge time domain signal for (a) new cutting tool (b) 0.2 mm flank wear cutting tool (c) 0.3 mm flank wear cutting tool (d) 0.4 mm flank wear cutting tool (e) 0.5 mm flank wear cutting tool. Cutting speed = 350 m/min, feed rate = 300 mm/min and depth of cut = 4 mm.

a

b

c

d

e
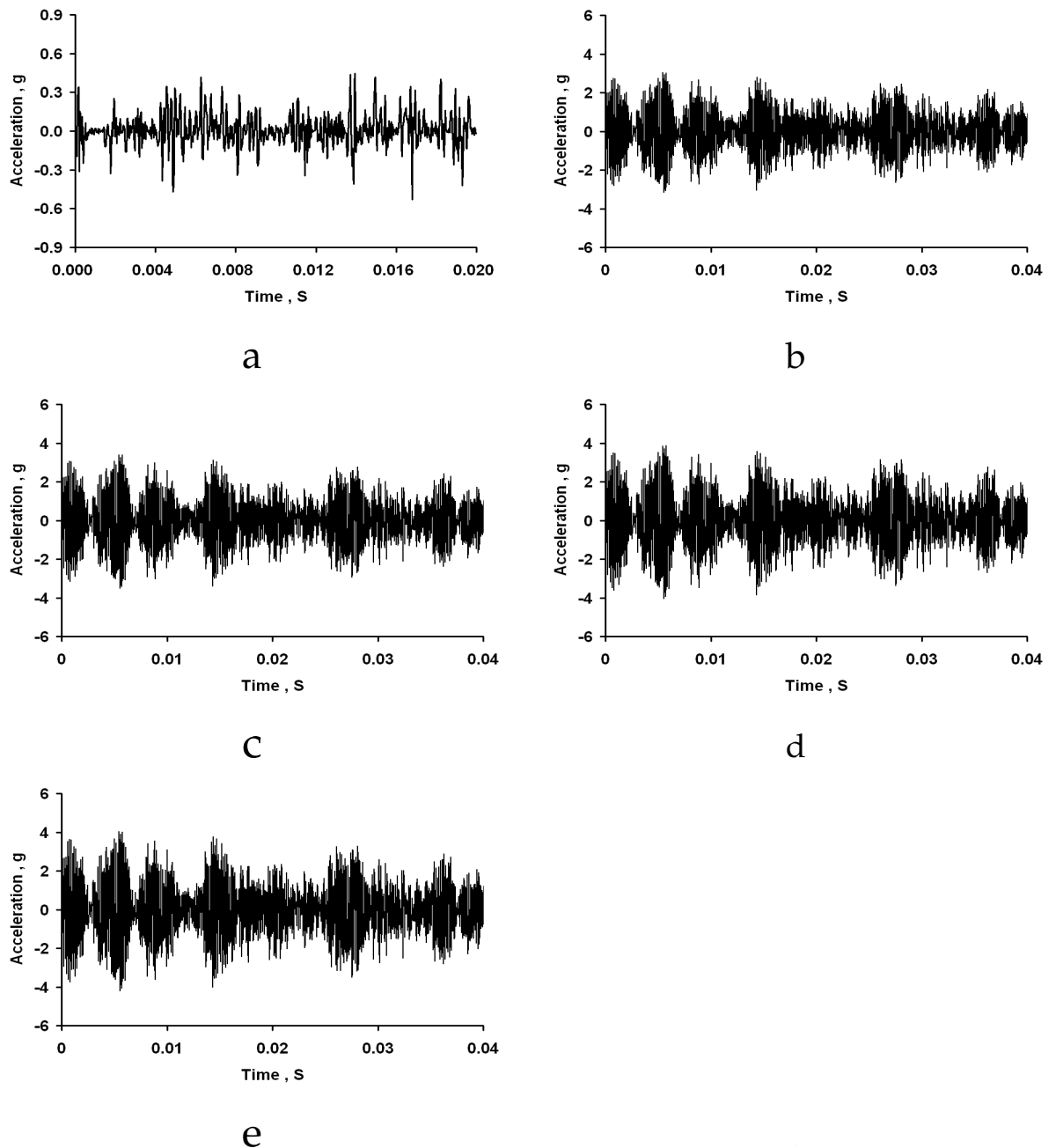
Figure 6.17: Typical accelerometer time domain signal in cutting direction for (a) new cutting tool (a) 0.2 mm chipping failure cutting tool (b) 0.3 mm chipping failure cutting tool (c) 0.4 mm chipping failure cutting tool (d) 0.5 mm chipping failure cutting tool. Cutting speed = 350 m/min, feed rate = 300 mm/min and depth of cut = 4 mm.
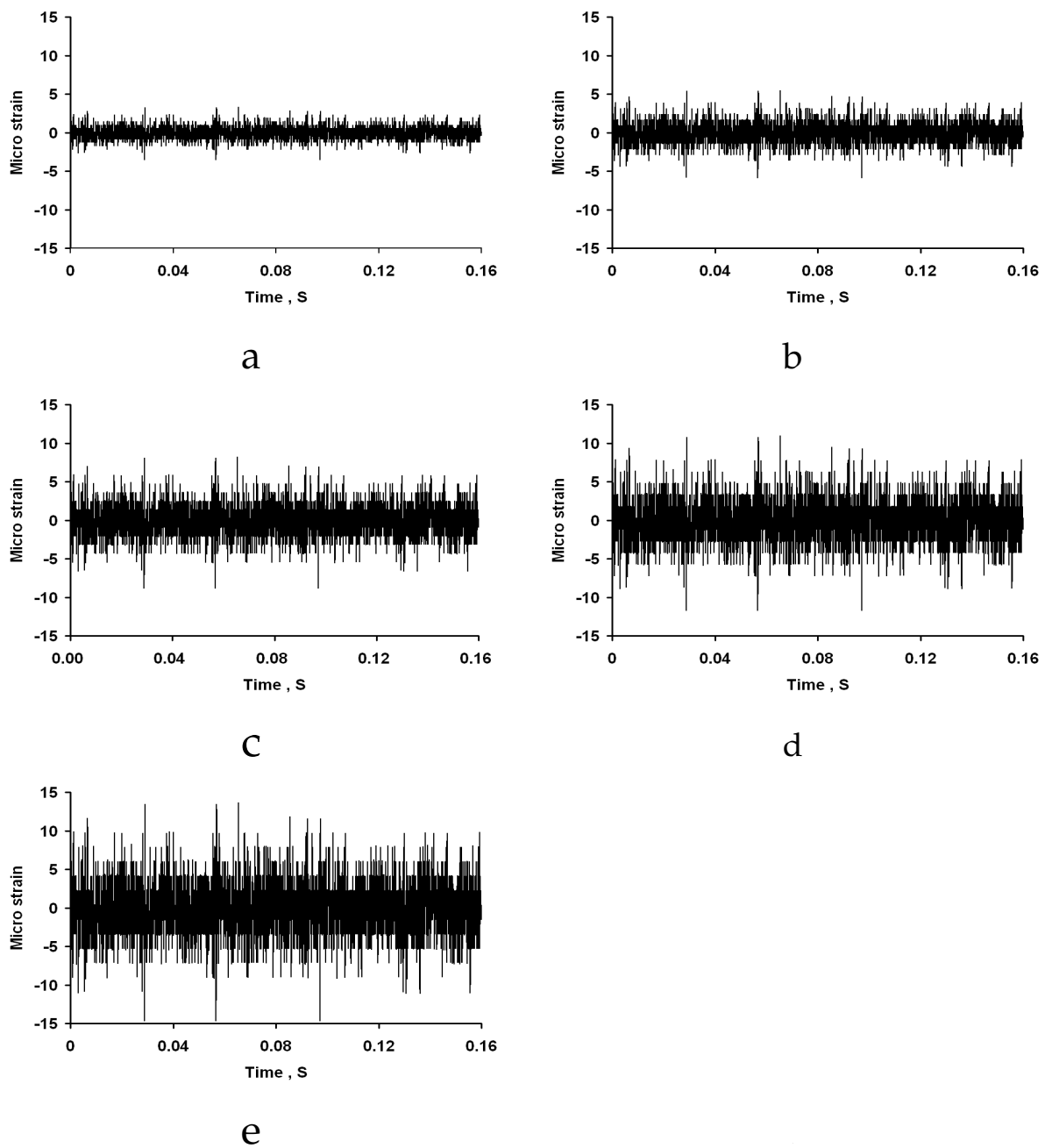
Figure 6.18: Typical strain gauge time domain signal for (a) new cutting tool (b) 0.2 mm chipping failure cutting tool (c) 0.3 mm chipping failure cutting tool (d) 0.4 mm chipping failure cutting tool (e) 0.5 mm chipping failure cutting tool. Cutting speed = 350 m/min, feed rate = 300 mm/min and depth of cut = 4 mm.
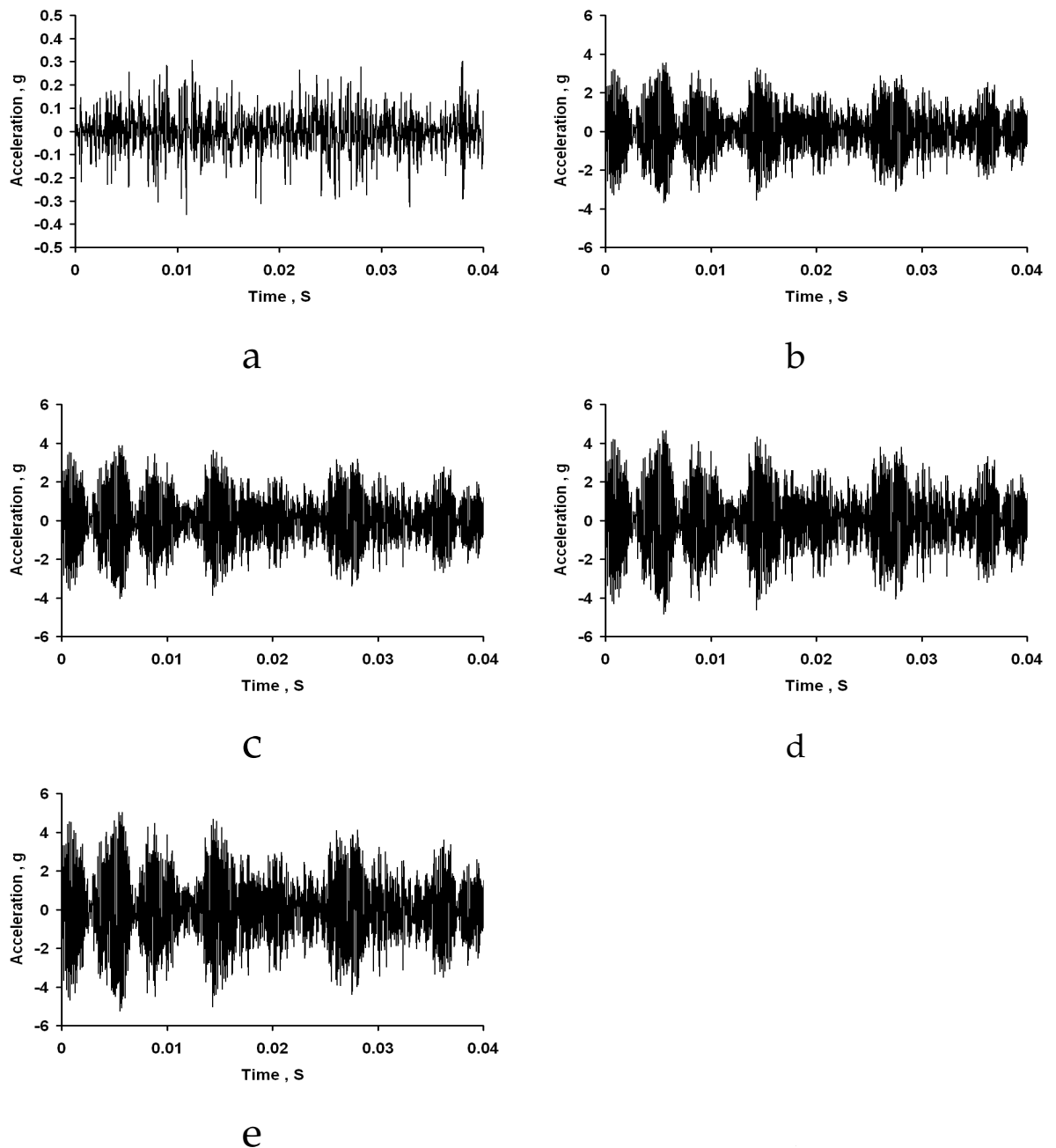
Figure 6.19: Typical accelerometer time domain signal in cutting direction for (a) new cutting tool (b) 0.2 mm chipping failure cutting tool (c) 0.3 mm chipping failure cutting tool (d) 0.4 mm chipping failure cutting tool (e) 0.5 mm chipping failure cutting tool. Cutting speed = 350 m/min, feed rate = 500 mm/min and depth of cut = 4 mm.
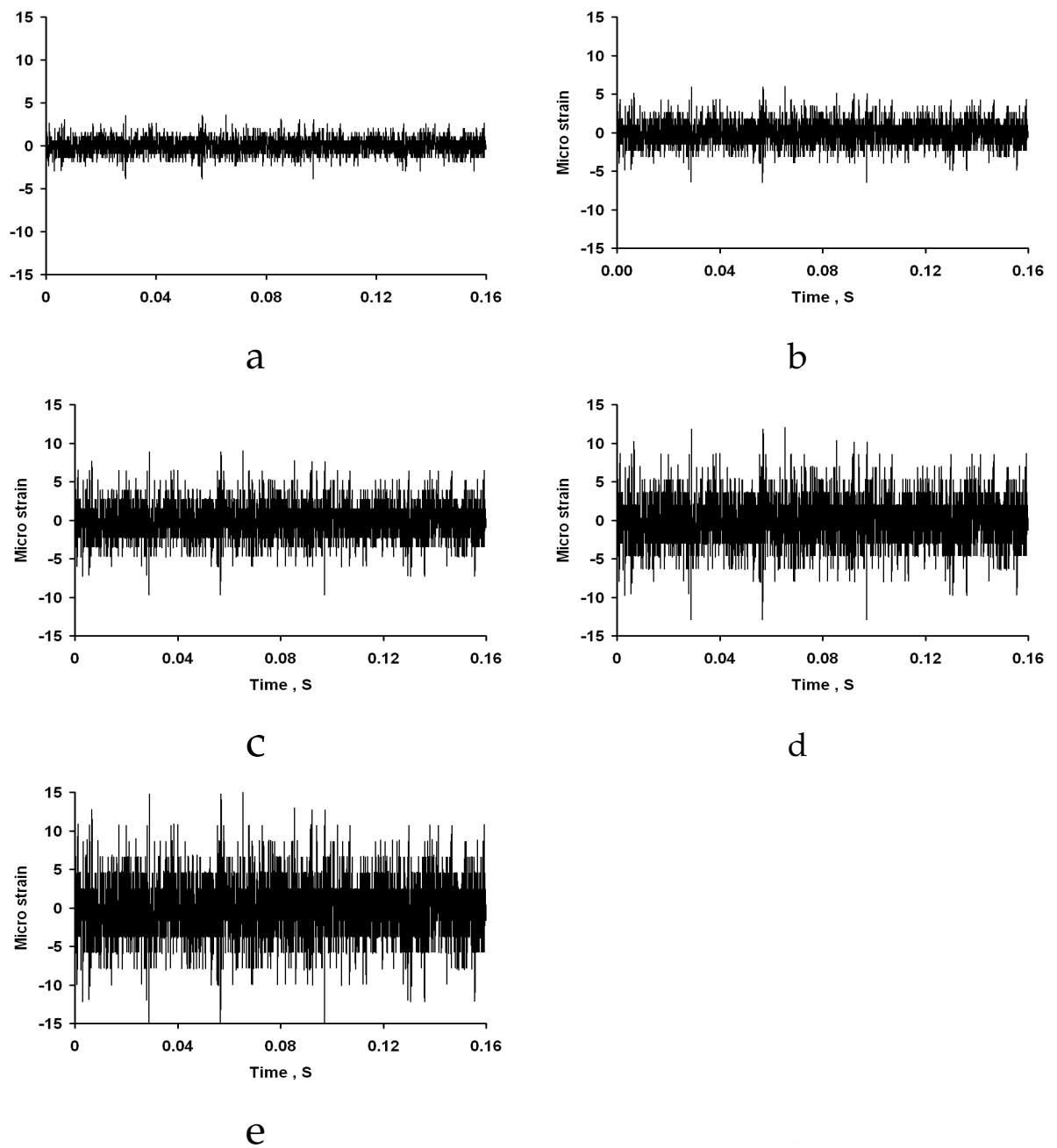
Figure 6.20: Typical strain gauge time domain signal for (a) new cutting tool (b) 0.2 mm chipping failure cutting tool (c) 0.3 mm chipping failure cutting tool (d) 0.4 mm chipping failure cutting tool (e) 0.5 mm chipping failure cutting tool. Cutting speed = 350 m/min, feed rate = 500 mm/min and depth of cut = 4 mm.

cutting like chip formation. In FEM, it is assumed that a part is divided into many small elements and it is subjected to deformation due to application of external load. The main idea in finite element method is to solve a complex problem by replacing it with a simple problem. By using the existing mathematical methods, in practice real or approximate solutions cannot be found for many problems. However, finite element method can be used to find approximate solutions for these problems. In finite element method, the solution zone is composed of adjacent sub parts which are called finite elements. It can be assumed that these sub parts are held together by nuts and screws. It is also assumed that when the bonding is removed, the sub parts are separated.

An analysis calculates the effects of steady state conditions on a structure, while ignoring inertia and damping effects, such as those caused by time-varying load. In a static analysis a rigidity matrix is calculated for each element according to the given specifications. These matrices are aggregated and the rigidity matrix of the system is generated. The solution is the displacements of the nodes that gives the unit displacements and strains. In this work, modal analysis is carried out to analyse dynamic behaviour of cutting tool using ANSYS. DNMG type of insert and the tool holder are modelled as of the same material. The mechanical properties of the tool holder are given in Table 6.2. The tool holder is fixed from the nodes that lie at the bottom and the top of the model in all degrees of freedom. Besides, dynamic force also exists that act onto the tool holder.

Basic modal analysis involves Eigen value problems to calculate natural frequency of the any system. The governing equation for Eigen value analysis of the system is given by (equation 6.28)

$$M\frac{\partial^2 x}{\partial^2 t} + Kx = f(t) \tag{6.28}$$

where M is mass of the system, K is stiffness of the system and x is the displacement. Considering the homogeneous part of equation 6.28 and assuming that the displacement response is harmonic is given by 6.29,

$$x(t) = X(\omega)e^{i\omega t} \tag{6.29}$$

The structural Eigen problem can be written in the form,

$$K\phi_j = \lambda_j M\phi_j, j = 1, 2, 3, ... \tag{6.30}$$

where, $\lambda_j = \omega_j^2$ is the jth Eigen value and ϕ_j is the jth Eigen vector. Solving the above equation 6.30, we can find out the natural frequencies and mode shapes of the systems.

In this thesis, modal analysis (ANSYS software) is used to determine the mode shapes and the natural frequencies of the cutting tool structure that are important in the design of a model for dynamic analysis. This can also be a starting point for a more detailed harmonic response analysis.

Firstly, a model is built to define the element types (hexagonal shape), material properties and the model geometry and the boundary condition are then defined. As the next step, first 4 mode shapes are determined and natural frequencies (with the values) are calculated. The natural frequencies and mode shapes are important parameters for dynamic loading conditions. From this we found following four natural frequencies as shown in Table 6.3. To validate the ANSYS model, Rap test has been conducted (Figure 5.3). Both the experimental (Rap test) and ANSYS results were compared. The mode shapes of the cutting tool vibration is shown in Figures 6.21-6.24. In this Rap test, accelerometer is kept on the tool holder and signal is recorded up to 5 kHz in the FFT analyser. From this analysis, it is observe that the accelerometer responses are showing peaks at a particularly in natural frequency of the tool in dynamic cutting

Table 6.2: Mechanical properties of the tool holder and workpiece

Tool mechanical properties	Tool holder	workpiece
Density	8.10 g/cm^3	7.85 g/cm^3
Poission ratio	0.3	0.3
Young's modulus	210 kN/mm^2	200 kN/mm^2
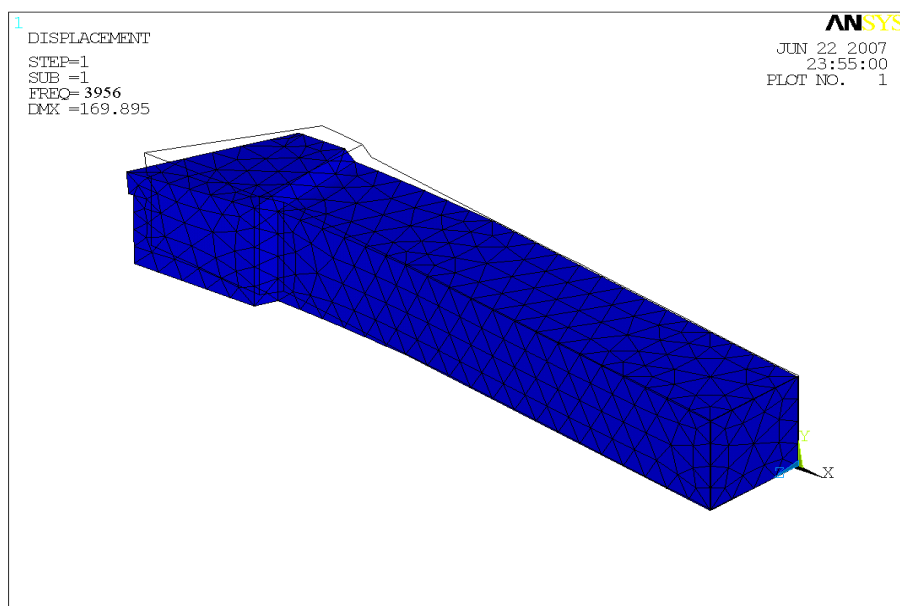
Figure 6.21: Mode of vibration in feed direction

conditions. This is very helpful to extract the information from various signals both accelerometer and strain gauge responses.

6.5   Finite Element Analysis of workpiece

In the area of cutting tool condition monitoring, most of the research papers deal with FEM analysis of cutting tool and only a few papers analysed workpiece. During experimentation (cutting operations) the accelerometer responses were
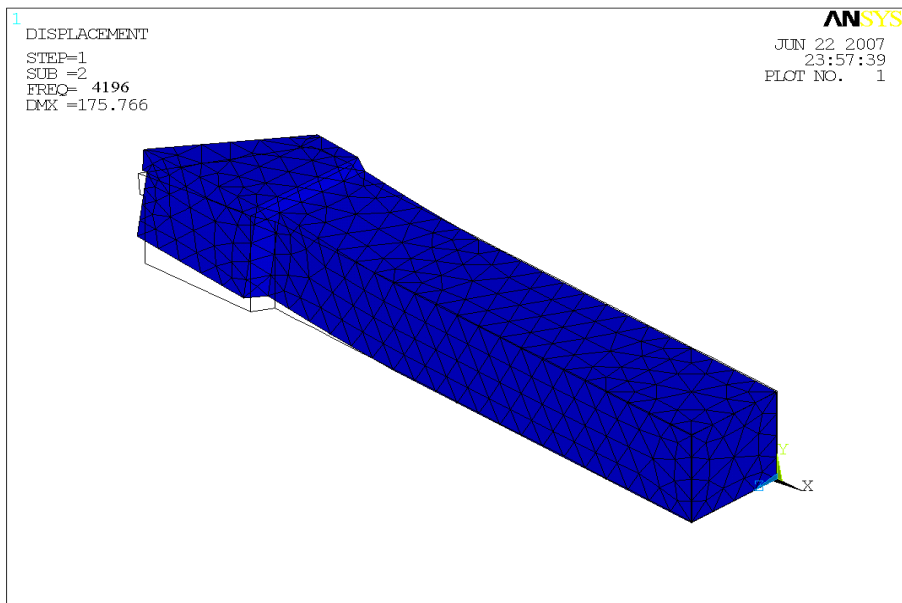
Figure 6.22: Mode of vibration in cutting direction
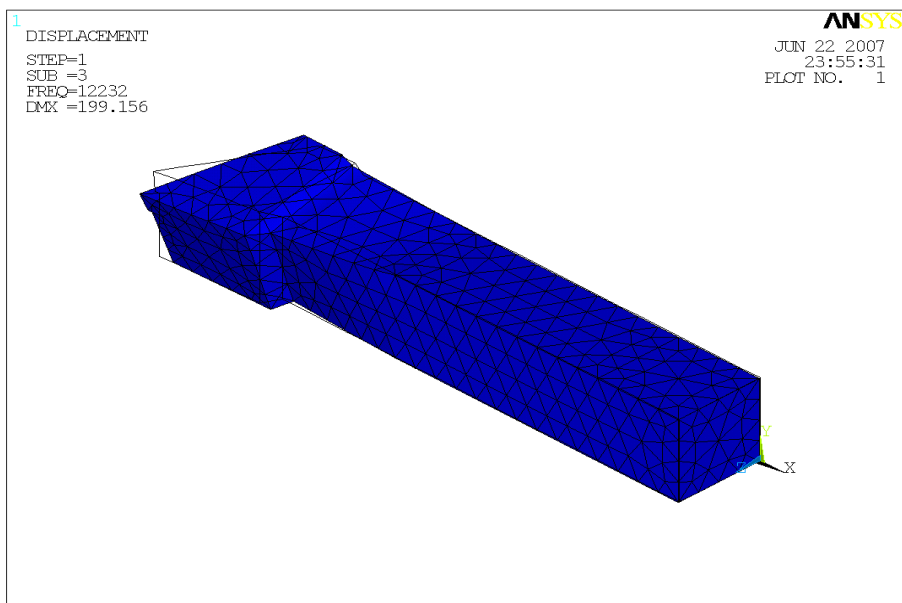
Figure 6.23: Torsional mode of vibration
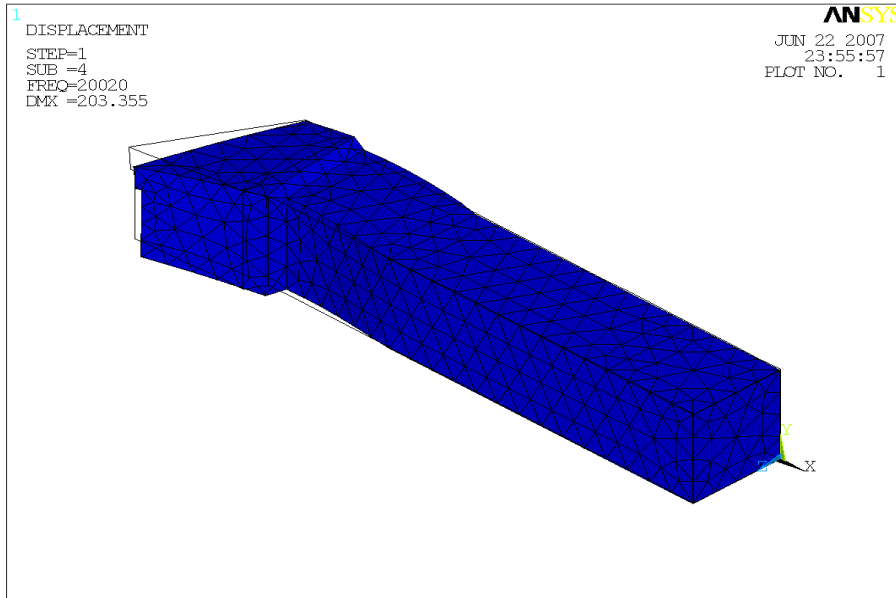
Figure 6.24: Mode of vibration in longitudinal direction

Table 6.3: Comparison of natural frequency of cutting tool

Mode number	FEM analysis, Hz	Rap test result, Hz
1	3956	3910
2	4196	4127
3	12232	limited up to 5 kHz
4	20020	limited up to 5 kHz

Table 6.4: Comparison of natural frequency of workpiece

Mode number	FEM analysis, Hz	Rap test result, Hz
1	316	340
2	986	937
3	1407	limited up to 1 kHz
4	2595	limited up to 1 kHz
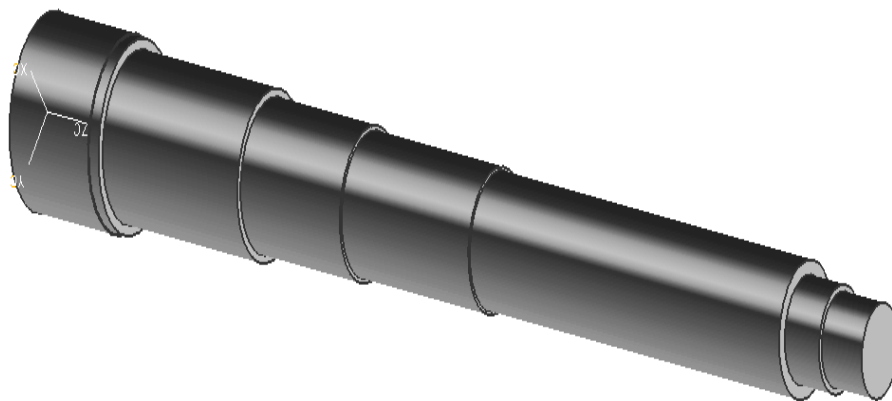
Figure 6.25: Typical assumed workpiece

observed in the frequency range of 300-500 Hz and show a negligible (small) amplitude of vibration (peaks). This is due to response of workpiece. The workpiece model has been developed (Figure 6.25) using ANSYS to study the dynamic behaviour. Then the above procedure (FEM model of cutting tool) and analysis (modal using ANSYS) is repeated for workpiece. These ANSYS results were validated (Table 6.4) with experimental results (Rap test as shown in Figure 6.30)and various mode shapes are shown in Figures (6.26 -6.29).

6.5.1 Remarks

Main aim of the thesis is to develop the sensor based TCM system. To achieve this goal, FEM modelling and analysis have been carried out to study the
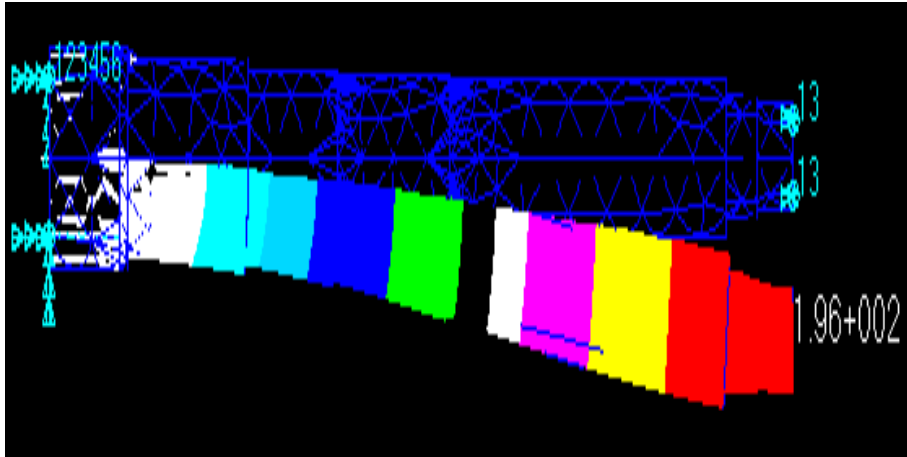
Figure 6.26: First mode of vibration workpiece
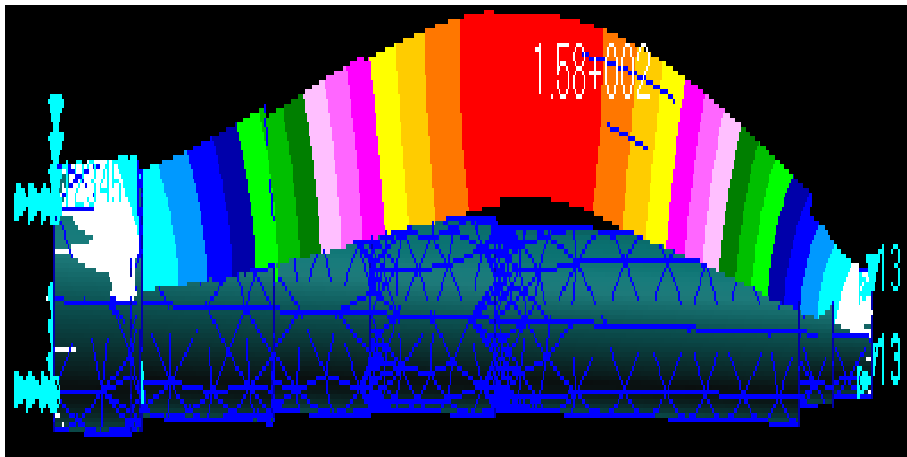
Figure 6.27: Second mode of vibration workpiece
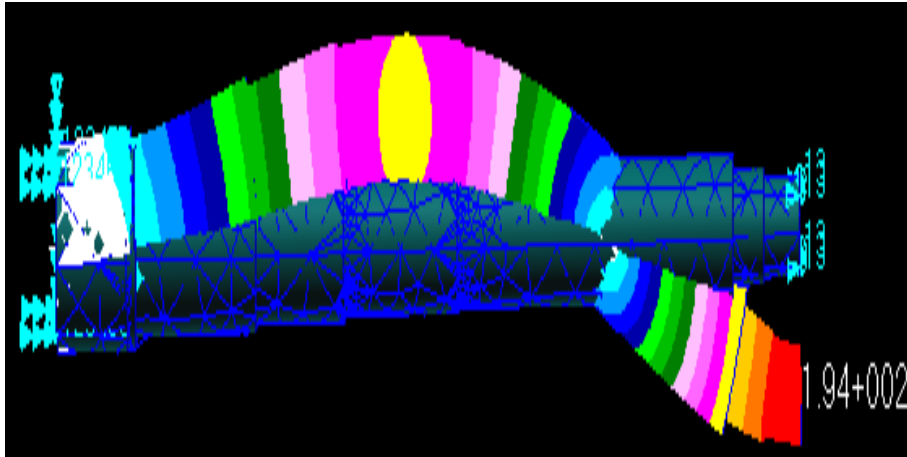
Figure 6.28: Third mode of vibration workpiece
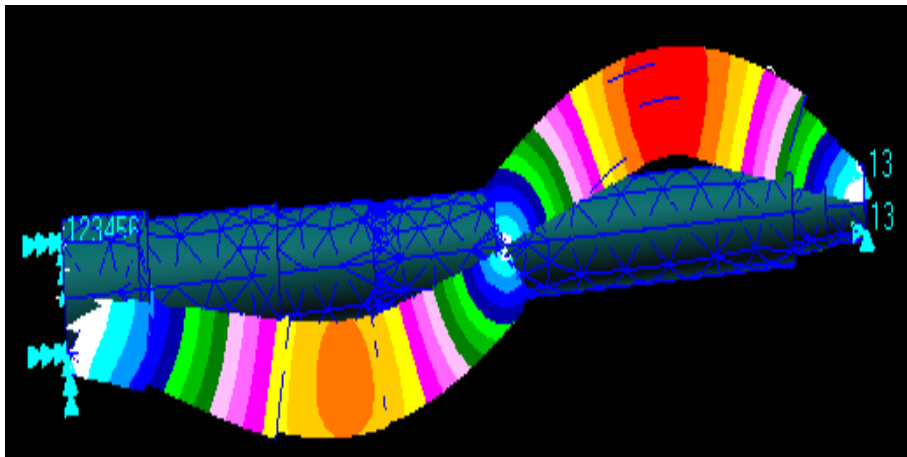
Figure 6.29: Fourth mode of vibration - workpiece
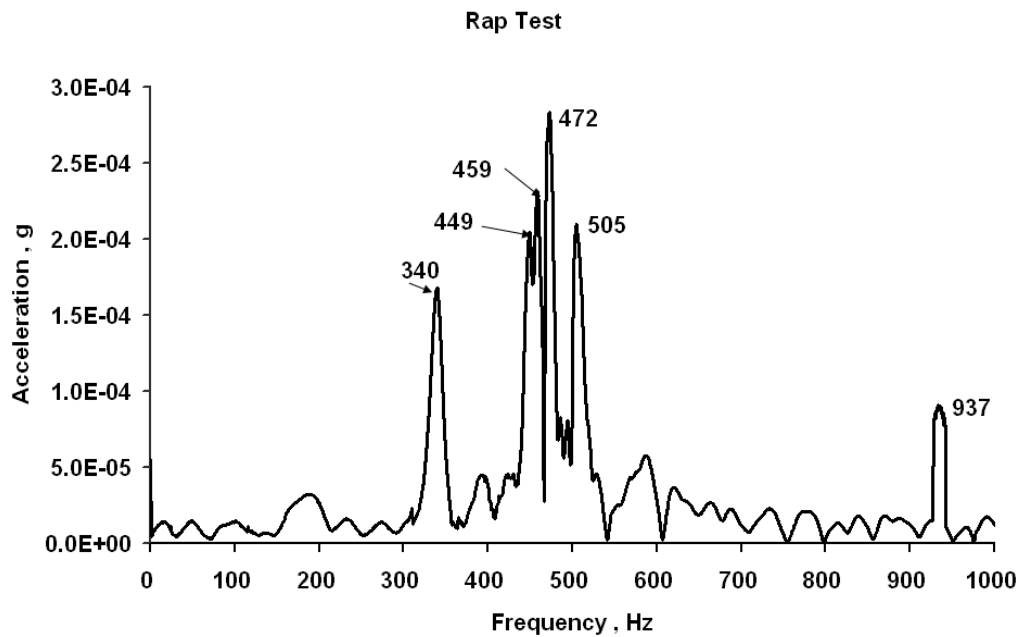
Figure 6.30: Rap test - Workpiece

dynamic behaviour of the cutting tool. Solid modelling has been carried out to using ANSYS software. The natural frequencies of the cutting tool and workpiece are obtained from modal analysis. This method provides simple approach to estimate the various modes of frequency in dynamic cutting conditions. In general, sensor will yield various signals with different amplitudes and frequencies, and it depends on various factors such as material properties, stiffness, spindle speed and so on. From the FEM analysis and experimental results (Rap test), it is found that first natural frequency of the cutting tool is 3.91 kHz (Figure5.3). This analysis is very much useful to extract the information from the sensors output in particular frequency domain analysis. It is observed that, while analysing the sensor output signals, some frequencies (Figure 6.30) are dominating in the range of 300 Hz to 500 Hz at low level amplitudes. These frequencies are natural frequencies of the workpiece at different modes. These frequencies may be ignored because of its low amplitude (in the order of 10^{-5}) when compared with tool vibration amplitude (in the

order of 10^{-3}). This analysis is mainly focused on cutting tool vibration and its mode shapes.

6.6   Frequency Domain based diagnosis

Typical Fast Fourier Transforms of the time domain signals are given in Figures 6.31 - 6.35. For frequency domain based diagnosis the (a) back-propagation algorithm and the (b) probabilistic network are employed. For statistical parameter based diagnosis only back-propagation methodology is used. The training and the test data, during the present study were generated on a CNC GILDMISTER turning center.

6.6.1   Feature extraction

Extraction of relevant information from the acquired data is critical for development of an effective diagnostic system. Prominent features are extracted from the signals and fed as a input to train a neural network. In the present work an algorithm is developed to automatically develop the feature vector from the power spectrum signal. There are two important sets of frequency components namely (i) operating frequency of spindle speed and (ii) the cutting tool natural frequency. In this analysis, it is observed that 3.91 kHz is the predominant frequency (varies between 3.8 kHz to 4.2 kHz) in the response signals (Figure 6.34). This is the natural frequency of the cutting tool. This is verified and validated with experimental Rap Test result (Figure 5.3).

6.6.2   Inputs for Neural Network

From the power spectrum signal the necessary information is extracted at particular frequency (say 3.91 kHz) and these amplitudes of vibration from the accelerometer and strain gauge signals are shown in the Table 6.5 for different
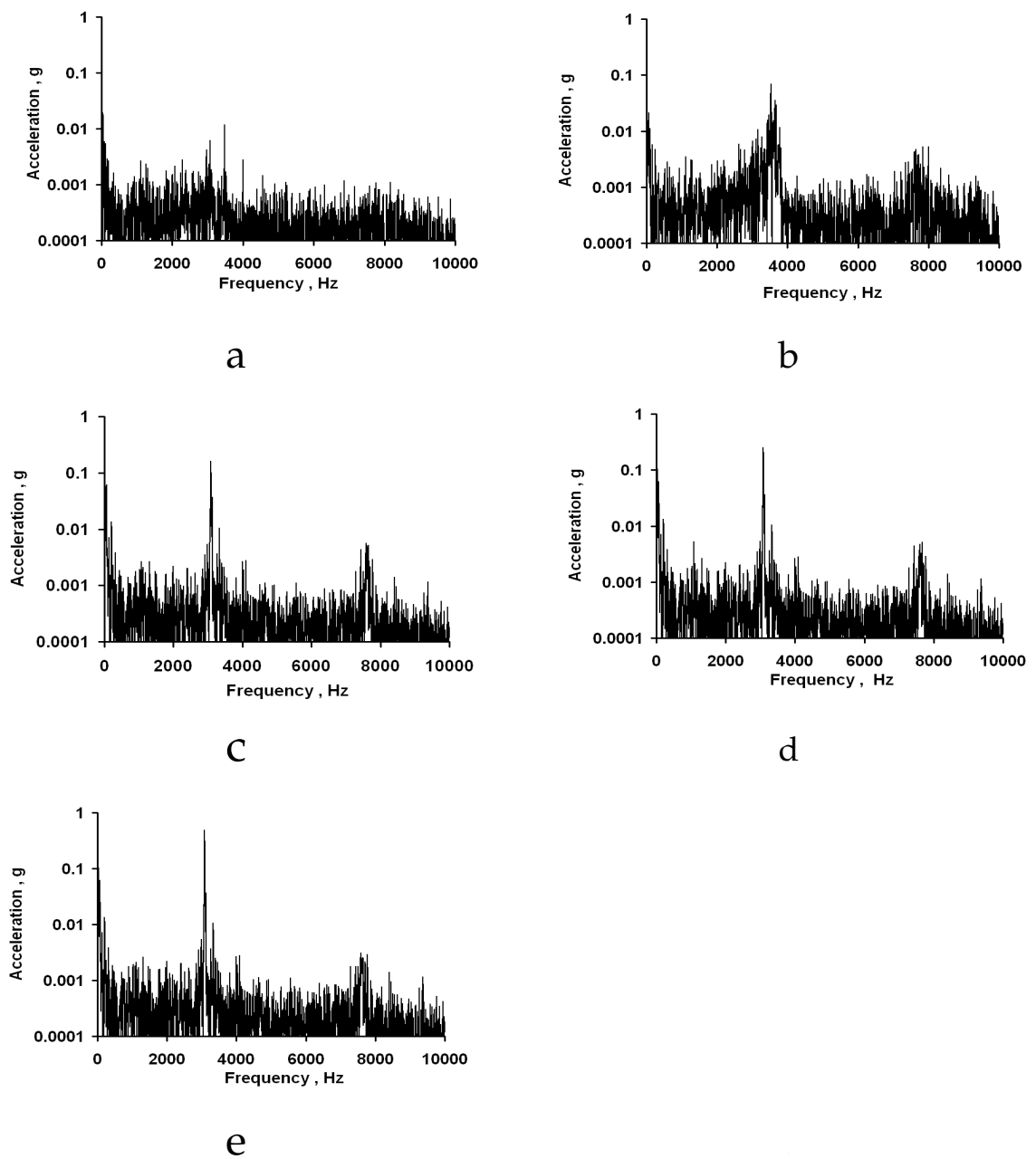
Figure 6.31: Typical accelerometer power spectrum signal in cutting direction for (a) new cutting tool (b) 0.2 mm flank wear cutting tool (c) 0.3 mm flank wear cutting tool (d) 0.4 mm flank wear cutting tool (e) 0.5 mm flank wear cutting tool. Cutting speed = 500 m/min, feed rate = 500 mm/min and depth of cut = 5 mm.
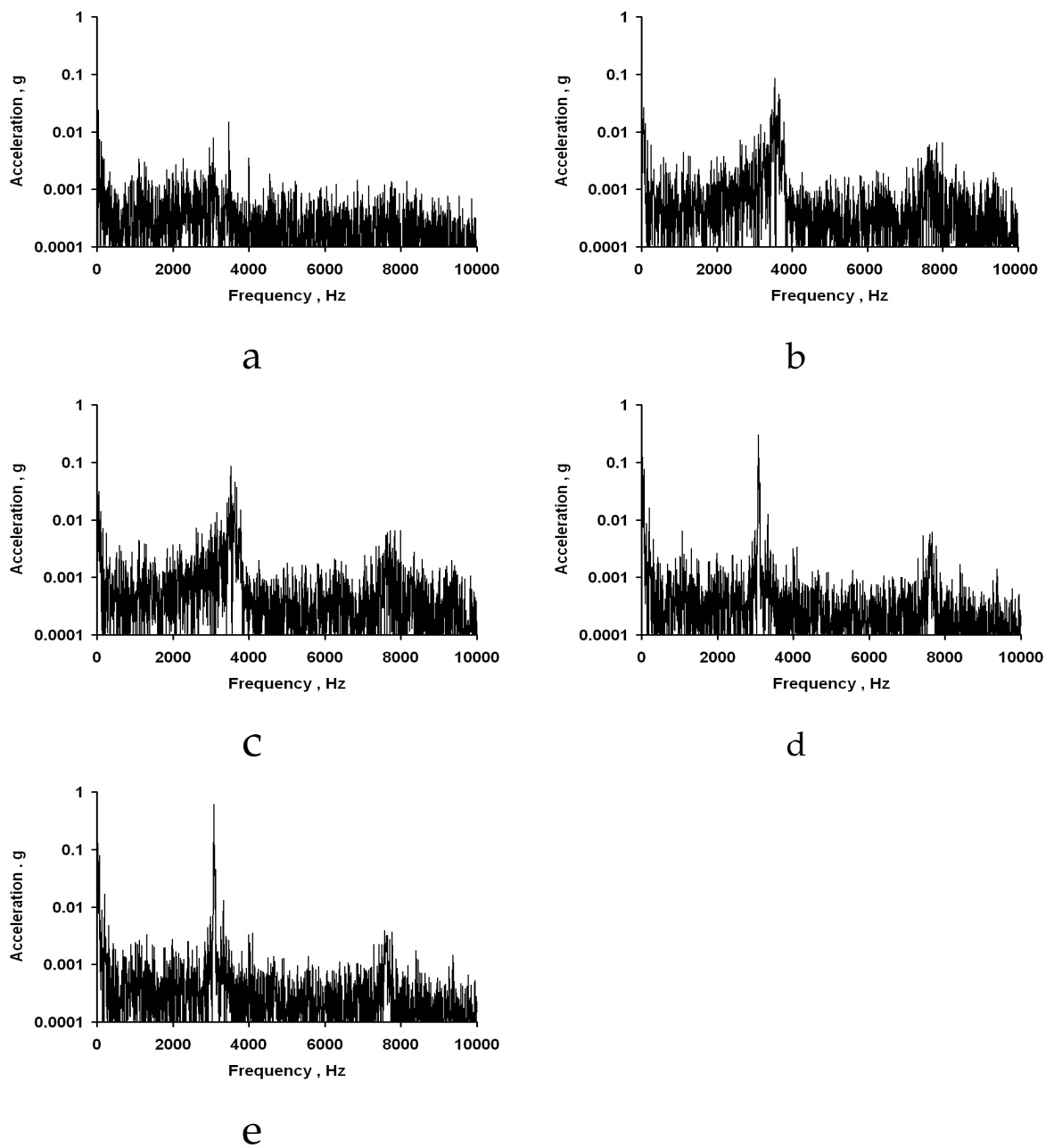
Figure 6.32: Typical accelerometer power spectrum signal in feed direction for (a) new cutting tool (b) 0.2 mm flank wear cutting tool (c) 0.3 mm flank wear cutting tool (d) 0.4 mm flank wear cutting tool (e) 0.5 mm flank wear cutting tool. Cutting speed = 500 m/min, feed rate = 500 mm/min and depth of cut = 5 mm.
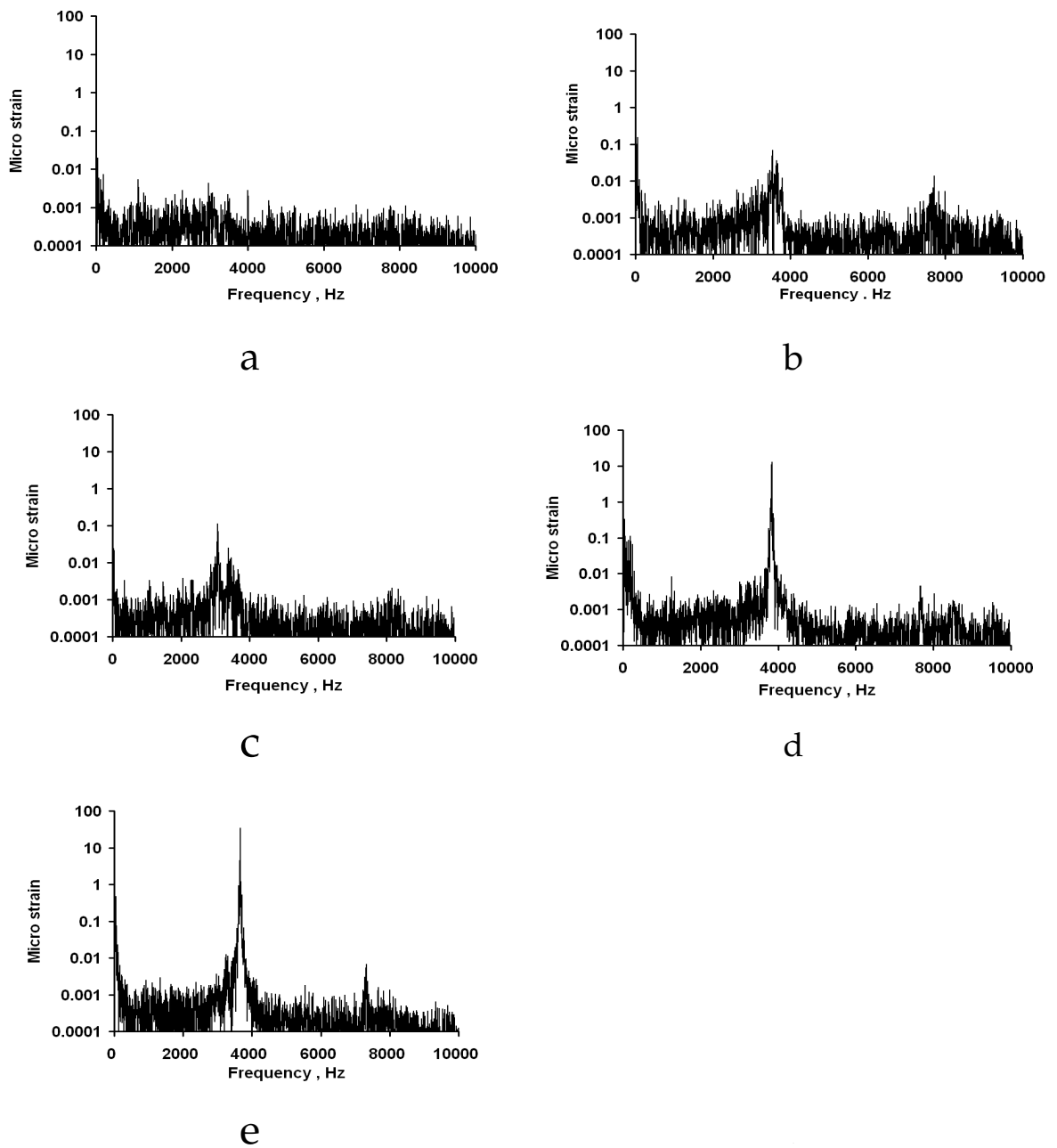
Figure 6.33: Typical strain gauge power spectrum signal for (a) new cutting tool (b) 0.2 mm flank wear cutting tool (c) 0.3 mm flank wear cutting tool (d) 0.4 mm flank wear cutting tool (e) 0.5 mm flank wear cutting tool. Cutting speed = 500 m/min, feed rate = 500 mm/min and depth of cut = 5 mm.
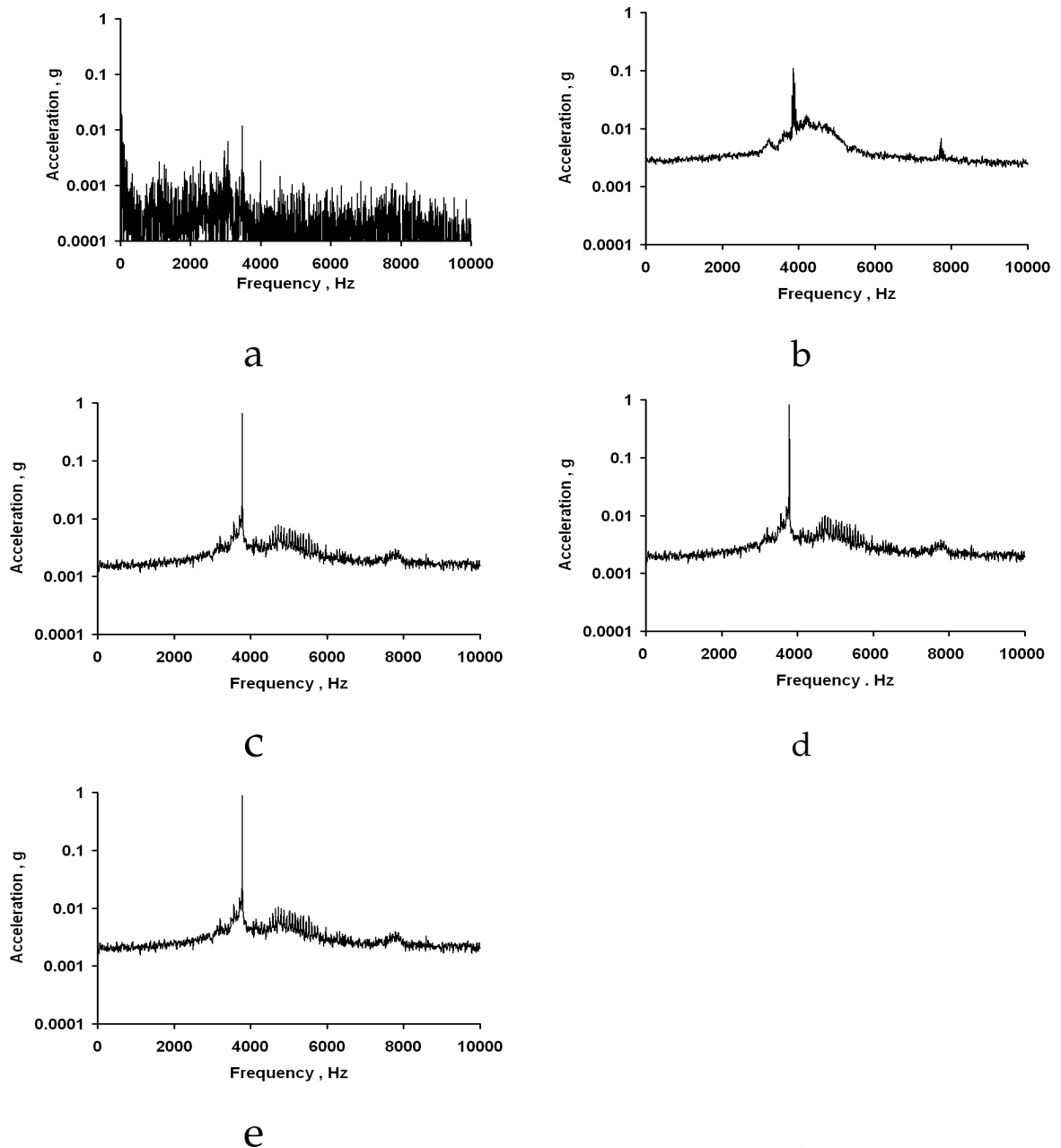
Figure 6.34: Typical accelerometer power spectrum signal in cutting direction for (a) new cutting tool (b) 0.2 mm chipping failure cutting tool (c) 0.3 mm chipping failure cutting tool (d) 0.4 mm chipping failure cutting tool (e) 0.5 mm chipping failure cutting tool. Cutting speed = 350 m/min, feed rate = 400 mm/min and depth of cut = 4 mm.
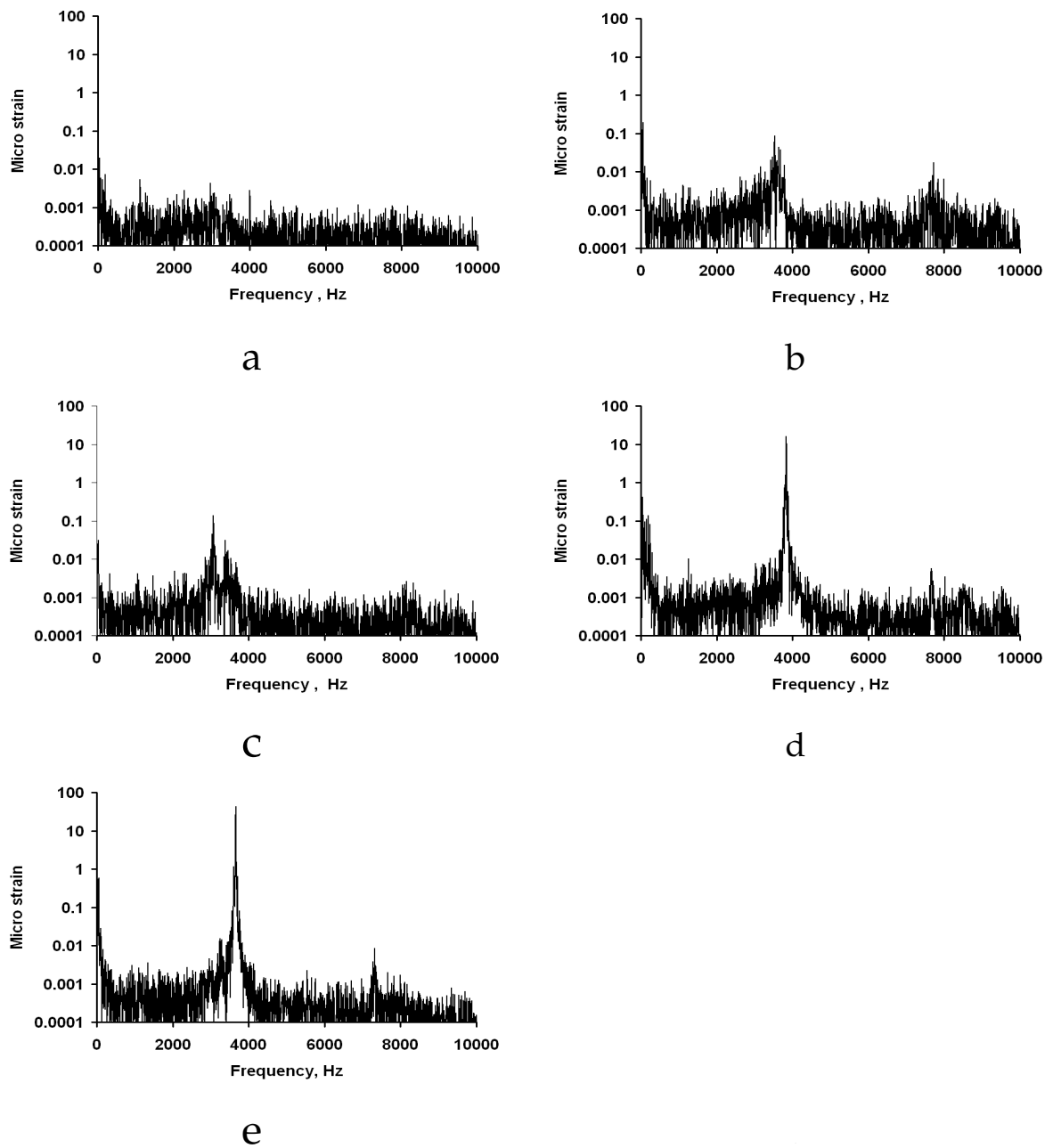
Figure 6.35: Typical strain gauge power spectrum signal for (a) new cutting tool (b) 0.2 mm chipping failure cutting tool (c) 0.3 mm chipping failure cutting tool (d) 0.4 mm chipping failure cutting tool (e) 0.5 mm chipping failure cutting tool. Cutting speed = 350 m/min, feed rate = 400 mm/min and depth of cut = 4 mm.

levels of flank wear. These are also shown in in Figure 6.36. The data from Figure 6.36 is used as input to train the neural network.

Table 6.5: Typical input vectors for neural networks

Ex No	Sensor number	FW = 0.5 mm	FW = 0.4 mm	FW = 0.3 mm	FW = 0.2 mm	New insert
1	1	0.2330	0.1580	0.0298	0.0091	0.0107
	2	0.2670	0.2450	0.0103	0.0089	0.0068
	3	7.4488	4.2373	0.0141	0.0211	0.0014
2	1	0.0528	0.0079	0.0131	0.0043	0.0026
	2	0.2370	0.0883	0.0065	0.0058	0.0037
	3	0.0274	0.1118	0.0013	0.0057	0.0004
3	1	0.0456	0.0196	0.0026	0.0009	0.0020
	2	0.1570	0.0277	0.0035	0.0025	0.0017
	3	0.0100	0.0017	0.0006	0.0023	0.0002

Sensor 1 - Accelerometer in cutting direction , Sensor 2 - Accelerometer in feed direction, Sensor 3 - Strain gauge and FW - Flank wear

6.6.3 Target Vectors for Training

The target vectors of neural networks are fixed as shown in Table 6.6. In Table 6.6, the first column (1 0 0 0 0) indicates the level of flank wear as 0.5 mm. Similarly the second column indicated the level of flank wear as 0.4, third indicate that level of flank failure as 0.3, and so on.

Table 6.6: Typical target vectors

Flank wear, mm	0.5	0.4	0.3	0.2	0.0
	1	0	0	0	0
Target	0	**1**	0	0	0
vectors	0	0	**1**	0	0
	0	0	0	**1**	0
	0	0	0	0	**1**
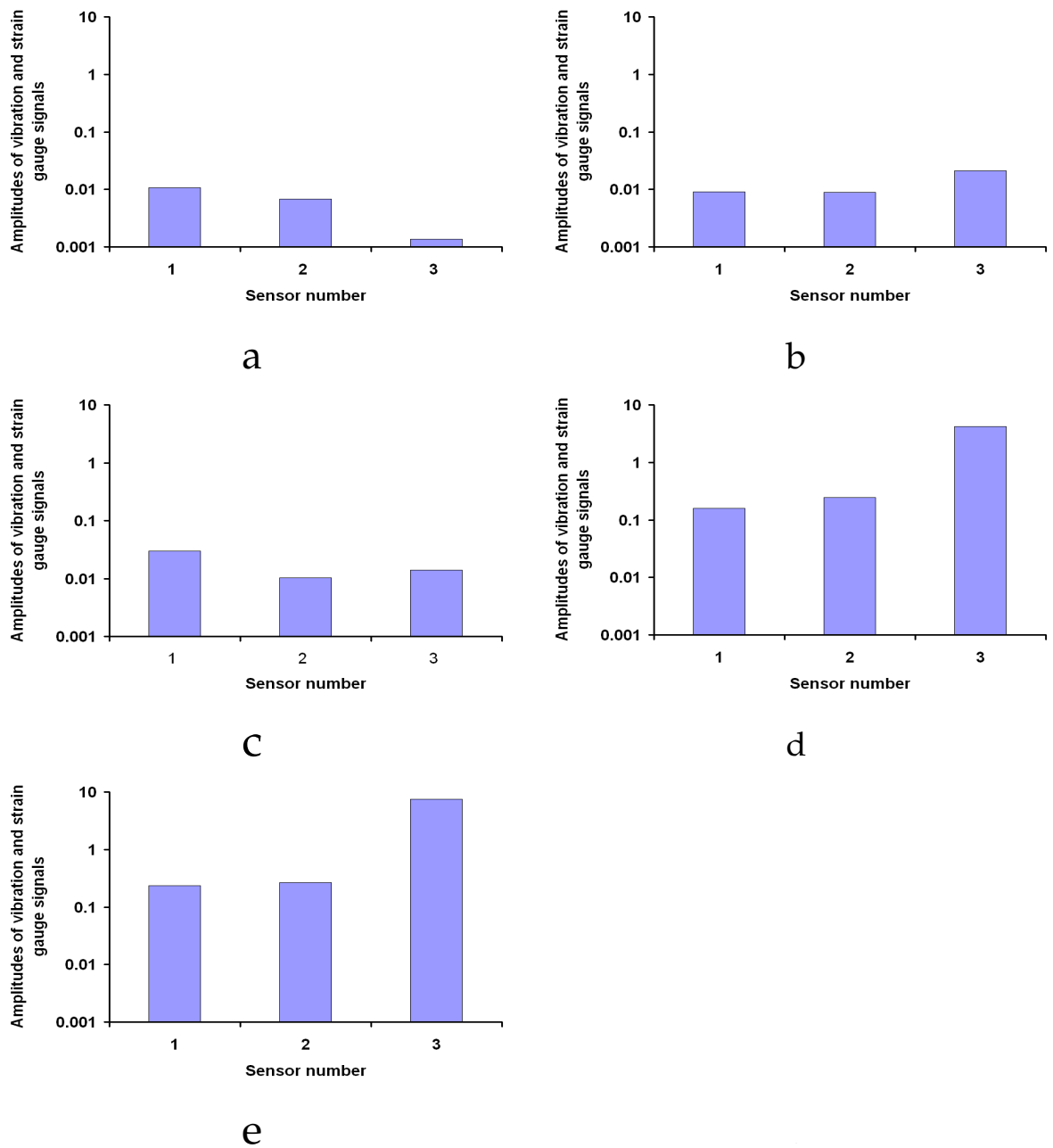
Figure 6.36: Typical input training vectors for (a) new cutting tool (b) 0.2 mm flank wear cutting tool (c) 0.3 mm flank wear cutting tool (d) 0.4 mm flank wear cutting tool (e) 0.5 mm flank wear cutting tool. Cutting speed = 500 m/min, feed rate = 500 mm/min and depth of cut = 5 mm.

6.6.4   Network Training and Testing

The neural network architecture, number of layers, nodes, transfer function and training pattern chosen in the present study are shown in Table 6.7. We have conducted 27 experiments with different combinations of machining conditions. On taking flank wear levels of 0, 0.2, 0.3, 0.4 and 0.5 mm as a parameter, the total number of experiments becomes 135(=27x5) as shown in Tables 4.4 - 4.6. Out of these, 110 experiments with different machining conditions have been selected for training and remaining 25 experiments are reserved for testing. Additionally, training algorithms, number of nodes, transfer functions and number of layers are varied to study the behaviour of networks and to arrive at an optimum configuration.

For single flank wear, the number of input terms in an input vector is 3, i.e. output responses of two accelerometers - in terms of vibration amplitude, g in cutting, and feed directions, and third one is strain gauge bridge output.

In this neural networks model, six layers feed forward back propagation neural networks with one input, four hidden layers and one-output layer were used. The training is carried out for five levels of flank wear (0, 0.2, 0.3, 0.4 and 0.5 mm). Different combinations of architecture were tried out for five different levels of flank wear.

The behaviour of neural networks architecture depends upon various parameters like input patterns to networks, target vectors (Table 6.6), number of layers, number of neurons, activation function, training function, number of epochs and so on. In this thesis an attempt has been made to classify the flank wear levels by using ANN.

The *trainrp* is found to be most robust training algorithm in terms of accuracy and time taken. The performance of various neural network architectures have been analyzed and some of them are described in Table 6.7. Out of these trials, Trial number 15 gives better convergence (Figure 7.27a), less computation time and

response of network is good enough to classify the flank wear levels. In Trial No 17, the network is not allowed to run for 20000 epochs because the rate of divergence increases with increases in number of epochs (after 1500 cycles) as shown in Figure 7.27b. It never converged to achieve the target level of accuracy 1×10^{-3} within 20000 epochs. On trial and error basis, the training of networks is allowed to run up to the maximum number of epochs like Trial No 5. However, this trial did not converge to the target level as shown in Figure 7.27c. Similarly, an attempt has been made to reduce the computational timings by selecting proper architecture of neural works (Trial No 15 of architecture 130-120-120-120-5). The same architecture was used for both training and testing exercises. The typical testing results are shown in Tables 6.8 and 6.9 respectively for the the Trial No 15 and 18 for the experiment number 25.

Table 6.7: Neural network architecture parameters

Trial No	Network architecture	Epochs	Transfer functions	Comments	Prediction %
1	100-100-100-100-5	20000	*logsig,logsig,logsig,tansig,logsig*	Not converged, attained max epochs	92.8
2	110-110-110-110-5	20000	*logsig,logsig,logsig,tansig,logsig*	Not converged, attained max epochs	94.1
3	120-120-120-120-5	7390	*logsig,logsig,logsig,logsig,tansig,logsig*	Converged	100
4	125-125-120-5	5386	*logsig,logsig,logsig,logsig,tansig,logsig*	Converged	100
5	125-125-125-5	20000	*logsig,logsig,logsig,logsig,tansig,logsig*	Not converged, attained max epochs	98.6
6	130-130-130-120-5	4049	*logsig,logsig,logsig,logsig,tansig,logsig*	Converged	100
7	130-130-130-125-5	5029	*logsig,logsig,logsig,logsig,tansig,logsig*	Converged	100
8	130-130-130-130-5	9251	*logsig,logsig,logsig,logsig,tansig,logsig*	Training stopped (non convergence)	84.5
9	140-140-130-120-5	6351	*logsig,logsig,logsig,logsig,tansig,logsig*	Training stopped (non convergence)	82.4
10	140-140-130-125-5	3351	*logsig,logsig,logsig,logsig,tansig,logsig*	Training stopped (non convergence)	68.3
11	140-140-140-120-5	4051	*logsig,logsig,logsig,logsig,tansig,logsig*	Training stopped (non convergence)	74.6
12	150-140-130-120-5	6851	*logsig,logsig,logsig,logsig,tansig,logsig*	Training stopped (non convergence)	78.9
13	150-150-120-5	4901	*logsig,logsig,logsig,logsig,tansig,logsig*	Training stopped (non convergence)	72.5
14	150-150-150-5	20000	*logsig,logsig,logsig,logsig,tansig,logsig*	Not converged, attained max epochs	83.5
15*	**130-120-120-120-5**	**1863**	*logsig,logsig,logsig,logsig,tansig,logsig*	**Converged**	100
16	120-120-120-5	4113	*logsig,logsig,logsig,logsig,tansig,logsig*	Converged	100
17	140-130-130-120-5	1851	*logsig,logsig,logsig,logsig,tansig,logsig*	Training stopped (non convergence)	68.7
18	130-120-100-5	2052	*logsig,logsig,logsig,logsig,tansig,logsig*	Converged	100
19	130-130-120-5	3311	*logsig,logsig,logsig,logsig,tansig,logsig*	Converged	100

*Trial No 15, the architecture of 130-120-120-120-5 is giving best convergence, less computation time and response of training is good enough to classify the flank wear at various levels.

Table 6.8: Output data for Trial No 15 (130-120-120-120-5)

	Ex No 25 (Flank wear levels, mm)				
	0.5	**0.4**	**0.3**	**0.2**	**0.0**
Output	**1.000**	0.000	0.000	0.002	-0.011
vectors	-0.003	**0.999**	0.000	-0.005	0.003
	-0.001	-0.001	**0.991**	-0.004	0.011
	-0.001	0.000	-0.003	**0.991**	0.013
	-0.001	-0.001	0.002	-0.005	**0.954**

Table 6.9: Output data for Trial No 18 (130-120-120-100-5)

	Ex No 25 (Flank wear levels, mm)				
	0.5	**0.4**	**0.3**	**0.2**	**0.0**
Output	**1.000**	0.029	0.059	0.100	0.100
vectors	0.053	**0.982**	0.065	-0.100	-0.100
	0.008	0.008	**0.993**	-0.086	-0.100
	-0.049	-0.048	-0.038	**1.000**	-0.099
	0.070	0.069	-0.091	-0.100	**0.963**

6.7 Network model to predict both flank wear and chipping failure

An ANN model for predicting and making a distinction between flank and chipping problems of different severity levels has also been attempted. The Chipping failure data are shown in the Tables 6.10 and 6.11. For Flank Wear experimental data is the same as given previously in Tables 4.4, 4.5 and 4.6.

The combined input vectors for doing such prediction is typically shown in Figures 6.38 and 6.39 and Table 6.12. The target vectors of neural networks are fixed as shown in Table 6.13. In Table 6.13, the first column (1 0 0 0 0 0 0 0 0 0) indicates the level of flank wear as 0.5 mm. Similarly the second column indicates the level of chipping failure as 0.5, third indicates the level of flank failure as 0.4.

Table 6.10: Accelerometer data for chipping failure

	Experimental conditions			Acceleration , g for different levels of chipping failure (mm)				
No	**CS**	**FR**	**DOC**	**0.5**	**0.4**	**0.3**	**0.2**	**0.0**
1	500	500	5	0.4194	0.2923	0.0519	0.0155	0.0177
2	500	500	4	0.0950	0.0147	0.0228	0.0074	0.0043
3	500	500	3	0.0821	0.0363	0.0046	0.0014	0.0033
4	500	300	5	0.1366	0.0551	0.0230	0.0192	0.0116
5	500	300	4	0.0700	0.0147	0.0087	0.0098	0.0020
6	500	300	3	0.0626	0.0065	0.0082	0.0038	0.0023
7	500	100	5	0.0886	0.0061	0.0034	0.0048	0.0101
8	500	100	4	0.0558	0.0054	0.0034	0.0034	0.0052
9	500	100	3	0.0428	0.0023	0.0005	0.0010	0.0009
10	350	500	5	0.4950	0.4311	0.1827	0.0338	0.0183
11	350	500	4	0.3600	0.0370	0.0381	0.0090	0.0059
12	350	500	3	0.0569	0.0205	0.0066	0.0050	0.0056
13	350	300	5	0.4554	0.0844	0.0430	0.0218	0.0136
14	350	300	4	0.2772	0.0346	0.0157	0.0145	0.0101
15	350	300	3	0.0495	0.0096	0.0128	0.0072	0.0027
16	350	100	5	0.3402	0.0644	0.0183	0.0112	0.0106
17	350	100	4	0.1244	0.0213	0.0168	0.0016	0.0065
18	350	100	3	0.0193	0.0014	0.0045	0.0019	0.0015
19	200	500	5	0.4770	0.4903	0.4037	0.0587	0.0252
20	200	500	4	0.4176	0.1082	0.0419	0.0154	0.0157
21	200	500	3	0.3168	0.0120	0.0161	0.0148	0.0086
22	200	300	5	0.4338	0.1149	0.0454	0.0751	0.0218
23	200	300	4	0.2934	0.0720	0.0191	0.0167	0.0150
24	200	300	3	0.2844	0.0141	0.0101	0.0076	0.0032
25	200	100	5	0.1908	0.1134	0.0252	0.0219	0.0185
26	200	100	4	0.1103	0.0344	0.0170	0.0157	0.0087
27	200	100	3	0.0335	0.0077	0.0135	0.0086	0.0061
	CS=Cutting speed			FR=Feed rate		DOC=Depth of cut		

Table 6.11: Strain gauge data for chipping failure

Experimental conditions			Micro strain for different levels of chipping failure (mm)				
No	CS	FR	DOC	0.5	0.4	0.3	0.2	0.0
1	500	500	5	16.3874	8.5170	0.0269	0.0390	0.0024
2	500	500	4	0.0604	0.2246	0.0025	0.0105	0.0007
3	500	500	3	0.0220	0.0033	0.0012	0.0042	0.0004
4	500	300	5	1.8846	0.0422	0.0048	0.0136	0.0022
5	500	300	4	0.0492	0.0062	0.0021	0.0032	0.0003
6	500	300	3	0.0038	0.0022	0.0004	0.0010	0.0004
7	500	100	5	0.1100	0.7851	0.0013	0.0001	0.0013
8	500	100	4	0.0311	0.0159	0.0005	0.0010	0.0003
9	500	100	3	0.0033	0.0021	0.0005	0.0002	0.0002
10	350	500	5	30.738	11.630	0.7487	0.0393	0.4716
11	350	500	4	1.3068	0.0284	0.1381	0.0343	0.0025
12	350	500	3	0.2588	0.0090	0.0115	0.0289	0.0005
13	350	300	5	2.3883	3.6624	0.2421	0.0331	0.0243
14	350	300	4	0.7416	0.0208	0.0457	0.0036	0.0006
15	350	300	3	0.1599	0.0033	0.0303	0.0020	0.0003
16	350	100	5	0.1402	0.1601	0.0027	0.0003	0.0014
17	350	100	4	0.1067	0.0201	0.0024	0.0012	0.0005
18	350	100	3	0.0593	0.0023	0.0013	0.0018	0.0000
19	200	500	5	31.169	28.083	24.411	1.2135	0.6423
20	200	500	4	9.3221	0.6400	10.756	0.0245	0.0272
21	200	500	3	0.7077	0.1461	0.0320	0.0012	0.0109
22	200	300	5	5.4740	5.0013	0.8272	0.0447	0.0333
23	200	300	4	0.9535	0.0283	0.0613	0.0081	0.0218
24	200	300	3	0.2994	0.0073	0.0378	0.0007	0.0082
25	200	100	5	0.3190	0.1980	0.0210	0.0056	0.0013
26	200	100	4	0.2075	0.0570	0.0021	0.0015	0.0025
27	200	100	3	0.0629	0.0035	0.0017	0.0009	0.0002
CS = Cutting speed			FR = Feed rate		DOC = Depth of cut			
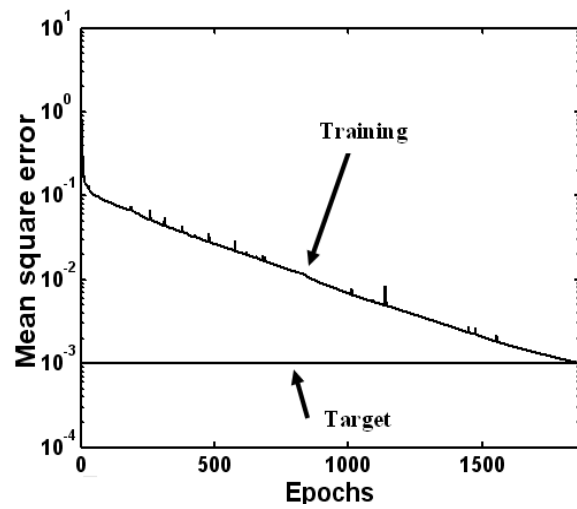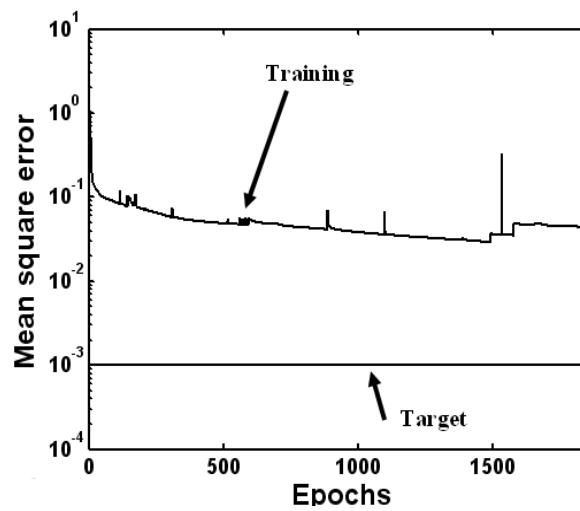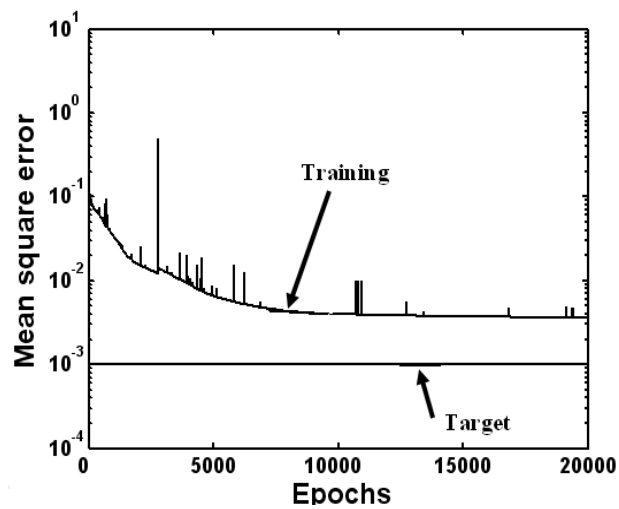
Figure 6.37: (a) Convergence pattern of back propagation networks for Trial No 15 (b) Convergence pattern of back propagation networks for Trial No 17 (c) Convergence pattern of back propagation networks for Trial No 5.
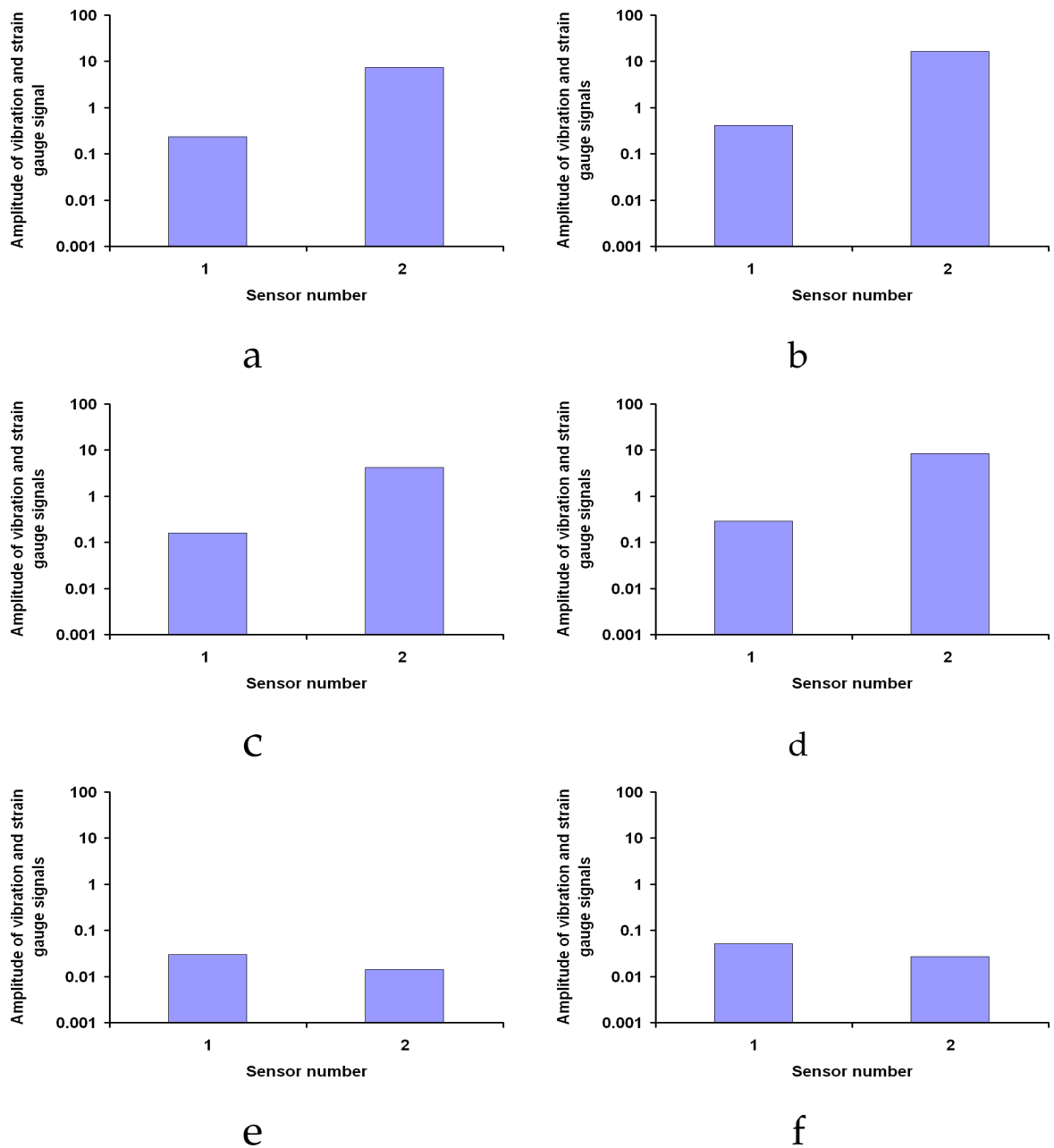
Figure 6.38: Typical input training vectors for (a) 0.5 mm flank wear cutting tool (b) 0.5 mm chipping failure cutting tool (c) 0.4 mm flank wear cutting tool (d) 0.4 mm chipping failure cutting tool (e) 0.3 mm flank wear cutting tool (f) 0.3 mm chipping failure cutting tool. Cutting speed = 500 m/min, feed rate = 500 mm/min and depth of cut = 5 mm.
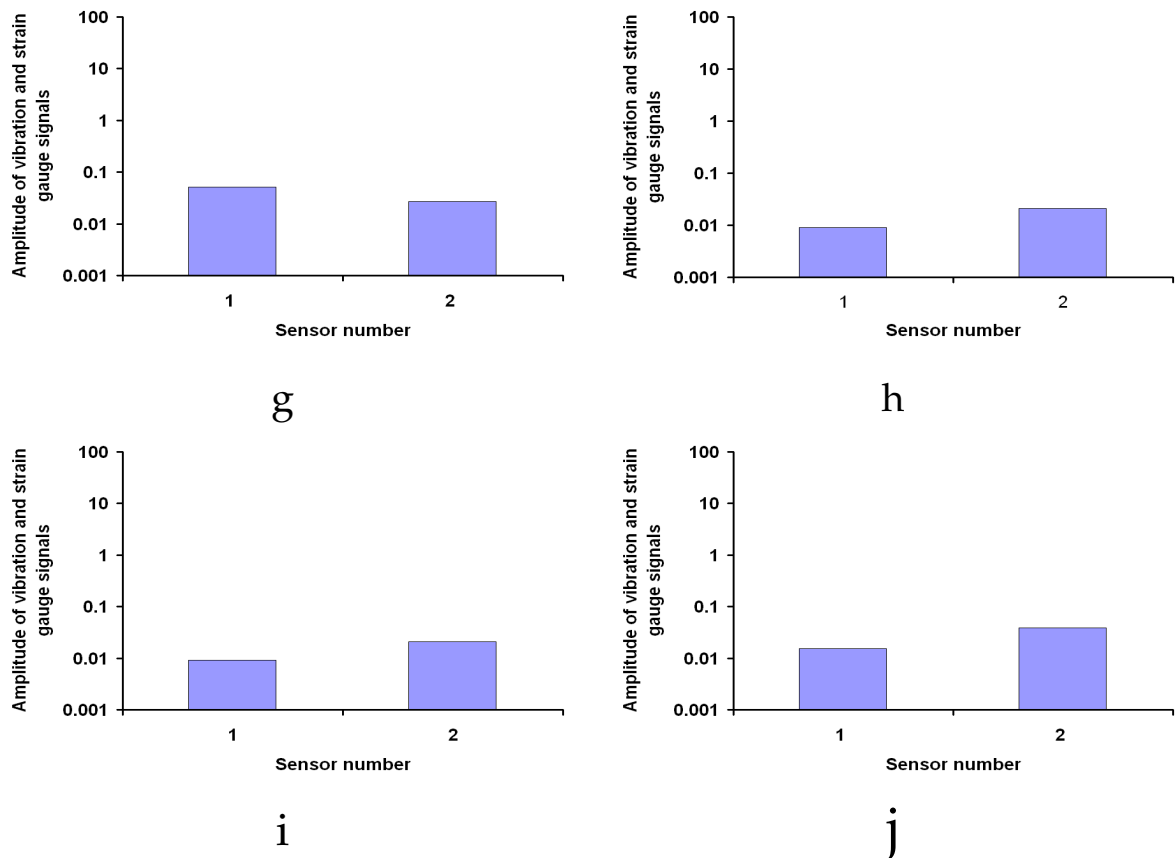
Figure 6.39: Typical input training vectors for (g) 0.2 mm flank wear cutting tool (h) 0.2 mm chipping failure cutting tool (i) new cutting tool (Flank wear) (j) new cutting tool (Chipping failure). Cutting speed = 500 m/min, feed rate = 500 mm/min and depth of cut = 5 mm.

Table 6.12: Typical input vectors for training the neural network

Ex No	Sensor number	F.W 0.5 mm	C.F 0.5 mm	F.W 0.4 mm	C.F 0.4 mm	F.W 0.3 mm	C.F 0.3 mm	F.W 0.2 mm	C.F 0.2 mm	F.W 0.0 mm	C.F 0.0 mm
1	1	0.2330	0.4194	0.1580	0.2923	0.0298	0.0519	0.0091	0.0155	0.0107	0.0177
	2	7.4488	16.387	4.2373	8.5170	0.0141	0.0269	0.0211	0.0390	0.0014	0.0024
2	1	0.0528	0.0950	0.0079	0.0147	0.0131	0.0228	0.0043	0.0074	0.0026	0.0043
	2	0.0274	0.0604	0.1118	0.2246	0.0013	0.0025	0.0057	0.0105	0.0004	0.0007
3	1	0.0456	0.0821	0.0196	0.0363	0.0026	0.0046	0.0009	0.0014	0.0020	0.0033
	2	0.0100	0.0220	0.0017	0.0033	0.0006	0.0012	0.0023	0.0042	0.0002	0.0004
4	1	0.0759	0.1366	0.0298	0.0551	0.0132	0.0230	0.0113	0.0192	0.0070	0.0116
	2	0.8566	1.8846	0.0210	0.0422	0.0025	0.0048	0.0074	0.0136	0.0012	0.0022
5	1	0.0389	0.0700	0.0079	0.0147	0.0050	0.0087	0.0058	0.0098	0.0012	0.0020
	2	0.0224	0.0492	0.0031	0.0062	0.0011	0.0021	0.0017	0.0032	0.0002	0.0003

Sensor 1- Accelerometer in cutting direction, Sensor 2- Strain gauge, F.W - Flank wear and C.F - Chipping failure

Table 6.13: Typical target vectors

Wear levels	F.W 0.5 mm	C.F 0.5 mm	F.W 0.4 mm	C.F 0.4 mm	F.W 0.3 mm	C.F 0.3 mm	F.W 0.2 mm	C.F 0.2 mm	F.W 0.0 mm	C.F 0.0 mm
Target vectors	1	0	0	0	0	0	0	0	0	0
	0	1	0	0	0	0	0	0	0	0
	0	0	1	0	0	0	0	0	0	0
	0	0	0	1	0	0	0	0	0	0
	0	0	0	0	1	0	0	0	0	0
	0	0	0	0	0	1	0	0	0	0
	0	0	0	0	0	0	1	0	0	0
	0	0	0	0	0	0	0	1	0	0
	0	0	0	0	0	0	0	0	1	0
	0	0	0	0	0	0	0	0	0	1

F.W – Flank wear failure and C.F – Chipping failure

6.7.1   Neural Network Training and Testing

Number of layers, nodes, transfer function and training pattern are varied as shown in Table 6.14 and their performances are compared. Feed forward back propagation algorithm is chosen for training and testing the experimental data. Out of 135 experiments, 110 experiments with different machining conditions were selected for training and remaining twenty five experimental data were reserved for testing.

In this work, six layers feed forward back propagation neural networks with one input, four hidden layers and one-output layer were used. The training is carried out for five levels of flank wear as well as chipping failure (0, 0.2, 0.3, 0.4 and 0.5 mm). Different combinations of architecture were tried out for five different levels of flank wear. Trial number 6 gave better convergence (Figure 6.40a), consumed less computation time and the response of network was good enough to classify the flank wear levels. On trial and error basis, the training of networks is allowed to run up to the maximum number of epochs. Trial number 4 did not converge to the target level as shown in Figure 6.40b. An attempt was made to reduce the computational timings by selecting proper architecture of neural works. Trial number 6 with architecture 150-140-130-120-10 consumed less time. The same architecture was used for both training (target vectors are shown in Table 6.13) and testing the experimental data. The typical testing results are shown in Tables 6.15 and 6.16 for Trial No 6 and 7 respectively.

Table 6.14: Neural network architecture parameters

Trial No	Network architecture	Epochs	Transfer functions	prediction %	Comments
1	100-100-100-100-10	20000	*logsig,logsig,logsig, logsig,tansig,logsig*	92.18	Close to target and attained maximum epochs
2	110-110-110-110-10	20000	*logsig,logsig,logsig, logsig,tansig,logsig*	75.26	Not converged, divergence and low prediction
3	120-120-120-120-10	20000	*logsig,logsig,logsig, logsig,tansig,logsig*	85.36	Close to target, attained maximum epochs
4	140-140-130-120-10	20000	*logsig,logsig,logsig, logsig,tansig,logsig*	95.27	Close to target and attained maximum epochs
5	140-140-130-125-10	20000	*logsig,logsig,logsig, logsig,tansig,logsig*	94.3	Close to target, attained maximum epochs
6	**150-140-130-120-10**	**4113**	*logsig,logsig,logsig, logsig,tansig,logsig*	**100**	**Converged**
7	150-140-130-130-10	5218	*logsig,logsig,logsig, logsig,tansig,logsig*	100	Converged
8	150-150-150-150-10	7257	*logsig,logsig,logsig, logsig,tansig,logsig*	100	Converged
9	200-175-150-150-10	20000	*logsig,logsig,logsig, logsig,tansig,logsig*	98.47	Close to target, attained maximum epochs
10	130-130-120-120-10	16425	*logsig,logsig,logsig, logsig,tansig,logsig*	89.6	Converged

*Trial No 6, the architecture of 150-140-130-120-10 is giving best convergence, less computation time and response of training is good enough to classify the flank wear at various levels.
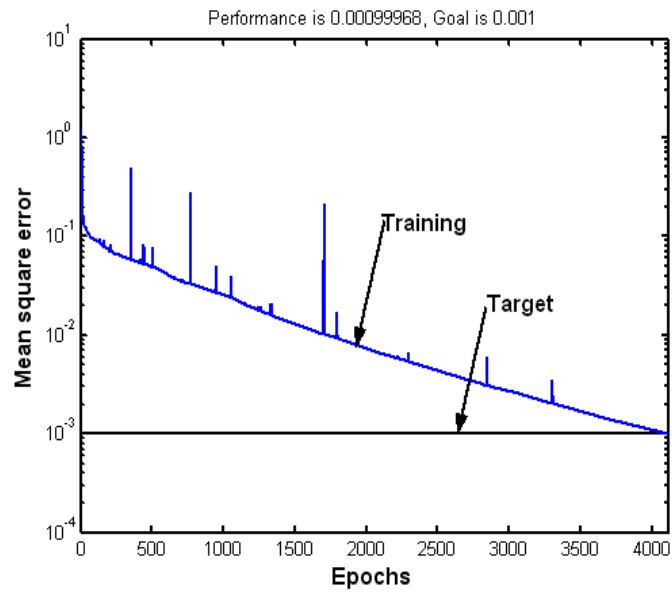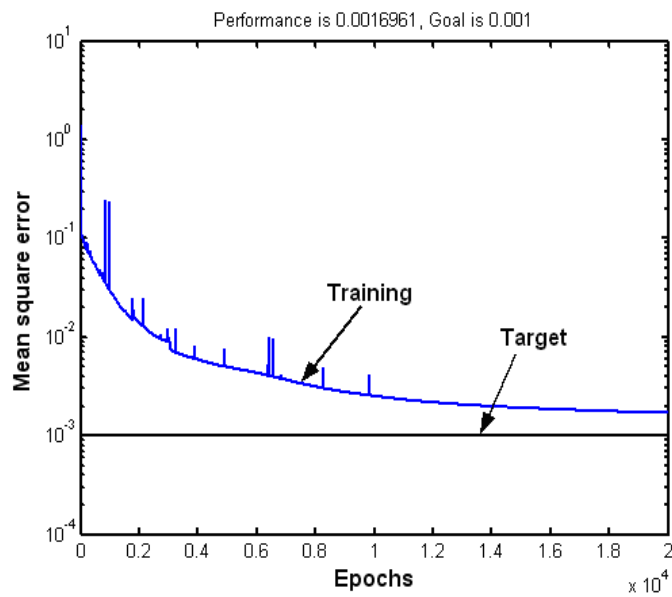
Figure 6.40: (a) Convergence pattern of neural networks for Trial No 6 (b) Convergence pattern of neural networks for Trial No 4.

Table 6.15: Typical output vectors for Trial No 6 (150-140-130-120-10)

Wear levels	F.W 0.5 mm	C.F 0.5 mm	F.W 0.4 mm	C.F 0.4 mm	F.W 0.3 mm	C.F 0.3 mm	F.W 0.2 mm	C.F 0.2 mm	F.W 0.0 mm	C.F 0.0 mm
Output vectors	1	0.000	0.000	0.002	-0.011	0.041	0.001	0.003	0.015	-0.037
	-0.003	**0.999**	0.000	-0.005	0.003	0.000	0.005	-0.002	0.076	-0.058
	-0.001	-0.001	**0.991**	-0.004	0.011	0.001	-0.002	0.0015	0.004	0.000
	-0.001	0.000	-0.003	**0.991**	0.013	0.002	-0.002	0.000	0.0084	0.024
	-0.001	-0.001	0.002	-0.005	**0.954**	0.005	-0.011	-0.003	0.002	0.0051
	0.000	-0.005	0.003	0.000	0.000	**1.000**	0.002	-0.011	-0.002	0.076
	0.001	0.003	0.0215	-0.037	-0.001	-0.001	**0.988**	0.047	0.000	0.002
	-0.003	0.002	0.002	-0.011	-0.001	0.000	0.008	**0.992**	0.000	-0.005
	-0.011	-0.002	-0.005	0.003	-0.001	0.001	0.000	0.0048	**0.929**	0.006
	0.047	0.000	-0.004	0.011	0.000	-0.005	0.001	-0.002	0.071	**0.951**

F.W - Flank wear and C.F - Chipping failure

Table 6.16: Typical output vectors for Trial No 7 (150-140-130-130-10)

Wear levels	F.W 0.5 mm	C.F 0.5 mm	F.W 0.4 mm	C.F 0.4 mm	F.W 0.3 mm	C.F 0.3 mm	F.W 0.2 mm	C.F 0.2 mm	F.W 0.0 mm	C.F 0.0 mm
Output vectors	**0.964**	-0.027	0.100	0.100	0.100	0.100	-0.033	0.100	0.100	0.100
	0.017	**0.973**	-0.100	-0.100	-0.057	-0.100	-0.038	0.100	-0.100	-0.042
	-0.001	0.032	**0.935**	-0.098	-0.099	-0.007	-0.004	0.091	0.004	-0.099
	-0.032	0.003	0.100	**0.971**	-0.098	0.100	0.009	0.100	0.100	-0.077
	0.057	0.040	-0.097	-0.099	**0.935**	-0.100	0.079	-0.099	-0.100	0.100
	-0.012	0.052	0.100	0.100	0.100	**0.992**	0.025	0.100	0.100	0.100
	-0.059	-0.049	-0.100	-0.013	-0.023	0.008	**0.978**	-0.036	0.073	-0.100
	0.021	-0.007	-0.093	0.082	-0.098	0.039	-0.012	**0.915**	-0.091	-0.100
	0.009	-0.093	0.100	0.099	-0.080	0.061	0.100	0.006	**0.999**	-0.098
	0.067	0.058	-0.097	-0.089	0.100	0.024	0.019	-0.100	-0.096	**0.939**

F.W - Flank wear and C.F - Chipping failure

6.8   Probabilistic Neural Networks (PNN)

Probabilistic neural network based three-layer feed forward network consisting of an input layer, a pattern layer and a summation layer as shown in Figure 6.41.
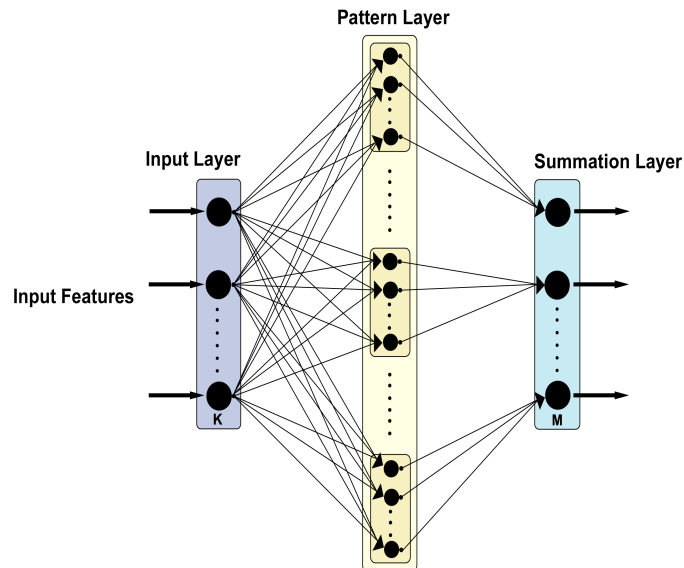
Figure 6.41: Structure of the probabilistic neural network (PNN)

The network is trained for five different wear levels with the same training data sets (Tables 4.4, 4.5 and 4.6) that were used for the Back propagation network. One hundred and ten data sets were used for training and twenty five sets were used for validation. The advantage of the PNN networks is that they are fast in comparison to other type of networks. Performance of the PNN network in classifying the faults correctly is shown in Figure 6.42. It is observed that 0.4 mm and 0.5 mm levels of flank wear get classified well. At lower of flank wear levels, the strain as well as vibration signatures do not show much variation and therefore data sets to PNN do not change much between flank wear levels from 0 to 0.3 mm.
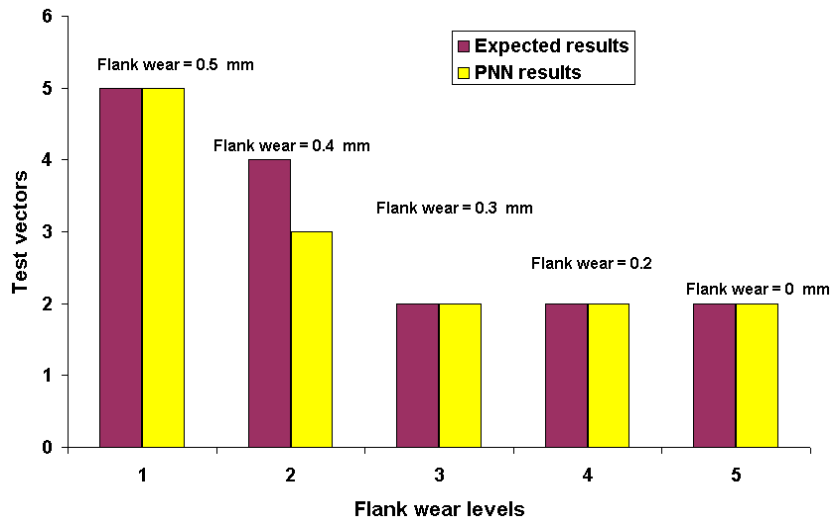
Figure 6.42: Typical performance of probabilistic neural network

6.9   Network model based on statistical parameters

It was also decided to carry out an exercise characterization of the cutting phenomenon using statistical parameters of the time domain vibration and strain gauge signals.

For these signals, following four statistical parameters were evaluated [73] as follows: Mean (μ), Standard deviation (σ), Skewness (S) and Kurtosis (K).

Mean:

$$\mu = \overline{X} = \frac{1}{N} \sum_{i=1}^{N} X_i \qquad (6.31)$$

Standard deviation:

$$\sigma = \sqrt{\frac{1}{N} \sum_{i=1}^{N} (X_i - \mu)^2} \qquad (6.32)$$

Skewness (S) is a measure of the asymmetry of the data around the sample mean. The skewness of a normal distribution (or any perfectly symmetric distribution) is zero. Skewness is the third statistical moment of distribution given by,

$$S = \frac{1}{N} \sum_{i=1}^{N} \frac{E(X_i - \mu)^3}{\sigma^3} \qquad (6.33)$$

where $E(X_i)$ is the expected value of X_i for i^{th} value of data.

Kurtosis of a distribution is the fourth statistical moment defined as

$$K = \frac{1}{N} \sum_{i=1}^{N} \frac{E(X_i - \mu)^4}{\sigma^4} \qquad (6.34)$$

Above defined statistical parameters are calculated using a Matlab code and the computed quantities are shown in Table 6.17.

Table 6.17: Typical input vectors for neural networks

Sensors	Statistical parameters	New insert	FW = 0.2 mm	FW = 0.3 mm	FW = 0.4 mm	FW = 0.5 mm
Accelero-meter in cutting direction	Mean	0.0003	0.0006	0.0016	0.0023	0.0054
	Std deviation	0.1295	0.1324	0.1553	0.165	0.2228
	Skewness	0.0032	0.0088	0.0173	0.0204	0.0424
	Kurtosis	1.4094	2.0114	2.198	2.5671	2.6551
Accelero-meter in feed direction	Mean	0.0001	0.0004	0.0012	0.0023	0.0055
	Std deviation	0.0523	0.0591	0.0735	0.1007	0.2199
	Skewness	0.0422	0.0459	0.0479	0.0868	0.1102
	kurtosis	1.4222	4.1572	4.1659	6.5615	6.8949
Strain gauge signal	Mean	0.0056	0.0416	1.2927	8.1621	24.179
	Std deviation	0.6057	0.8076	4.7507	24.746	64.218
	Skewness	0.0048	0.0713	0.1553	3.5505	3.8316
	Kurtosis	2.1843	2.9487	2.9652	16.78	17.487

FW - Flank wear

6.9.1 Statistical Parameter Variation with Machining Conditions

These statistical parameters are also shown in Figures 7.33 - 7.36. It can be seen from these figures that all the statistical parameters increase with increase in flank wear. As the flank wear increases, frictional force between the flank face of the cutting tool and work piece surface also increases which causes an increase in cutting force and feed force both. Hence, there is an increase in the values of the

mean vibration level, g, in the cutting direction as well as in the feed direction (Figure 7.33a and Figure 7.33b). Increase in the magnitude of force also increases strain as shown in Figure 7.33c. However, increase in strain is not significant up to 0.2 mm flank wear because the change in the cutting force is also small due to modest variation in the flank wear. It is noted that the magnitude of mean vibration signal, g (Figure 7.33a) decreases with increase in cutting speed. This is due to increase in cutting speed decreases the cutting force. In addition to that the same effect is observed in the response of strain gauge (Figure 7.33c).

Standard deviation (equation 6.32) is the most common measure of statistical dispersion, and it indicates the degree of spread of the values in a data set from its mean. Since the vibration amplitude, g is increasing with increase in flank wear, the standard deviation (dispersion) of vibration amplitude also increases with increase in flank wear. Variation in standard deviations of vibration amplitude with flank wear is shown in Figure 7.34a for sensor 1 (Accelerometer) which is placed in cutting direction and sensor 2 (Accelerometer) which is placed in feed direction as shown in Figure 7.34b. Figure 7.34c shows the effect of a change in flank wear on the standard deviation of micro strain. As discussed in the preceding section, a change in micro strain is small till 0.2 mm flank wear hence the change in standard deviation is also small till 0.2 mm flank wear as shown in Figure 7.34c. It is noted that the magnitude of mean acceleration, g (Figure 7.34a and Figure 7.34b) decreases with increase in cutting speed. This is due to the fact that increase in cutting speed decreases the cutting force. In addition, the same effect is observed in the response of strain gauge (Figure 7.34c).

Skewness (equation 6.33) is a measure of asymmetry (time domain in the present case) in the data around the mean. Skewness of the data set indicates whether deviations from the mean are going to be positive or negative. It is conventionally defined in such a way as to make it non-dimensional. It is a pure number that characterizes only the shape of the distribution. Skewness (level of
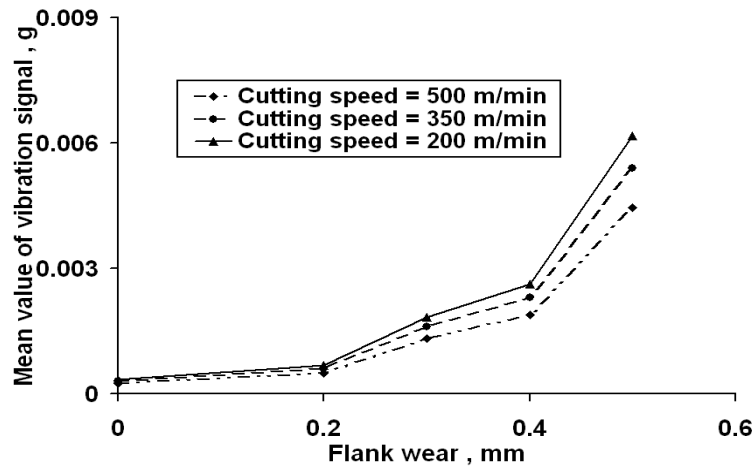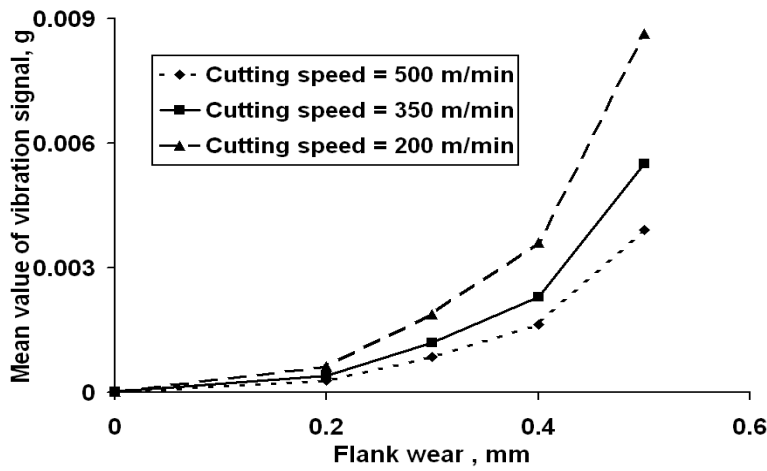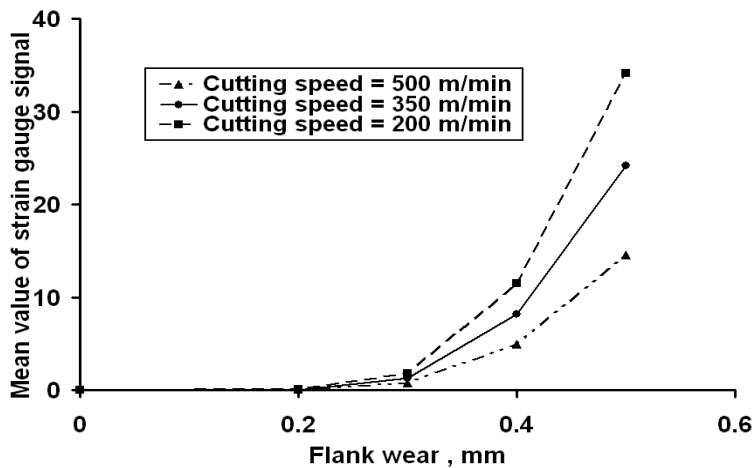
Figure 6.43: (a) Relationship between mean value of vibration signal and flank wear in cutting direction (b) Relationship between mean value of vibration signal and flank wear in feed direction (c) Relationship between mean value of micro strain signal and flank wear (depth of cut = 4 mm and feed rate = 300 mm/min).

Figure 6.44: (a) Relationship between standard deviation of vibration signal and flank wear in cutting direction (b) Relationship between standard deviation of vibration signal and flank wear in feed direction (c) Relationship between strain gauge signal and flank wear (depth of cut = 4 mm and feed rate = 300 mm/min).

asymmetry) increases with increase in flank wear level due to rubbing action of the cutting tool at the flank face as shown in Figure 7.35. Skewness of vibration amplitude increases more in case of sensor 2 (feed direction) as compared to sensor 1 (cutting direction) and their values are positive. This indicates the higher mean value of the amplitude of vibration with increase in flank wear which is clear from Figure 7.35a and Figure 7.35b. Further, positive skewness also indicates that the mean value is smaller than the median and modal values of the amplitude of vibration. Similar behaviour is seen for the case of variation in micro strain with flank wear (Figure 7.35c). It is noted that the magnitude of acceleration, g (Figure 7.35a) decreases with increase in cutting speed. This is due to decrease in cutting force due as the cutting speed increases. In addition, the same effect is observed in the response of strain gauge (Figure 7.35c).

Kurtosis (equation 6.34) is also a non-dimensional quantity and, in the present reference, it is a measure of peak value of time domain data. The peaks of vibration and strain level increase with increase in flank wear level (due to increase in cutting force which obviously increases the peak value of the time domain data) as shown in Figure 7.36. It is noted that the magnitude of acceleration, g (Figure 7.36a) decreases with increase in cutting speed. This is due to decrease in cutting force (if cutting speed increases it obviously decreases the cutting force). Similar effect is observed in the response of strain gauge (Figure 7.36c).

It is seen (Table 6.17) that the variation in kurtosis value is smaller when the flank wear changes from 0 to 0.5 mm in the cutting direction (Figure 7.36a). But its value changes substantially in case of feed direction (example, sensor 2 and Figure 7.36b by a factor of 4). It also indicates that at higher flank wear the degree of peakedness of the amplitude of vibration increases. Further, the frequency of distribution [73] of amplitude of vibration is platykurtic ($\beta_2 < 3$) in case of sensor 1 and leptokurtic ($\beta_2 > 3$) in case of sensor 2. It means that the amplitude of vibration in cutting direction (sensor 1) does not change

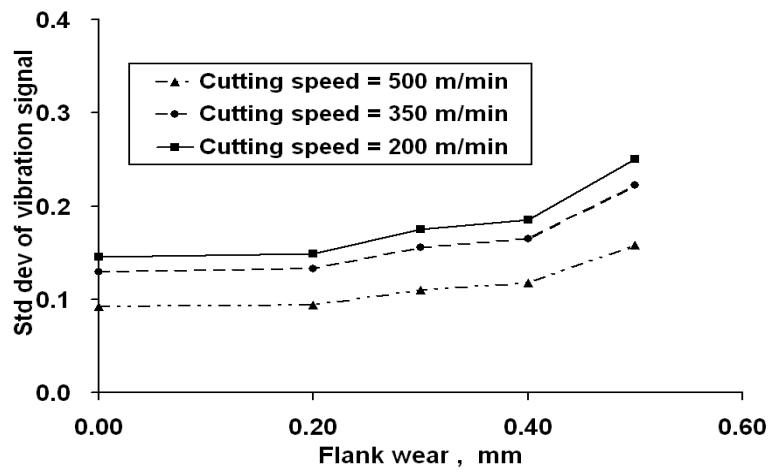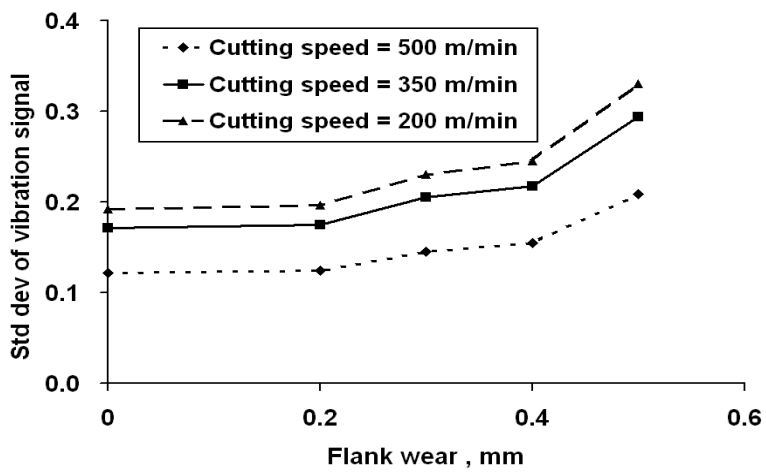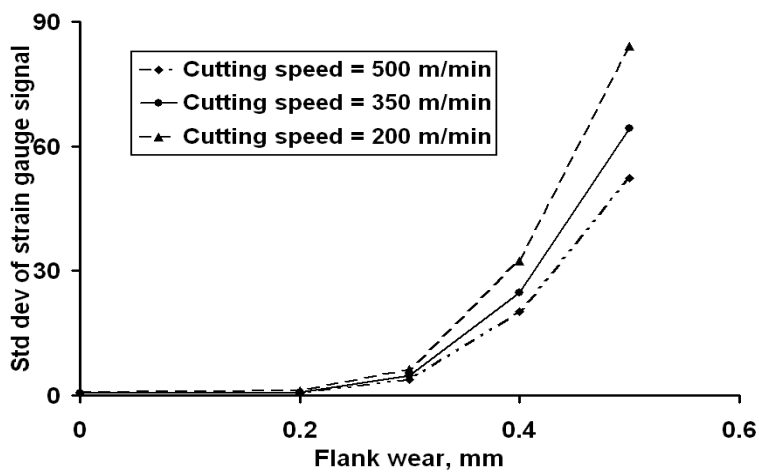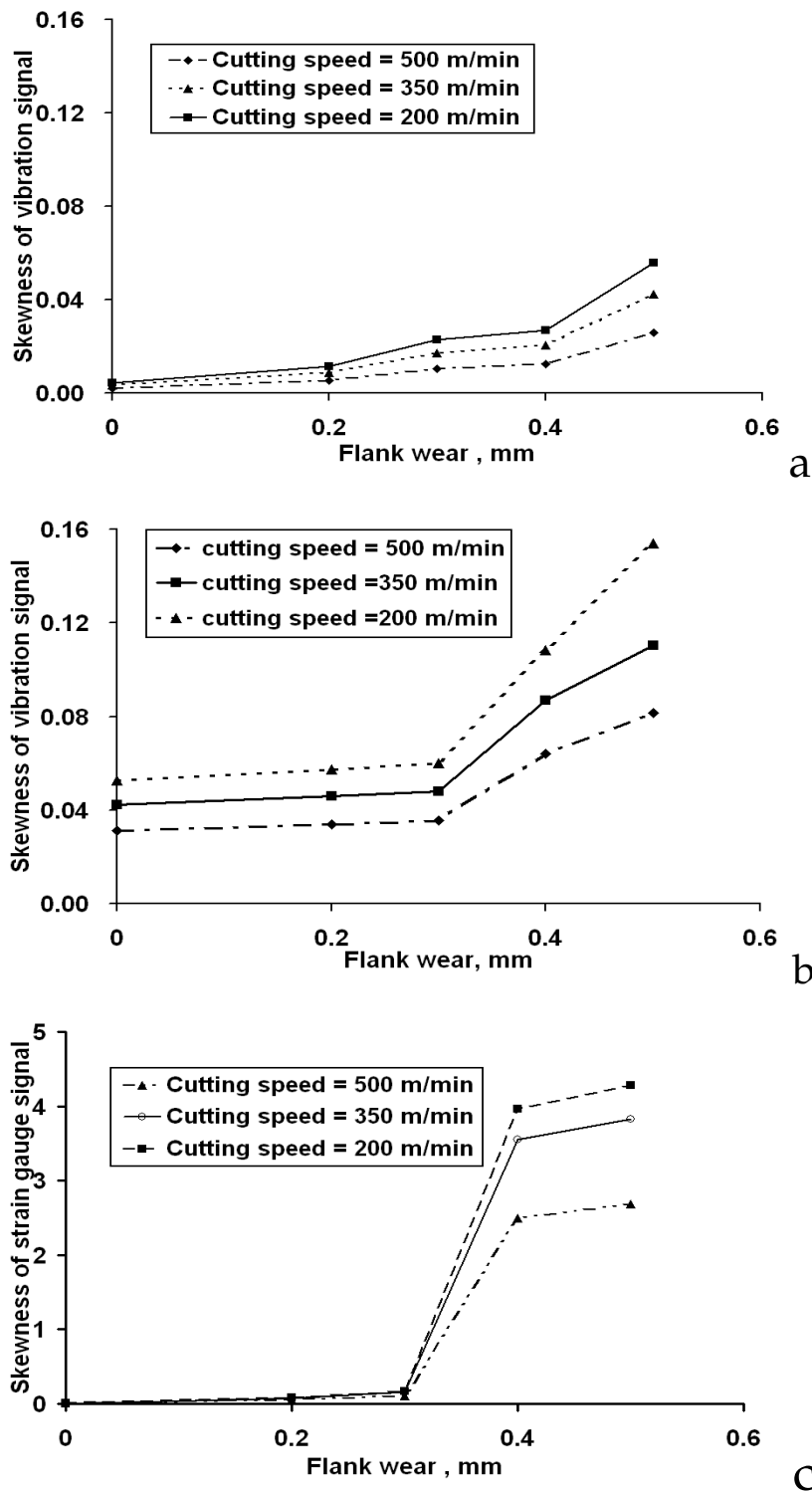Figure 6.45: (a) Relationship between skewness of vibration signal and flank wear in cutting direction (b) Relationship between skewness of vibration signal and flank wear in feed direction (c) Relationship between skewness of strain gauge signal and flank wear(depth of cut = 4 mm and feed rate = 300 mm/min).

substantially (distributions curve is flat) while changes substantially in the case of feed direction (sensor 2).

6.9.2 Statistical Inputs for Neural Network

These four statistical parameters, namely, (i) Mean, (ii) Standard deviation, (iii) Skewness and (iv) kurtosis were used as input vectors to the neural networks. For each level of flank wear, the number of terms in the input vector is 12 as given in Table 6.17. These terms are a combination of outputs of two accelerometers signals (4+4) and one strain gauge signals (4) as shown in Figure 6.47.

Networks are trained for five levels of flank wear ranging from 0 to 0.5 and target vectors of neural networks are fixed for training as listed in Table 6.18. In Table 6.18 , first column (1 0 0 0 0) indicates the level of flank wear 0.5 mm. Similarly second, third, fourth, and fifth columns indicate the levels of flank wear as 0.4, 0.3, 0.2 and 0 mm, respectively.

Table 6.18: Typical target vectors

Flank wears in mm	0.5	0.4	0.3	0.2	0.0
	1	0	0	0	0
Target	0	**1**	0	0	0
vectors	0	0	**1**	0	0
	0	0	0	**1**	0
	0	0	0	0	**1**

6.9.3 Network Training and Testing

Different architectures were tried and finally a four layer feed forward back propagation neural network with one input layer, two hidden layers and one-output layer was adopted. The training is carried out for five levels of flank wear (0, 0.2, 0.3, 0.4 and 0.5 mm) using 110 experimental data sets. The
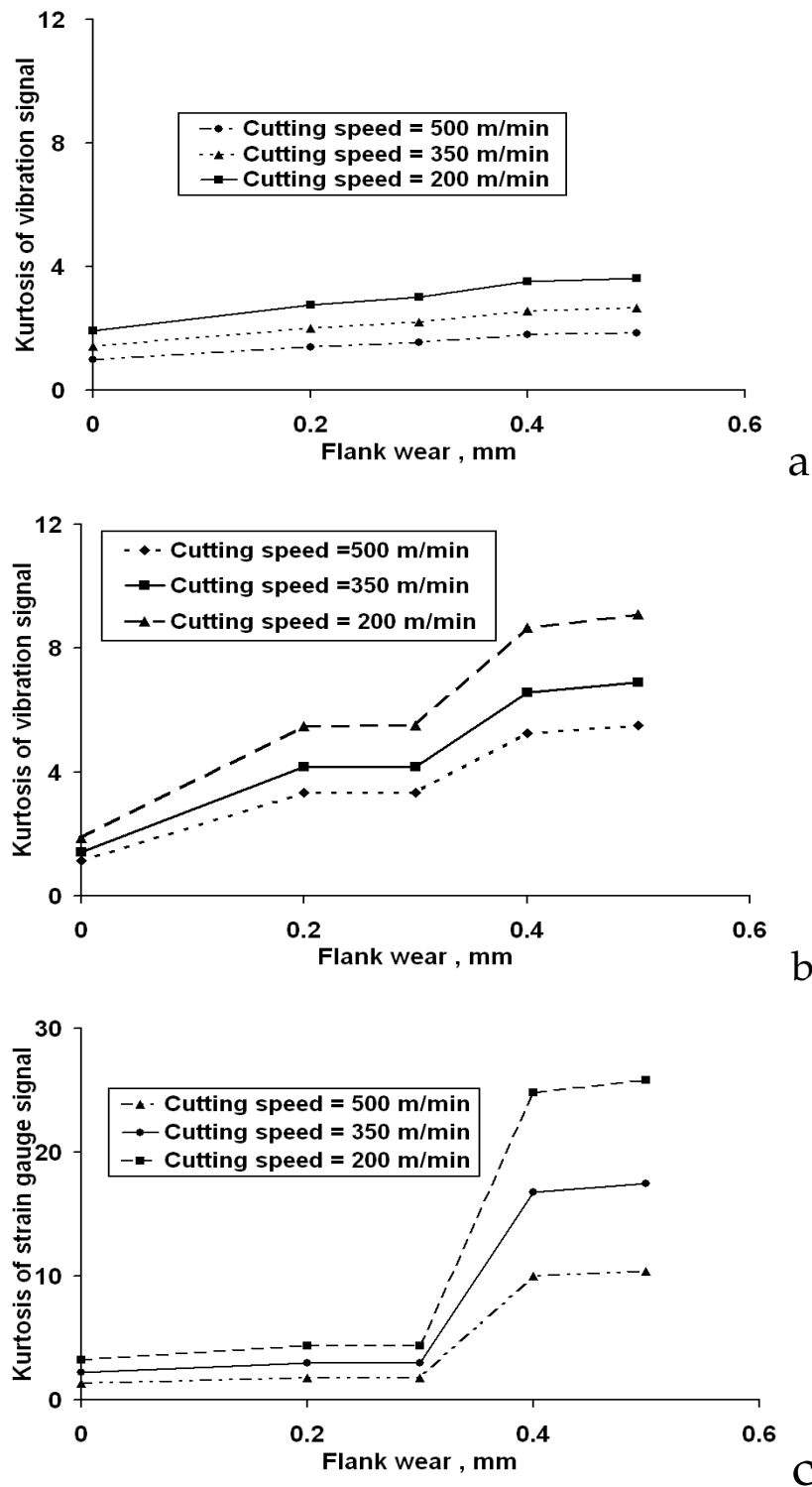
Figure 6.46: (a) Relationship between kurtosis of vibration signal and flank wear in cutting direction (b) Relationship between kurtosis of vibration signal and flank wear in feed direction (c) Relationship between kurtosis of strain gauge signal and flank wear (depth of cut = 4 mm and feed rate = 300 mm/min).
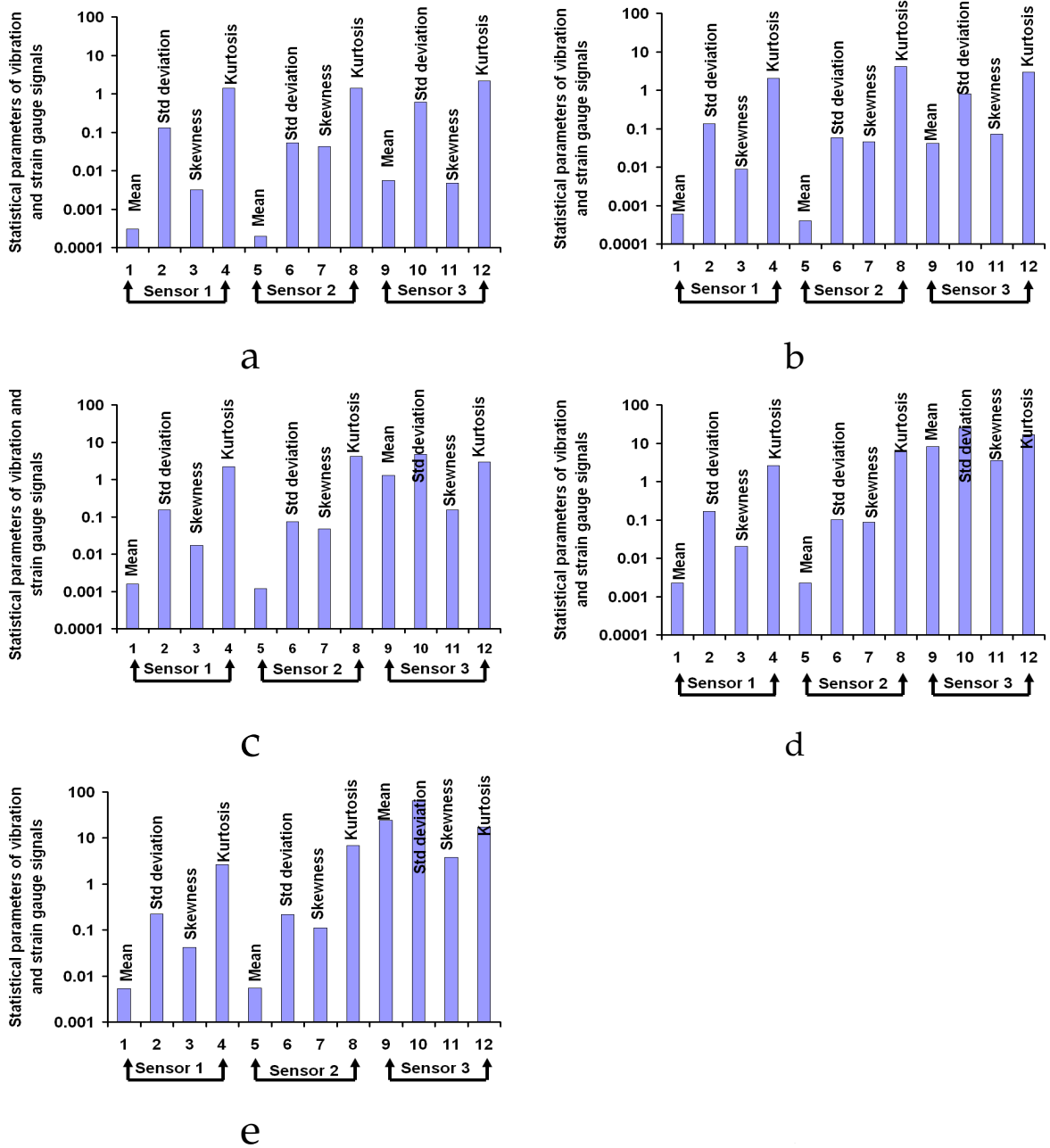
Figure 6.47: Typical input training vectors for (a) new cutting tool (b) 0.2 mm flank wear cutting tool (c) 0.3 mm flank wear cutting tool (d) 0.4 mm flank wear cutting tool (e) 0.5 mm flank wear cutting tool. Cutting speed = 500 m/min, feed rate = 500 mm/min and depth of cut = 5 mm. Sesnor 1 - Accelerometer in cutting direction , Sesnor 2 - Accelerometer in feed direction and Sesnor 3 - Strain gauge

remaining 25 experimental data were reserved for testing the neural network model.

After fixing the number of layers to four, the number of neurons in the individual layers are varied to obtain an optimum network. The convergence patterns of these networks (Trial No 5 and 8) are shown in Figure 6.48a and Figure 6.48b. The desired level of accuracy ($= 1 \times 10^{-4}$) is generally obtained within 15000 epochs for all the architectures as shown in Table 6.19.

Best results were obtained with *logsig* and *tansig* activation functions, the *trainrp* is found to be most robust training algorithm in terms of accuracy and time taken (Table 6.19, Trial No 5).

After training, the same neural network architecture is tested with new data. The testing results are shown in Tables 6.20 and 6.21 for Trial No 5 and 8. These Tables 6.20 and 6.21 results and earlier results clearly indicate that with statistical data as input, the ANN is able to identify the state of flank wear of a given tool.

6.10   Remarks

Development of ANN models for tool failure prediction have been described in this chapter. Frequency domain and statistical input based ANNs have been developed. Probabilistic Networks based on Bayes' Rule have also been developed. Experimental data of measured acceleration, g and micro strain are utilized to train the network models. Trained models are used in predicting flank wear and chipping failure for various different cutting conditions. The developed prediction system is found to be capable of accurate in predicting tool failure - both flank wear and chipping, for the range it has been trained.

All data, experimentally obtained and collected from the sensors, have been used to create ANN models. On the basis of prediction accuracy, these models can be extended and extrapolate for other machining conditions.
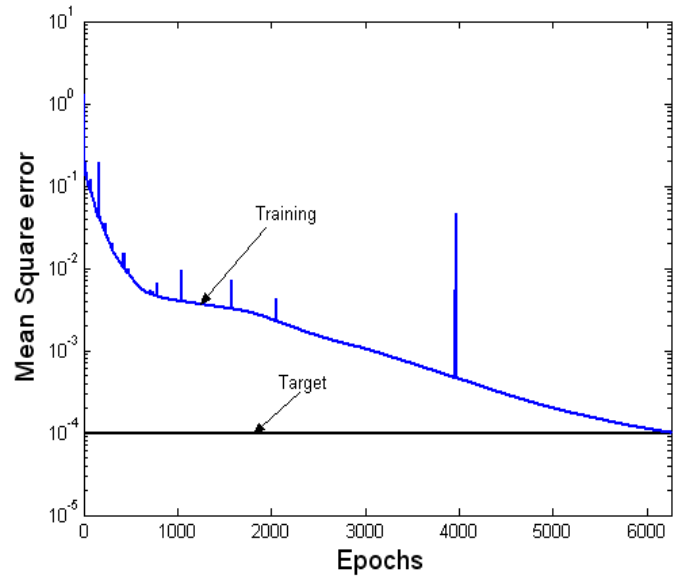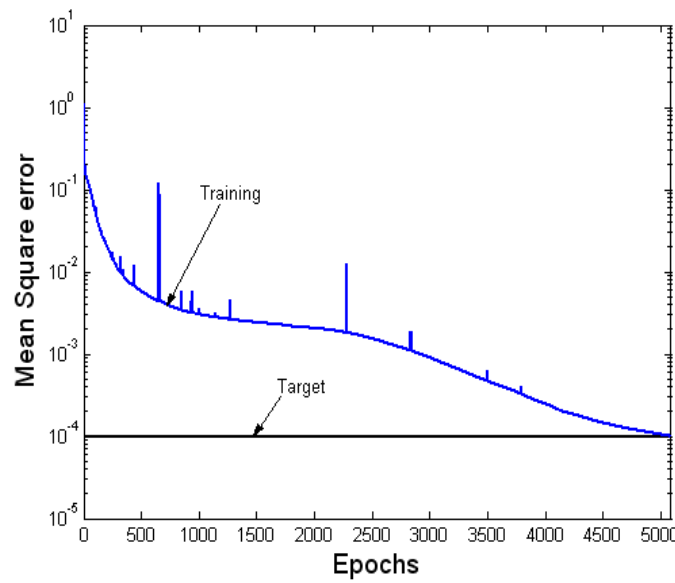
Figure 6.48: (a) Convergence pattern of back propagation networks for Trial No 5. (b) Convergence pattern of back propagation networks for Trial No 8.

Table 6.19: Neural network architecture of time domain analysis

Trial No	Network architecture	Epochs	Transfer functions	Comments	prediction %
1	100-100-50-5	14600	*logsig,logsig, logsig,tansig*	Converged	100
2	100-100-75-5	15000	*logsig,logsig, logsig,tansig*	Not converged	97.8
3	100-100-100-5	15000	*logsig,logsig, logsig,tansig*	Not converged	94.3
4	125-125-50-5	10777	*logsig,logsig, logsig,tansig*	Converged	100
5*	**125-125-100-5**	**6258**	*logsig,logsig, logsig,tansig*	**Converged**	100
6	150-150-50-5	8315	*logsig,logsig, logsig,tansig*	Converged	100
7	200-100-50-5	15000	*logsig,logsig, logsig,tansig*	Not converged	87.8
8	200-200-75-5	5090	*logsig,logsig, logsig,tansig*	Converged	100
9	200-200-100-5	4800	*logsig,logsig, logsig,tansig*	Converged	100
10	250-200-100-5	8315	*logsig,logsig, logsig,tansig*	Not converged	81.5
11	250-250-100-5	13292	*logsig,logsig, logsig,tansig*	Converged	100
12	250-250-250-5	2030	*logsig,logsig, logsig,tansig*	Converged	100
13	275-275-150-5	4939	*logsig,logsig, logsig,tansig*	Converged	100
14	300-250-200-5	15000	*logsig,logsig, logsig,tansig*	Not converged	80.1
15	300-300-50-5	15000	*logsig,logsig, logsig,tansig*	Not converged	78.2
16	300-300-100-5	15000	*logsig,logsig, logsig,tansig*	Not converged	75.2
17	300-300-150-5	4634	*logsig,logsig, logsig,tansig*	Converged	100

*Trial No 5, the architecture of 125-125-100-5 gives best convergence, less computation time and response of training is good enough to classify the flank wear at various levels.

Table 6.20: Typical output for test data for Trial No 5 (125-125-100-5)

	Flank wears in mm				
	0.5	0.4	0.3	0.2	0.0
	0.998	0.001	0.000	0.001	0.001
	0.007	**0.999**	0 0.000	0.001	0.001
Output vectors	0.009	0.001	**0.999**	0.001	0.001
	0.000	0.010	0.000	**1**	0.010
	0.000	0.001	0.001	0.001	**0.999**

Table 6.21: Typical output for test data for Trial No 8 (200-200-75-5)

	Flank wears in mm				
	0.5	0.4	0.3	0.2	0.0
Output	**0.9947**	0.0165	0.1000	0.1000	0.0888
vectors	-0.0914	**0.9418**	0.0999	-0.1000	-0.0873
	-0.0631	0.0303	**0.9214**	-0.0046	-0.0957
	-0.0774	-0.0891	-0.0712	**1.0000**	-0.0826
	0.0421	0.0528	-0.0986	-0.0804	**0.9725**

In the design of neural networks, our major concern was to obtain a good generalization capability. These ANN models may also utilized to determine optimum number of neurons in hidden layer and its structure optimisation.

Chapter 7

Conclusions

7.1 Conclusions

The development of practical and reliable condition monitoring methods for detecting flank wear and chipping failure in turning operation is essential for realization of intelligent and flexible manufacturing systems. In this thesis, the problem of detection of flank wear and chipping failure in turning operation has been studied using vibration and strain measurement methods. Based on the findings of this thesis, following conclusions are drawn:

- An artificial wear can be created in a controlled manner by using EDM process, which emulates the real flank wear and chipped off cutting edge where machining responses are similar to actual flank wear and chipped off cutting edge.

- Vibration and strain monitoring during turning operation can be useful for predicting flank wear as well as chipping failure. For this purpose, four statistical moments are estimated using time domain data and then they are used in ANN analysis as the input data. Four layer ANN response then can be used to classify the flank wear at different levels. Frequency domain analysis has also been carried out and features were fed in to six layer ANN

as input data. The responses of ANN are good enough to classify the flank wear and chipping failure at different levels.

- From the experimental results the amplitude of vibration in cutting direction (sensor 1) does not change substantially (kurtosis distribution curve is flat) while it does change in feed direction (sensor 2) (kurtosis distribution curve is more like a normal distribution). This indicates that the responses of vibration signals in feed direction are superior to cutting direction which classifies the flank wear levels as per the condition monitoring aspects.

- Neural networks model has been developed and used to predict the condition of the cutting tool. On the basis of the condition of the cutting tool this neural network model may be further employed to develop an adaptive feed back system to control the machining process.

- The neural networks code was tested employing various training algorithms available in the Matlab toolbox and finally optimum architecture (Trial No 15) was selected. Among these algorithms, the trainrp was found to be most robust and easily applicable to classify the flank wear levels while using logsig and tansig as activation functions.

- A multiple regression model has been developed for flank wear level prediction as well as chipping failure. The model have been validated with the experimental results.

- The amplitude of vibration (acceleration, g) and amplitude of strain are more for the chipped off tool when compared with flank wear tool.

- The response of accelerometer signals and strain gauge bridge signals were studied with different machining conditions. The acceleration, g increases with increasing feed rate and depth of cut and decreases with increase in

cutting speed. The strain increases with increase in feed rate and depth of cut and decreases with increase in cutting speed.

7.2   Future work

The present study involving the following

- Creation of artificial wear which emulates real flank wear and cutting edge chipping wear

- Development of computer based instrumentation to condition, record and analyse the signals obtained from strain gauge bridge using LabVIEW.

- Development of an algorithm to extract the relevant features of signals obtained from strain gauge bridge and accelerometer sensors and compiling them to form a training vector.

- Development of ANN code to train and test the neural network.

- Development of Regression models to correlate the different levels of wear with machining input parameters.

- Development of FEM model to find the natural frequencies of cutting tool with different modes.

In this study, ANN models have been developed to predict the condition of a cutting tool to predict whether it has flank wear or a chipped off cutting edge. To develop such models, features are extracted from strain and vibration signals at the natural frequency of cutting tool. These features are used as input vectors for training the neural network. Apart from these features, a few more frequencies can be extracted from the signals. In future these data may be useful for validating the ANN models. The following work can be carried out in future for further improvements.

- Old worn-out DNMG inserts can be collected and a prepare CAD model of real life failed tool bit geometry using 3D scanner or CMM (Reverse engineering) representing actual flank wear, can be prepared.

- EDM process can be employed to create identical flank wear, chipping failure and crater wear geometry on test tools.

- In future, all three types of tool wear- flank, crater and chipping failure can be considered simultaneously and their interactions can be studied using solid tools or non grooved DNMG inserts i.e. DNMG inserts have a configuration with out chip breaker.

- Cutting fluids may also be used with DNMG inserts fitted with cutting tools after proper sealing of sensors from the cutting fluids.

While considerable research has been explined in several papers to implement ANN concepts in cutting tool condition monitoring system. Still there is no solution for finding the number of layers, number neurons for particular type of wear. Future research should be engaged in evolutionary algorithms for structure optimisation. The problem of how to find an optimal architecture is currently one of the central issues of research on neural networks.

Though a lot of work has been done there is still a demand for a reliable and universal monitoring system. Such a system would involve two inherent components: hardware and software. Presently, the hardware component is more developed and many sensors and transducers have been employed in industrial conditions. However, the software component requires improvement, as there are more difficult and complex tasks yet to be solved.

Bibliography

[1] S.K. Choudhury and J.B. Bajpai "Investigation in orthogonal turn-milling towards better surface finish," *Journal of Materials Processing Technology*, Vol.170(3) , pp. 487-493, 2005.

[2] T.Childs,K.Maekawa,T.Obikawa and Y.Yamane "Metal Machining Theory and applications," *Butterworth Heinemann*, New Delhi, 2001.

[3] E. Daniel Kriby, Ms. Zhe Zhang and J.C. Chen "Development of an accelerometer-based surface roughness prediction system in turning operations using multiple regression techniques," *Journal of Industrial Technology*, Vol.20(4) , pp. 1-8, 2004.

[4] C.G.Harris, J.H.Williams and A.Davies, "Condition monitoring of machine tools," *International journal of production research*, vol. 27(9), pp. 1445-1464, 1989.

[5] T. Blum and I. Inasaki, "A study on acoustic emission from the orthogonal cutting process,"*ASME Trans. Journal of Engineering for Industry* vol.112 (3), pp. 203211,1990.

[6] D.E.Dimla, P.M.Lister and N.J.Leighton, "Neural networks solutions to the tool condition monitoring problem in metal cutting - A critical review of methods ," *International Journal of Machine Tools and Manufacturers*, vol. 37, pp. 1219-1241, 1997.

[7] B.Sick "On-line and indirect tool wear monitoring in turning with artificial neural networks: a review of more than a decade of research," *Mechanical Systems and Signal Processing*, vol. 16, pp. 487-546, 2002.

[8] G.H.Lim " Tool wear monitoring in machine turning ," *Journal of Material Processing Technology*, vol. 51, pp. 25-36, 1995.

[9] I.N. Tansel and C. McLaughlin, "On-line monitoring of tool breakage with unsupervised neural network," *Trans. NAMR I/SME* , pp. 364370,1991.

[10] G.Byrne,D.Dornfeld, I.Inasaki, G.Ketteler and W.Knig, R.Teti "Tool condition monitoring (TCM) - The status of research and industrial application," *Annals of CIRP*, vol. 44(2), pp. 541-567, 1995.

[11] S.K.Choudhury and K.K.Kishore "Tool wear measurement in turning using force ratio," *International Journal of Machine Tools and Manufacture*, vol. 40, pp. 899-909, 2000.

[12] X.P. Li and A.Y.C. Nee "Monitoring cutting conditions for tool scheduling in CNC machining," *Manufacturing Systems*, vol. 25 (4), pp. 377-383, 1996.

[13] Vinod yadav, V.K.Jain and Prakash M.Dixit , " Thermal stress due to electrical discharge machining, "*International Journal of Machine Tools and Manufacture*, Vol.42, pp.877-888,2002.

[14] P.W. Prickett and C. Johns, " An overview of approaches to end milling tool monitoring, "*International Journal of Machine Tools and Manufacture* , Vol.39(1), pp.105-122,1999.

[15] L.C. Lee, K.S. Lee and C.S. Gan, "On the correlation between dynamic cutting force and tool wear," *International Journal of Machine Tools and Manufacture*,Vol. 29 (3) , pp. 295303,1989.

[16] D. Choi, W.T. Kwon and C.N. Chu, "Real-time monitoring of tool fracture in turning using sensor fusion," *International Journal of Advanced Manufacturing Technology*, vol.(15)5 pp. 305-310,1999.

[17] K. Jemielniak and O. Otman, "Tool failure detection based on analysis of acoustic emission signals," *Journal of Material Processing Technology* ,vol.76, pp. 192197 , 1998.

[18] S. Kakade, L. Vijayaraghavan and R. Krishnamurthy, "In-process tool wear and chip-form monitoring in face milling operation using acoustic emission," *Journal of Material Processing Technology*,Vol.44 , pp. 207-214, 1994.

[19] S.X. Zheng, R. McBride, J.S. Barton, J.D.C. Jones, K.F. Hale and B.E. Jones, "Intrinsic optical fiber sensor for monitoring acoustic emission,"*Sensors and Actuators*,Vol.31 , pp. 110114, 1992.

[20] W. Kenig, K. Kutzner and U. Schehl, "Tool monitoring of small drills with acoustic emission,"*International Journal of Machine Tools and Manufactures*, Vol.32 (4) , pp. 487493,1992.

[21] T. Moriwaki and M. Tobito, "A new approach to automatic detection of life of coated tool based on acoustic emission measurement," *ASME Trans. Journal of Engineering for Industry*, Vol. 112 (3) , pp. 212218,1990.

[22] J. Roget, P. Souquet and N. Gsib, " Application of acoustic emission to the automatic monitoring of tool condition during machining,"*ASNDT Materials Evaluation*, Vol.46 , pp. 225229,1988.

[23] D.E.Dimla, "Sensors signals for tool-wear monitoring in metal cutting operations-A Review of methods," *International Journal of Machine tools and Manufacture*,Vol.40, pp 1073-1098,2000.

[24] D. Yan, T.I. El-Wardany and M.A. Elbestawi, "A multi-sensor strategy for tool failure detection in milling," *International Journal of Machine Tools and Manufacture*, Vol.35(3), pp. 383398,1995.

[25] D.A. Dornfeld, "Application of acoustic emission techniques in manufacturing,"*NDT and E International*, Vol 25(6), pp. 259269,1992.

[26] T.J.Ko and D.W.Cho, " Cutting state monitoring in milling by a neural network," *International Journal of Machine Tools and Manufacture*,Vol.34(5), pp 659-676,1994.

[27] D.A. Dornfeld, "In process recognition of cutting states,"*JSME International Journal,(Series C: Dynamics Control)*, Vol 37 (4) , pp. 638650, 1994.

[28] L.Gould, "Sensing tool and drive element conditions in machine tools," *Sensor*, pp 5-13,1988.

[29] J. Paulo Davim, "A note on the determination of optimal cutting conditions on the surface finish obtained in turning using design experiments," *Journal of Materials Processing Technology*, Vol.116, pp 305-308, 2001.

[30] D. E. Dimla and P. M. Lister, "On-line metal cutting tool condition monitoring.: I: force and vibration analyses," *International Journal of Machine Tools and Manufactures*,Vol.40(5), pp 739-768,2000.

[31] S.Purushothaman and Y.G. Srinivasa "A back propagation applied to tool wear monitoring ," *International Journal of Machine Tools and Manufacturers*, vol. 34, pp. 625-631, 1994.

[32] Y.L.Yao and X.Fang, "Assessment of chip forming patterns with tool wear progression in machining via neural networks," *International Journal of Machine Tools and Manufactures*,Vol.33(1), pp 89-102,1993.

[33] H.V.Ravindra, Y.G.Srinivasa and R.Krishnamurthy, "Modelling of tool wear based on cutting forces in turning, "*Wear*, 169, pp.25-32,1993.

[34] L.C.Lee,K.S.Lee and C.S.Gan, "On the correlation between dynamic cutting force and tool wear, "*International Journal of Machine Tools and Manufacturers*, Vol.29(3), pp.295-303,1989.

[35] M.J.M.Marques and R.M.D.Mesquita, "Monitoring the wear of sintered high speed steel tools," *Journal of Material Processing Technology*,25, pp 195-213,1991.

[36] J.S.Kim,and B.H.Lee, "An analytical model of dynamic cutting forces in chatter vibrations ," *International Journal of Machine tools and manufactures*,Vol.31(3), pp 371-381,1991.

[37] S.E.Oraby and D.R.Hayhurst, "Development of models for tool wear force relationships in metal cutting," *International Journal of Machine Tools and Manufactures*,Vol.33(2), pp 125-138,1991.

[38] Y.Yao,X.D.Fang and G.Arndt, "Comprehensive tool wear estimation in finish -machining via multivariate time series of 3D cutting forces," *Annals of CIRP*,Vol.39(1), pp 57-60,1990.

[39] Y.Yao,and X.D.Fang, "Modelling of multivariate time series for tool wear estimation in finish-turning ," *International Journal of Machine Tools and Manufactures*,Vol.32(4), pp 495-508,1992.

[40] A.Ghasempoor,J.Jeswiet and T.N.Moore, " Real time implementation of on-line tool condition monitoring in turning," *International Journal of Machine tools and Manufactures*,Vol.39, pp 1883-1902,1999.

[41] L.Dan and J.Mathew, "Tool wear and failure monitoring techniques for turning-a review, "*International Journal of Machine Tools and Manufacturers*, Vol.30(4), pp.579-598,1990.

[42] D.E.Dimla, P.M.Lister and N.J.Leighton, "Neural networks solutions to the tool condition monitoring problem in metal cutting- A critical review of methods, "*International Journal of Machine Tools and Manufacturers*, Vol37(9), pp.1219-1241,1997.

[43] Y.Yao,X.D.Fang and G.Arndt, "On-line estimation of groove wear in the minor cutting edge for finish machining," *Annals of CIRP*,Vol.40(1), pp 41-44,1991.

[44] J. Rotberg, S. Braun and E. Lenz, " Mechanical signature analysis in interrupted cutting, "*Annals of CIRP*, Vol.36(1), pp.249-252,1987.

[45] C.Y.Jiang,Z.Zhang and H.J.Xu, "In-process monitoring of tool wear stage by frequency band energy method," *Annals of CIRP*,Vol.36(1), pp 45-48,1987.

[46] J. Lin, "Inverse estimation of the tool-work interface temperature in end milling," *International Journal of Machine Tools and Manufactures*,35(5), pp 751-760,1995.

[47] R. S. Raman, A. Shaikh and P.H. Cohen, "A mathematical model for tool temperature sensing," *ASME Computational Methods in Materials Processing*,61, pp 181-193,1992.

[48] D.A.Stephenson and A.Ali, "Tool Temperature in Interrupted Metal Cutting, "*ASME Trans. Journal of Engineering for Industry*, Vol.115, pp.432-437,1992.

[49] J.G.Chow, P.K.Wright, " On-line estimation of tool/chip interface temperatures for a turning operation, "*ASME Trans. Journal of Engineering for Industry*, Vol.110, pp.56-64,1988.

[50] E. Usui, T. Shirakashi and T. Kitagawa, "Analytical prediction of cutting tool wear, "*Wear*, Vol.100,issues 1-3, pp.129-151,1984

[51] M.C.Shaw," The importance of temperature in grinding, *"Journal of Mechanical Working Technology*, Vol.17, pp.343-355,1988.

[52] Noori-Khajavi and R. Komanduri, " Frequency and time domain analyses of sensor signals in drilling-I. Correlation with drill wear, *"International Journal of Machine Tools and Manufactures*, Vol.35(6), pp.775-793,1995.

[53] M. Zhou, M. Andersson and J.E. Sthl, " A system for monitoring cutting tool spontaneous failure based on stress estimation, *"Journal of Materials Processing Technology*, Vol.48, pp.231-237,1995.

[54] M.P.Groover, " Introduction to Fundamentals of Modern Manufacturing systems ," *John Wiley publishers*, 3rd Edition (2006) Delhi.

[55] G.C. Sen and A. Bhattacharyya, "Principles of metal cutting, *"New central book agency*, (1969) New Delhi.

[56] TaeguTec, "Manual for turning operation ," *Taegutec Tooling system*,TaeguTec India Ltd, India.

[57] W.G.Cochran and G.M.Cox "Experimental Designs," 2nd ed. *John Wiley and Sons*, New York, 1967.

[58] Williams.J.Endres and Raja K.Kountanya, "The Effects of Corner radius and Edge radius on Tool Flank wear," *Journal of Manufacturing Processes*, vol.4(2), pp. 89-95, 1994.

[59] M.Thomas and Y.Beauchamp, "Statistical investigations of modal parameters of cutting tools in dry turning," *International Journal of Machine Tools and Manufacturers*, vol.43(11), pp. 1093-1106, 2003.

[60] C.Scheffer,H.Kratz,P.S.Heyns and F.Klocke, "Development of tool wear-monitoring for hard turning," *International Journal of Machine Tools and Manufacturers*, vol.43, pp. 973-985, 2003.

[61] I.W.Mayes, " Use of neural network for on-line vibration monitoring, "*Proceedings of institute of mechanical engineers* , Vol.208, 1994.

[62] M.F.Elkordy, K.C.Chang and G.C.Lee " Application of neural networks in vibration signature analysis, "*Journal of engineering mechanics*, Vol.120 (2),1994.

[63] M.Kram, M.Ghassemzadeh, N.Dai, M.Gandikota and A.M.Trzyanadlowski " Validation and recovery of vibration data in electro machine systems using neural network software, "*IEEE transactions on industrial applications* , Vol.30 (6), 1994.

[64] K.G.Ahn, H.J.Pahk, M.Y.Jung and D.W.Cho " A hybrid-type active vibration isolation system using neural networks software, "*Journal of Sound and Vibration* , Vol.192(4), 1996.

[65] S.J.Huang and R.J.Lian " A combination of fuzzy logic and and neural network algorithms for active vibration control, "*Proceedings Institute of Mechanical Engineers*, Vol.210, 1996.

[66] S.Haykin " Neural networks. A comprehensive foundation , "*Macmillan*, New York, 1994.

[67] A.C.McCormick and A.K.Nandi " Real time classification of rotating shaft loading conditions using ANN, "*IEEE transactions on neural networks*, Vol.8 (3), 1997.

[68] D.O.Hebb " Organization of behaviour, "*Science editions*, New York), 1961.

[69] Y.Han, L.Xiu, Z.Wang, Q.Chen, S.Tan " Artificial neural network controlled fast valving in a power generation plant, "*IEEE Transactions on Neural Networks*, Vol.8 (2), 1997.

[70] S. V. T. Elanayar and Y. C. Shin , " Radial basis function neural network for approximation and estimation of nonlinear stochastic dynamic systems, "*IEEE Transactions on Neural Networks*, Vol.5, pp.594-603,1994.

[71] R.J.Kuo and P.H.Cohen , " Multi-sensor integration for on-line tool wear estimation through radial basis function networks and fuzzy neural network , "*Neural Networks*, Vol.12(2), pp.355-370,1999.

[72] N.K.Bose and P.Liang , " Neural network foundations, with graphs, algorithms and applications , "*Tata Mc Graw-Hill*, New Delhi, 1996.

[73] B.S.Grewal, "Higher Engineering Mathematics," *Khanna Publishers*, 39th Edition (2005) Delhi.

[74] S.Rangwala and D.Dornfeld, " Sensor Integration using Neural networks for intelligent tool condition monitoring,"*Journal of Engineering for industry*,Vol 112, pp.219-228, 1990.

[75] E.Daniel Kriby,Ms.Zhe Zhang,J.C.Chen, "Development of an accelerometer-based surface roughness prediction system in turning operations using multiple regression techniques, *Journal of Industrial Technology*, Vol.20(4), pp 1-8, 2004.

[76] B.Y.Lee and Y.S.Tarng , "Application of the Discrete Wavelet Transform to the Monitoring of Tool Failure in End Milling Using the Spindle Motor," *International Journal of Advanced Manufacturing Technology*, Vol. 15(4),pp 238-243,2004.

[77] S.Rangwala,D.Dornfeld, "Sensor Integration using Neural networks for intelligent tool condition monitoring," *Journal of Engineering for industry*,Vol.112,pp 219-228,August 1990.

[78] Tugrul Ozel,Abhijit Nadgir, "Prediction of flank wear by using neural networks modeling when cutting hardened H-13 steel with chamfered

and honed CBN tools," *International Journal of Machine Tools and Manufacturers*,Vol.42,pp 287-297,2002.

[79] K.F.Martin, "A Review by discussion on Condition monitoring and fault diagnosis in machine tools," *International Journal of Machine Tools and Manufacturers*, vol. 34(4), pp. 527-551, 1994.

[80] Oleg Raybov,Kazuo Mori and Nagayoshi kasashima "Laser displacement meter applications for milling diagnostics," *Optics Lasers in Engineering*, vol. 30, pp. 251-263, 1998.

[81] Xiaoli Li, "A brief review: Acoustic emission method for tool wear monitoring during turning," *International Journal of Machine Tools and Manufacturers*,Vol.42, pp 157-165,2002.

[82] S.Purushothaman and Y.G.Srinivasa, "A Back propagation algorithm applied to tool wear monitoring," *International Journal of Machine Tools and Manufacturers*,Vol.34(5), pp 625-631,1994.

[83] Y.S.Tarng,Y.W.Hsieh and S.T.Hwang, "Sensing tool breakage in face milling with a neural network," *International Journal of Machine Tools and Manufacturers*,Vol.34(3), pp 341-350,1994.

[84] D.A.Dornfeld, "Neural network sensor fusion for tool condition monitoring ," *Annals of CIRP*,Vol.39(1), pp 101-105,1990.

[85] K.S.Lee,L.C.Lee, and S.C.Teo, "On line tool wear monitoring using a PC," *Journal of Material Processing Technology*,29, pp 3-13,1992.

[86] S.E.Oraby and D.R.Hayhurst, "Development of models for tool wear force relationships in metal cutting," *International Journal of Machine Tools and Manufacturers*,Vol.33(2), pp 125-138,1991.

[87] L.C.Lee,K.Y.Kim and X.D.Liu, "Characterisation of tool wear and failure," *Journal of Material Processing Technology*,40, pp 143-153,1994.

[88] J.Rotberg,S.Braun and E.Lenz, "Mechanical signature analysis in interrupted cutting," *Annals of CIRP*,Vol.36(1), pp 249-252,1987.

[89] I.Grabec, " Chaotic dynamics of the cutting process," *International Journal of Machine Tools and Manufacturers*,Vol.28(1), pp 19-32,1988.

[90] M.K.Khraisheh, C.Pezeshki and A.E.Bayoumi, " Time series based analysis for primary chatter in metal cutting," *Journal of Sound and Vibration*,Vol.180(1), pp 67-87,1988.

[91] M.E.Merchant, "Mechanics of metal cutting process," *Journal of Applied Physics*,16, pp 318-324,1945.

[92] T.I.El.Wardany,D.Gao and M.A.Elbestawi, "Tool condition monitoring in drilling using vibration signature analysis,"*International Journal of Machine Tools and Manufacturers*, Vol.36(6), pp.687-711,1996.

[93] R. Radulescu and S.G. Kapoor, "An analytical model for prediction of tool temperature fields during continuous and interrupted cutting," *ASME Trans. Journal of Engineering for Industry*,116(2), pp 135-143,1994.

[94] W.S. McCulloch and W. Pitts, "A logical calculation of the ideas immanent in nervous activity," *Bulletin of Mathematical Biophysics*, vol. 5, pp. 115-133, 1943.

[95] Jack M.Zurada , "Introduction to Artificial Neural systems," *Jaico publishing house*, New Delhi,1999.

[96] S. Rangwala and D. Dornfeld, " Sensor integration using neural networks for intelligent tool condition monitoring,"*ASME Trans. Journal of Engineering for Industry*, Vol.112(3), pp.219-228,1990.

[97] N.H. Abu-Zahra and T.H. Nayfeh, " Calibrated method for ultrasonic on-line monitoring of gradual wear during turning operations, "*International Journal of Machine Tools and Manufactures*, Vol.37(10), pp.1475-1484,1997.

[98] S. Kurada and C. Bradley, " A review of machine vision sensors for tool condition monitoring, "*Computers in Industry*, Vol.34(1), pp.55-72,1997.

[99] D.C.D. Oguamanam, H. Raafat and S.M. Taboun, " A machine vision system for wear monitoring and breakage detection of single-point cutting tools, "*Computers in Industrial Engineering*, Vol.26(3), pp.575-598,1994.

[100] Y.S. Wong, A.Y.C. Nee, X.Q. Li and C. Reisdorf, " Tool condition monitoring using laser scatter pattern, "*Journal of Materials Processing Technology* , Vol.63, pp.205-210,1997.

[101] M. Shiraishi, " Scope of in-process measurement, monitoring and control techniques in machining processes-Part 1: In-process techniques for tools, "*Precision Engineering* , Vol.10(4), pp.179-189,1988.

[102] J.I. El Gomayel and K.D. Bregger, " On-line tool wear sensing for turning operations, "*ASME Trans. Journal of Engineering for Industry*, Vol.108, pp.44-47,1986.

[103] N. Constantinides and S. Bennett, " An investigation of methods for on-line estimation of tool wear, "*International Journal of Machine Tools and Manufactures* , Vol.27(2), pp.225-237,1987.

[104] A. Ravichandran and B. Yegnanarayana, "Studies on object recognition from degraded images using neural networks," *Neural Networks*, vol. 8, pp. 481-488, 1995.

[105] C.M. Bishop, *Neural Networks for pattern Recognition*, Oxford university press, 2003.

[106] W.T. Miller, III, "Real time application of neural network for sensor based control of robot with vision," *IEEE Transaction on Systems Man and Cybernetics*, vol. 19, pp. 825-831, 1989.

[107] K.S. Narendra and K. Parthasarathy, "Gradient methods for the optimization of dynamical systems containing neural networks," *IEEE Transaction on Neural Networks*, vol. 2, pp. 252-262, 1991.

[108] L.R. Rabiner, "A tutorial on hidden Markov models and selected applications in speech recognition," *Proc. IEEE*, vol. 77, pp. 257-286, 1989.

[109] L.R. Rabiner and B.H. Juang, *Fundamental of Speech Recognition*, Englewood Cliffs, New Jersey, Prentice-Hall, 1993.

[110] P.P. Raghu, R. Poongodi and B. Yegnanarayana, "A combined neural network approach for texture classification," *Neural Networks*, vol. 8, pp. 975-987, 1995.

[111] P.P. Raghu and B. Yegnanarayana, "Segmentation of Gabor-Filtered textures using deterministic relaxation," *IEEE Transactions on Image Processing*, vol. 5, pp. 1625-1636, 1996.

List of Publications

1. **H.Chelladurai**, V.K.Jain and N.S. Vyas, "Development of a cutting tool condition monitoring system for high speed turning operation by vibration and strain analysis ", *International Journal of Advanced Manufacturing Technology*, 37(2008),471-485.

2. **H.Chelladurai**, V.K.Jain and N.S. Vyas, "Cutting Tool Condition Monitoring System for High Speed Turning Operations", *International Journal of Manufacturing Technology and Management*, (Accepted for publication)

3. **H.Chelladurai**, V.K.Jain and N.S. Vyas, "Cutting tool condition monitoring under high speed turning operations", *International Journal of Machining and Machinability of Materials* , (Accepted for publication).

4. **H.Chelladurai**, V.K.Jain and N.S. Vyas, "Cutting Tool Condition Monitoring for High Speed Turning Operations", *in proc. of 22nd National and First International Conference on All India Manufacturing Technology Design and Research (AIMTDR)*, pp. 439-445, Dec. 23-26, 2006, IIT Roorkee, India.